공학박사 학위논문

Missile Acceleration Autopilot Design Based on State-Dependent Riccati Equation Method

State-Dependent Riccati Equation 기법을 이용한
유도탄의 가속도 자동조종장치 설계

2019 년 8 월

서울대학교 대학원
기계항공공학부

이 재 호

Missile Acceleration Autopilot Design Based on State-Dependent Riccati Equation Method

State-Dependent Riccati Equation 기법을 이용한
유도탄의 가속도 자동조종장치 설계

지도교수 김 유 단

이 논문을 공학박사 학위논문으로 제출함

2019 년 6 월

서울대학교 대학원

기계항공공학부

이 재 호

이재호의 공학박사 학위논문을 인준함

2019 년 6 월

위 원 장 김 현 진 (인)

부위원장 김 유 단 (인)

위 원 박 찬 국 (인)

위 원 탁 민 제 (인)

위 원 유 창 경 (인)

Missile Acceleration Autopilot Design Based on State-Dependent Riccati Equation Method

by

Jaeho Lee

Submitted to the Graduate School of
Seoul National University
in partial fulfillment of the requirements for the degree of

Doctor of Philosophy

Department of Mechanical and Aerospace Engineering
Seoul National University

Advisor: Prof. Youdan Kim

August 2019

Missile Acceleration Autopilot Design Based on State-Dependent Riccati Equation Method

by

Jaeho Lee

Approved as to style and content by:

H. Jin Kim, Chair, Ph.D.

Youdan Kim, Vice-Chair, Ph.D.

Chan Gook Park, Member, Ph.D.

Min-Jea Tahk, Member, Ph.D.

Chang-Kyung Ryoo, Member, Ph.D.

June 2019

Abstract

Missile Acceleration Autopilot Design Based on State-Dependent Riccati Equation Method

Jaeho Lee
Department of Mechanical and Aerospace Engineering
The Graduate School
Seoul National University

An acceleration autopilot for a tail-fin controlled skid-to-turn maneuver missile is designed using a state-dependent Riccati equation (SDRE) method. The asymptotic stability of the closed-loop system controlled by the designed autopilot is analyzed in a predefined missile operational range. To analytically represent the closed-loop system, the analytic solution of the state-dependent algebraic Riccati equation (ARE) is obtained and utilized in analyzing the asymptotic stability.

In the first part of this study, six-degrees-of-freedom equations are derived for the tail-fin controlled missile, and reduced equations for longitudinal and lateral motions are introduced based on a linear approximation. For the longitudinal dynamics of the missile, mathematical analyses of its characteristics and closed-loop system behavior are given. A valid transformation to normal form equations with a normal acceleration output is presented, and non-minimum phase behavior of the tail-fin controlled missile is analyzed, based on the normal form equations. For the closed-loop system behavior with an approximate model-based controller, input-output stability, specifying an external input as

a term causing the non-minimum phase behavior, is proved for the non-zero acceleration command. Furthermore, perfect regulation of the closed-loop system is shown for the zero acceleration command. A numerical example is given to illustrate the analytical results.

In the second part of this study, the asymptotic stability of the closed-loop system controlled by the SDRE method is analyzed in the predefined operational range of the missile. The analytic solution of the state-dependent ARE is obtained for two-dimensional nonlinear systems, where a matrix sign function and matrix principal square root are utilized. Next, a SDRE method-based missile acceleration autopilot is designed using the longitudinal dynamics of the missile. Incorporating assumptions about the properties of the tail-fin controlled missile in the normal operational range, the asymptotic stability of the closed-loop system controlled by the designed acceleration autopilot is analyzed, using the Lyapunov stability theorem. The analytical result of the asymptotic stability is demonstrated with a numerical simulation. Finally, a numerical simulation based on the six-degrees-of-freedom equations of the missile is performed to verify the control performance of the proposed autopilot.

Keywords: Missile Acceleration Autopilot, State-Dependent Riccati Equation, Asymptotic Stability, Nonlinear Analysis

Student Number: 2013-20698

Contents

List of Tables

List of Figures

Chapter 1

Introduction

1.1 Background and Motivation

A state-dependent Riccati equation (SDRE) method is one of the nonlinear control methodologies, which has emerged over the last decade as an effective design technique, particularly in aerospace engineering. The design procedure of the SDRE method begins by transforming a nonlinear system into a pseudo-linear system using a state-dependent coefficient (SDC) transformation. The SDRE method usually considers an autonomous input-affine nonlinear system. Motivated by a linear quadratic regulator (LQR), a state-dependent algebraic Riccati equation (ARE) for the transformed pseudo-linear system, including the state-dependent weighting matrices, is constructed and solved in the SDRE method. Next, the suboptimal control input with the solution of the state-dependent ARE is generated. The main feature of the SDRE method is the ability to directly handle the tradeoff between the state errors and control efforts, by adjusting the weighting matrices, as in the LQR method. Tuning of the control gains in other nonlinear control methods is far less intuitive. Furthermore, the SDRE method allows for design flexibility, such as a non-uniqueness of the SDC transformation.

There are many successful applications of the SDRE method to various problems. In particular, the SDRE method has been widely used in aerospace engineering to design a missile autopilot. A three-loop autopilot has been the representative method for missile acceleration autopilots, because it has good control performance. Typically, the three-loop autopilot is designed for a certain operating point, based on a linearized model of a missile. However, the control performance can also be guaranteed for the neighborhood near the design point, if the variation of the parameters between the operating points is sufficiently small and slow. The drawback is that the design procedure for many operating points requires heavy time-consuming tasks, and the stability cannot be guaranteed if the parameters change rapidly.

Nonlinear autopilots can resolve the issues of the three-loop autopilot, because they are designed for a nonlinear missile model, covering the entire flight envelope. Among them, the SDRE method is a suitable approach for tail-fin controlled missile autopilot design. This is because it is not based on nonlinear dynamic inversion, unlike the feedback linearization and sliding mode control schemes. Consequently, the SDRE method can directly handle non-minimum phase systems, such as a tail-fin controlled missile. Furthermore, the optimal property of the SDRE method, which approximately minimizes a quadratic cost function, is a great advantage in designing a missile autopilot. Other nonlinear control schemes cannot address the optimal properties of the controllers.

However, a major drawback of the SDRE method is that the state-dependent ARE should be numerically solved at each step, which is referred to as 'online computation' of the SDRE method. Online computation is inevitable in most cases, because obtaining the analytic solution of the state-dependent ARE is

very difficult. The two main problems of online computation for the SDRE method are i) high computational cost and ii) an analytic representation of the closed-loop system controlled by the SDRE method is not possible. The computational cost issue has been resolved to a large extent, by improvements in the microprocessor computational capacity. However, the second issue remains a major obstacle to using the SDRE method in practice, because the size and boundary of the asymptotic stable region cannot be properly quantified. In fact, most applications of the SDRE method depend on local asymptotic stability around the equilibrium points based on the point-wise controllability and observability.

Another difficulty of the SDRE method is treating system robustness, with respect to uncertainties and disturbances. In particular, the SDRE method is known to be sensitive to parametric uncertainties, because it is motivated by the LQR technique. Note that the linear model-based three-loop autopilot can handle system robustness, by examining the phase and gain margins for a certain operating point. Some nonlinear control schemes, such as backstepping and sliding mode control, allow further development for robust performance.

In this study, the analytic solution of the state-dependent ARE is obtained for two-dimensional nonlinear systems, thus providing an analytic representation of the closed-loop system. To design and analyze the SDRE method-based acceleration autopilot using the analytic solution, a short-period approximated model of the longitudinal missile motion is used. The longitudinal dynamics can also be applied to the lateral motion of the missile because of the axial symmetry of the skid-to-turn maneuver. First, the characteristics of the longitudinal dynamics for the tail-fin controlled missile are analyzed, and then the missile

acceleration autopilot is designed based on the longitudinal dynamics. Using the analytic solution of the state-dependent ARE, the closed-loop system controlled by the designed autopilot is represented analytically, and its asymptotic stability is analyzed based on the Lyapunov stability theorem.

To examine robustness with respect to parametric uncertainties, the analytical results of the SDRE method are investigated with a numerical example that includes the aerodynamic uncertainties. Furthermore, the control performance of the proposed autopilot, which is designed considering the short-period approximated model, is demonstrated using a full nonlinear dynamics model of the skid-to-turn missile with uncertainty.

1.2 Literature Survey

1.2.1 Application and Theoretical Studies on State-Dependent Riccati Equation Method

The SDRE method has been applied to controller design for various systems [1–9]. Missile autopilot design is a representative application of the SDRE method [2–6]. Also, other aerospace systems such as spacecraft [7, 8] and unmanned helicopter [9] have used the SDRE method for designing control systems. These studies used online computation to obtain the control input of the SDRE method, and thus only local asymptotic stability of the closed-loop system can be guaranteed. Therefore, the region of attraction cannot be clearly quantified. Local asymptotic stability of the SDRE method is valid in a sufficiently small region around the origin, based on the fact that the closed-loop system matrix is Hurwitz at the origin. Furthermore, the existence of a larger region of asymptotic stability, namely large-scale asymptotic stability of the SDRE method [10], has been proven. However, practical use is severely limited if global stability is not guaranteed or the region of attraction is not clearly quantified, although most applications of the SDRE method depend on large-scale asymptotic stability.

Many previous studies have focused on the applications of the SDRE method, rather than detailed theoretical investigation. Several studies have examined the stability issue of the SDRE method, based on the analytic representation of the closed-loop system [11–14]. For a two-dimensional nonlinear system with a single input, the global asymptotic stability of the SDRE method was shown [11, 12]. These studies dealt with a very simplified system, where some components of the SDC system and input matrices were set to zero,

and therefore, obtaining the analytic solution of the state-dependent ARE was much easier. Furthermore, strong assumptions are required to guarantee global asymptotic stability. In summary, the analytical results of Refs. [11,12] are limited to a special class of nonlinear systems. In addition, it was shown that the global stability of the SDRE method is guaranteed for scalar systems without any additional restriction and multivariable systems with the symmetric closed-loop system matrix [13,14]. However, general multivariable systems do not have a symmetric closed-loop system matrix.

1.2.2 Analytic Solution of the Algebraic Riccati Equation

The processes for obtaining the solutions of the state-dependent ARE and constant ARE are the same. The only difference is whether or not the solution is constant. The analytic representation of the closed-loop system for the constant ARE is possible, even though it is solved by a numerical algorithm. Most studies dealing with the constant ARE have used a numerical solution [15–17]. Among the numerical methods for solving the ARE, Potter's method is the most widely used. Here, the Hamiltonian matrix corresponding to the ARE is constructed, and its eigenvectors are computed numerically [15]. The Schur decomposition method was proposed to improve the numerical stability [16], and the matrix sign function is also used to numerically solve the ARE [17].

Some studies have been done on the derivation of the analytic solution of the ARE [18–29]. However, most of this research was confined to certain special classes, even for two-dimensional systems [18–24]. In some studies, a process was required to find special matrices satisfying another matrix quadratic equation, to analytically solve the ARE [25,26]. Ledyaev derived the mathematical

formulas of the algebraic and differential Riccati equations [27]. However, direct application to the analytic representation of the closed-loop system is difficult, because these solutions are expressed in terms of the matrix transfer functions including the integral terms. Recently, a method to obtain the analytic solution of the ARE for two-dimensional systems was introduced based on the analytic representation of the matrix sign function by obtaining the principal square root of the square of the Hamiltonian matrix [28]. Here, this method is further developed to derive the analytic solution of the state-dependent ARE component-wisely, without specifying a certain class of nonlinear systems [29].

1.2.3 Characteristics of the Tail-Fin Controlled Missile

The properties of the tail-fin controlled missile are well known, but in many cases, a rigorous mathematical analysis has not been performed. One of the well-known properties of the tail-fin controlled missile is a non-minimum phase behavior. The concept of non-minimum phase was defined early on for linear systems, and it is now well-established for nonlinear systems, based on the stability of the internal dynamics [30]. Several studies have performed an analysis of the non-minimum phase of the tail-fin controlled missile, using specific aerodynamic data [31] and singular perturbation theory in the normal operational range of the missile [32]. However, these studies were based on the zero-acceleration subspace of the missile, rather than the normal form equations. Additionally, the normal form equations of the missile longitudinal dynamics, specifying the angle of attack as the output, were used to design the missile acceleration autopilot [33].

For the tail-fin controlled missile system with unstable internal dynamics,

nonlinear inversion-based control schemes, such as feedback linearization and sliding mode control, cannot be directly applied to the design of an acceleration autopilot. Approximate input-output linearization (AIOL) has been frequently used for circumventing the non-minimum phase behavior of the missile. This method neglects the force induced by the fin deflection causing the non-minimum phase behavior [31, 32, 34, 35]. Most studies using the AIOL method for the design of a missile acceleration autopilot have assumed that the approximate model-based controller works well on the actual missile system. This approach was validated using numerical simulation only [36]. In Ref. [37], the boundedness of the tracking error on the actual system was proven, assuming that the desired command and specific term are sufficiently small.

1.2.4 Missile Acceleration Autopilot

The traditional design of a missile acceleration autopilot is a three-loop structure [38]. The three-loop structure has been widely used for acceleration control in linear-based autopilot design because of its robustness to disturbances, although the control gains should be designed for each operating point [39–41]. To deal with disturbances or modeling errors caused by the linearization, robust control theory, such as $\mathcal{H}_\infty$ control and μ-synthesis, has been applied to the design of a missile acceleration autopilot [42–44]. The gain-scheduling approach is a widely used method for designing autopilots, based on the linear missile model [45–47]. However, the gain-scheduling approach for a highly nonlinear system requires time-consuming work, and the control performance cannot be guaranteed for the entire flight envelope [48].

In contrast, missile autopilot designs that take account of the nonlineari-

ties of missile dynamics have been proposed in Refs. [2–6,49–54]. Several studies have used the feedback linearization method, nonlinear control scheme based on nonlinear dynamic inversion, to design a missile acceleration autopilot [49, 50]. However, the feedback linearization method requires precise model information to cancel out the nonlinearities of the missile system, and therefore, it might not be robust to disturbances [55]. The backstepping control [51, 52] and sliding mode control [53, 54], which are other nonlinear control schemes based on nonlinear dynamic inversion, have also been applied to the design of a missile acceleration autopilot. These methods allow for further development to increase robustness, with respect to uncertainties and disturbances. The SDRE method is one of the widely used techniques for designing a missile acceleration autopilot [2–6]. Considering the capability of the SDRE method to directly handle the unstable and/or non-minimum phase systems, it is a suitable approach for designing the autopilot of the tail-fin controlled missile [56].

1.3 Contributions

The main contributions of this study are summarized as follows.

Mathematical Analysis of the Tail-Fin Controlled Missile Dynamics

In this study, rigorous mathematical analyses of the properties of missile longitudinal dynamics are given. First, the non-minimum phase behavior of the tail-fin controlled missile is analyzed, based on the normal form equations with acceleration output. Although Ref. [33] proposed a valid transformation to the normal form equations of the missile, the angle of attack was specified as the output rather than the normal acceleration. Also, the analysis of the non-minimum phase behavior of the tail-fin controlled missile was performed based on the zero-acceleration subspace, without transforming into the normal form equations in Refs. [31, 32]. In this study, the non-minimum phase analysis is based on the internal dynamics, which is directly obtained from the normal form equations of the missile. Second, the behavior of the actual system controlled by the AIOL-based autopilot is analyzed. This result contains not only the boundedness of the tracking error as proved in Ref. [37], but also the $\mathcal{L}_p$-stability of the actual system. This is commonly used for input-output stability, where the term causing the non-minimum phase behavior is considered to be the external input.

Analytic Solution of the SDRE Method for Two-Dimensional Nonlinear Systems

To analytically present the closed-loop system controlled by the SDRE method-based autopilot, the analytic solution of the state-dependent ARE is derived for two-dimensional nonlinear systems. References [11, 12] have suggested an ana-

lytic solution of the state-dependent ARE for two-dimensional systems. However, some components of the SDC system and input matrices of the pseudo-linear system in the SDRE method were set to zero, so that the process of obtaining the analytic solution was greatly simplified. In this study, an analytic solution of the SDRE method is proposed for general two-dimensional nonlinear systems, without any restriction on the matrix components included in the pseudo-linear system. Whereas studies dealing with the derivation of the analytic solution of the ARE are confined to certain restrictions on the systems [18–24], the method proposed here needs only conditions for the existence of the positive definite stabilizing solution of the state-dependent ARE. The analytic solution of the ARE proposed in Ref. [27] cannot be directly applied to the analytic representation of the closed-loop system, because the analytic solution is expressed as the matrix transfer functions, including the integral terms. However, the method proposed in this study allows for the analytic representation of the closed-loop system, because the obtained solution is expressed component-wisely.

Asymptotic Stability of the Closed-Loop System Controlled by the SDRE-Based Autopilot

In this study, the asymptotic stable region for the SDRE method-based autopilot is clearly quantified, based on the Lyapunov stability theorem. Existing missile applications of the SDRE method have used online computation, which depends on the local asymptotic stability around the origin [2–6]. The local stability or lack of a well-quantified region of attraction prevents the SDRE method from being used in practice, because the autopilot may not provide

good performance for arbitrary initial states. Here, asymptotic stability in the predefined operational range of the missile is proven, using the analytic solution of the state-dependent ARE. References [11,12] have shown the global stability of a closed-loop system controlled by the SDRE method, using very simplified systems with strong assumptions. Therefore, the results are of limited use in the design of the missile autopilot. In contrast, the analytical result proposed in this study provides the theoretical basis and justifications for utilizing the SDRE method practically, in the design of a missile autopilot.

1.4 Dissertation Outline

This dissertation is organized as follows:

In Chapter 1, the background and motivation of this study are described, and related research works are given. The objectives and contributions of the study are presented.

In Chapter 2, six-degrees-of-freedom equations of the skid-to-turn maneuver tail-fin controlled missile are derived, and the reduced models for the longitudinal and lateral motions of the missile are presented. A brief description of the SDRE method is given.

In Chapter 3, the analytical results of the missile longitudinal dynamics are provided. The characteristics of the longitudinal dynamics of the tail-fin controlled missile are analyzed including the coordinate transformation to the normal form equations and non-minimum phase behavior. And the analytical results of the closed-loop system behavior with the approximate model-based controller are presented. Numerical example is provided to demonstrate the findings of the mathematical analyses.

In Chapter 4, the analytic solution of the SDRE method for two-dimensional systems is derived. The missile acceleration longitudinal autopilot is designed based on the SDRE method, and the stability analysis of the closed-loop system controlled by the designed autopilot is performed using the derived analytic solution of the SDRE method. By providing the numerical example, the analytical results of the SDRE method are verified.

In Chapter 5, the design procedure of the three-axes missile autopilot is provided based on the proposed longitudinal autopilot and roll stabilizer. For comparison, the SDRE method-based missile acceleration autopilot designed

for the full-order missile model is presented. Numerical simulation is performed for two autopilot cases to demonstrate the control performance of the designed autopilots.

In Chapter 6, concluding remarks and suggestions for further works are presented.

Chapter 2

System Model and State-Dependent Riccati Equation Method

2.1 System Model

2.1.1 Six-Degrees-of-Freedom Equations

In this study, the following assumptions are considered for deriving six-degrees-of-freedom equations of motions for the tail-fin controlled missile.

Assumption 2.1: The missile has symmetric, cruciform shape.

Assumption 2.2: The physical parameters of the missile including the mass, moment of inertia, reference length, and area are fixed.

Assumption 2.3: External forces and moments caused by the aerodynamic effects are considered, and the forces and moments caused by the gravity and thrusters are neglected.

Under **Assumptions 2.2** and **2.3**, the six-degrees-of-freedom equations of the missile with respect to the body-axes can be represented as follows [57],

$$m\dot{\mathbf{v}} + m(\omega \times \mathbf{v}) = F_a \tag{2.1}$$

$$I\dot{\omega} - \omega \times I\omega = M_a \tag{2.2}$$

where m and I are the mass and the moment of inertia matrix of the missile, respectively, $\mathbf{v} = [u\ v\ w]^T$ is the velocity vector, $\omega = [p\ q\ r]^T$ is the angular velocity vector, and $F_a = [F_X\ F_Y\ F_Z]^T$ and $M_a = [L\ M\ N]^T$ are the external force and moment vectors caused by the aerodynamic effects, respectively. Under **Assumption 2.1**, the moment of inertia matrix can be expressed as follows,

$$I = \begin{bmatrix} I_{xx} & 0 & 0 \\ 0 & I_{yy} & 0 \\ 0 & 0 & I_{zz} \end{bmatrix} \tag{2.3}$$

where $I_{yy} = I_{zz}$. Using the aerodynamic coefficients, the external forces are expressed as

$$\begin{aligned} F_X &= QSC_X \\ F_Y &= QSC_Y \\ F_Z &= QSC_Z \end{aligned} \tag{2.4}$$

where Q is the dynamic pressure, and S is the reference area. And C_X, C_Y, and C_Z are the non-dimensionalized aerodynamic force coefficients which can be expressed as the following nonlinear functions.

$$\begin{aligned} C_X &= f_{C_X}(\mathbf{M}, h, x_{\text{cm}}, \alpha, \beta, \delta_r, \delta_p, \delta_y) \\ C_Y &= f_{C_Y}(\mathbf{M}, h, x_{\text{cm}}, \alpha, \beta, \delta_r, \delta_p, \delta_y) \\ C_Z &= f_{C_Z}(\mathbf{M}, h, x_{\text{cm}}, \alpha, \beta, \delta_r, \delta_p, \delta_y) \end{aligned} \tag{2.5}$$

where $\mathbf{M}$ is the Mach number, h is the altitude, x_{cm} is the distance between the missile's nose and the center of mass, α and β are the angle of attack and sideslip angle, respectively, δ_r, δ_p, and δ_y are the roll, pitch, and yaw fin

deflections, respectively, and $f_i(\cdot)$ denotes a nonlinear function. Likewise, the external moments can be represented as follows,

$$\begin{aligned} L &= QSD\left(C_l + \frac{D}{2V}C_{l_p}p\right) \\ M &= QSD\left(C_m + \frac{D}{2V}C_{m_q}q\right) \\ N &= QSD\left(C_n + \frac{D}{2V}C_{n_r}r\right) \end{aligned} \tag{2.6}$$

where D is the reference length, V is the total velocity, C_l, C_m, and C_n are the non-dimensionalized aerodynamic moment coefficients, and C_{l_p}, C_{m_q}, and C_{n_r} are the non-dimensionalized aerodynamic damping coefficients. The non-dimensionalized aerodynamic moment coefficients are expressed as the following nonlinear functions.

$$\begin{aligned} C_l &= f_{C_l}(\mathbf{M}, h, x_{\text{cm}}, \alpha, \beta, \delta_r, \delta_p, \delta_y) \\ C_m &= f_{C_m}(\mathbf{M}, h, x_{\text{cm}}, \alpha, \beta, \delta_r, \delta_p, \delta_y) \\ C_n &= f_{C_n}(\mathbf{M}, h, x_{\text{cm}}, \alpha, \beta, \delta_r, \delta_p, \delta_y) \end{aligned} \tag{2.7}$$

Substituting Eqs. (2.3), (2.4) and (2.6) into Eqs. (2.1) and (2.2), the six-degrees-of-freedom equations of the tail-fin controlled missile can be obtained in scalar form as follows:

Translational Equations

$$\begin{aligned} \dot{u} &= rv - qw + \frac{QSC_X}{m} \\ \dot{v} &= pw - ru + \frac{QSC_Y}{m} \\ \dot{w} &= qu - pv + \frac{QSC_Z}{m} \end{aligned} \tag{2.8}$$

Rotational Equations

$$\begin{aligned}
\dot{p} &= \frac{QSD}{I_{xx}}\left(C_l + \frac{D}{2V}C_{l_p}p\right) \\
\dot{q} &= \frac{I_{zz}-I_{xx}}{I_{yy}}pr + \frac{QSD}{I_{yy}}\left(C_m + \frac{D}{2V}C_{m_q}q\right) \\
\dot{r} &= \frac{I_{xx}-I_{yy}}{I_{zz}}pq + \frac{QSD}{I_{zz}}\left(C_n + \frac{D}{2V}C_{n_r}r\right)
\end{aligned} \tag{2.9}$$

In addition, the dynamics of the angle of attack and sideslip angle can be derived using the obtained six-degrees-of-freedom equations. The angle of attack and sideslip angle are defined as follows,

$$\begin{aligned}
\alpha &= \tan^{-1}\frac{w}{u} \\
\beta &= \sin^{-1}\frac{v}{V}
\end{aligned} \tag{2.10}$$

Using Eq. (2.10) and the total velocity, the components of the velocity vector can be rewritten as

$$\begin{aligned}
u &= V\cos\alpha\cos\beta \\
v &= V\sin\beta \\
w &= V\sin\alpha\cos\beta
\end{aligned} \tag{2.11}$$

Differentiating the total velocity with respect to time and substituting Eqs. (2.8) and (2.11) into the resulting equation yield

$$\dot{V} = \frac{QS}{m}\left(C_X\cos\alpha\cos\beta + C_Y\sin\beta + C_Z\sin\alpha\cos\beta\right) \tag{2.12}$$

Differentiating Eq. (2.10) with respect to time and substituting Eqs. (2.8), (2.11), and (2.12) into the resulting equation, the following dynamics of the

angle of attack and sideslip angle can be obtained.

$$\begin{aligned}\dot{\alpha} &= q - (p\cos\alpha + r\sin\alpha)\tan\beta + \frac{1}{V\cos\beta}(a_z\cos\alpha - a_x\sin\alpha)\\ \dot{\beta} &= p\sin\alpha - r\cos\alpha - \frac{1}{V}(a_x\cos\alpha\sin\beta - a_y\cos\beta + a_z\sin\alpha\sin\beta)\end{aligned} \tag{2.13}$$

where a_x, a_y, and a_z are X-, Y-, and Z-axes accelerations of the missile body, respectively, which are defined as

$$\begin{aligned}a_x &= \frac{QSC_X}{m}\\ a_y &= \frac{QSC_Y}{m}\\ a_z &= \frac{QSC_Z}{m}\end{aligned} \tag{2.14}$$

2.1.2 Longitudinal and Lateral Motions of Equations

Based on the roll stabilization, the longitudinal and lateral motions of the missile can be presented separately neglecting the coupling effects between the roll-pitch-yaw channels. Under **Assumption 2.3** with a specified altitude, the aerodynamic force and moment coefficients of the longitudinal motion can be modeled using the small-perturbation theory and first-order Taylor expansion as follows,

$$\begin{aligned}\bar{C}_Z &= C_{Z_\alpha}(\mathbf{M},\alpha)\alpha + C_{Z_{\delta_p}}(\mathbf{M},\alpha)\delta_p\\ \bar{C}_m &= C_{m_\alpha}(\mathbf{M},\alpha)\alpha + C_{m_{\delta_p}}(\mathbf{M},\alpha)\delta_p\end{aligned} \tag{2.15}$$

where $C_{(\cdot)}(\mathbf{M},\alpha)$ represents the longitudinal aerodynamic coefficient expressed as a function of the Mach number and the angle of attack. Substituting Eq. (2.15) into Eqs. (2.9), (2.13), and (2.14), the longitudinal motion of the missile can be described based on the short-period approximation as follows [58],

$$
\begin{aligned}
\dot{\alpha} &= \frac{QS}{mV}\left(C_{Z_\alpha}(\mathbf{M},\alpha)\alpha + C_{Z_{\delta_p}}(\mathbf{M},\alpha)\delta_p\right) + q \\
\dot{q} &= \frac{QSD}{I_{yy}}\left(C_{m_\alpha}(\mathbf{M},\alpha)\alpha + C_{m_{\delta_p}}(\mathbf{M},\alpha)\delta_p + \frac{D}{2V}C_{m_q}(\mathbf{M},\alpha)q\right) \\
a_z &= \frac{QS}{m}\left(C_{Z_\alpha}(\mathbf{M},\alpha)\alpha + C_{Z_{\delta_p}}(\mathbf{M},\alpha)\delta_p\right)
\end{aligned}
\tag{2.16}
$$

Figure 2.1 shows the longitudinal geometry of the tail-fin controlled missile, where X_B and Z_B denote X- and Z-axes of the missile body, and x_{cf} and x_{cp} are the distances from the missile's nose to the center of pressures for the missile's tail-fin and body, respectively. Similarly, the aerodynamic force and moment coefficients of the lateral motion are modeled as follows,

$$
\begin{aligned}
\bar{C}_Y &= C_{Y_\beta}(\mathbf{M},\beta)\beta + C_{Y_{\delta_y}}(\mathbf{M},\beta)\delta_y \\
\bar{C}_n &= C_{n_\beta}(\mathbf{M},\beta)\beta + C_{n_{\delta_y}}(\mathbf{M},\beta)\delta_y
\end{aligned}
\tag{2.17}
$$

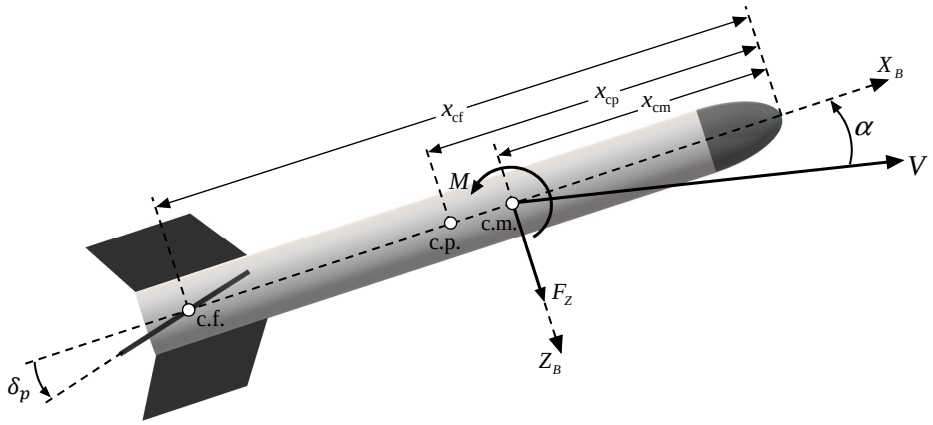

Figure 2.1 Tail-fin controlled missile geometry in the longitudinal motion

where $C_{(\cdot)}(\mathbf{M}, \beta)$ represents the lateral aerodynamic coefficient expressed as a function of the Mach number and the sideslip angle. Substituting Eq. (2.17) into Eqs. (2.9), (2.13), and (2.14), the lateral motion of the missile can be described based on the short-period approximation as follows,

$$\begin{aligned}
\dot{\beta} &= \frac{QS}{mV}\left(C_{Y_\beta}(\mathbf{M},\beta)\beta + C_{Y_{\delta_r}}(\mathbf{M},\beta)\delta_y\right) - r \\
\dot{r} &= \frac{QSD}{I_{zz}}\left(C_{n_\beta}(\mathbf{M},\beta)\beta + C_{n_{\delta_r}}(\mathbf{M},\beta)\delta_y + \frac{D}{2V}C_{n_r}(\mathbf{M},\beta)r\right) \\
a_y &= \frac{QS}{m}\left(C_{Y_\beta}(\mathbf{M},\beta)\beta + C_{Y_{\delta_y}}(\mathbf{M},\beta)\delta_y\right)
\end{aligned} \tag{2.18}$$

Remark 2.1: Because the missile has an axial symmetric shape with respect to X-axis of the missile body under **Assumption 2.1**, the longitudinal and lateral motions can be described in the same way based on the roll stabilization as in Eqs. (2.16) and (2.18), respectively. Therefore, the design schemes and analytical results for the longitudinal dynamics of the missile treated in this study can also be applied to the lateral dynamics of the missile.

2.2 State-Dependent Riccati Equation Method

This section introduces the traditional SDRE method-based controller design process for multi-input multi-output nonlinear systems. Let us consider the following autonomous input-affine nonlinear system.

$$\dot{x} = f(x) + g(x)u \tag{2.19}$$

where $x \in \mathbb{R}^n$ is the state vector, $u \in \mathbb{R}^m$ is the input vector, $f(x) \in \mathbb{R}^n$ is the system vector, and $g(x) \in \mathbb{R}^{n\times m}$ is the input matrix. Assuming that $f(0) = 0$ and $g(x) \neq 0$ for all x in a region of interest, the input-affine nonlinear system, Eq. (2.19), can be transformed into a pseudo-linear system using the SDC transformation as follows,

$$\dot{x} = F(x)x + B(x)u \tag{2.20}$$

where $F(x) \in \mathbb{R}^{n\times n}$ and $B(x) \in \mathbb{R}^{n\times m}$ are the state-dependent system and input matrices, respectively, satisfying $F(x)x = f(x)$ and $B(x) = g(x)$.

Motivated by the LQR technique, which is the linear control design scheme based on the optimal control theory, the SDRE method constructs the state-dependent ARE for the pseudo-linear system, Eq. (2.20), considering the following quadratic cost function.

$$J = \frac{1}{2}\int_0^\infty \left(x^T Q(x)x + u^T R(x)u\right) dt \tag{2.21}$$

where $Q(x) \in \mathbb{R}^{n\times n}$ and $R(x) \in \mathbb{R}^{m\times m}$ are weighting matrices. Note that the SDRE method can directly handle the tradeoff between the state errors and control efforts by adjusting the weighting matrices $Q(x)$ and $R(x)$ as in the

LQR method. Based on the quadratic cost function in Eq. (2.21), the state-dependent ARE can be constructed as follows,

$$F(x)^T X(x) + X(x)F(x) - X(x)B(x)R(x)^{-1}B(x)^T X(x) + Q(x) = 0 \quad (2.22)$$

where $X(x) \in \mathbb{R}^{n\times n}$ is the positive definite stabilizing solution of the state-dependent ARE, which exists if the following conditions are satisfied on the region of interest of x [59].

Condition 2.1: All state-dependent matrices of the pseudo-linear system are continuous matrix-valued functions.

Condition 2.2: The weighting matrices are continuous matrix-valued functions satisfying $Q(x) = Q(x)^T \geq 0$ and $R(x) = R(x)^T > 0$.

Condition 2.3: The pairs $(F(x), B(x))$ and $\big(F(x), \bar{Q}(x)\big)$ are point-wise controllable and observable, respectively, where $Q(x) = \bar{Q}(x)\bar{Q}(x)^T$.

The full-state feedback control input of the SDRE method including the solution of the state-dependent ARE is obtained as follows,

$$u = -R(x)^{-1}B(x)^T X(x)x \quad (2.23)$$

Substituting Eq. (2.23) into Eq. (2.20), the closed-loop system controlled by the SDRE method can be expressed as

$$\begin{aligned}\dot{x} &= F(x)x - B(x)R(x)^{-1}B(x)^T X(x)x \\ &= (F(x) - B(x)R(x)^{-1}B(x)^T X(x))x \\ &= A_c(x)x \end{aligned} \quad (2.24)$$

where $A_c(x) \in \mathbb{R}^{n\times n}$ is the closed-loop system matrix.

Remark 2.2: Because it is very difficult to obtain the analytic solution of the state-dependent ARE, Eq. (2.22), it is usually solved at each step using a numerical algorithm, which is referred as the online computation of the SDRE method. Therefore, the closed-loop system controlled by the SDRE method, which is presented in Eq. (2.24), cannot be represented analytically, and it is very hard to perform deep theoretical investigations for the SDRE method.

Chapter 3

Analysis of Missile Longitudinal Dynamics

3.1 Problem Statement

In this chapter, the missile longitudinal dynamics is analyzed using the equation derived in the previous chapter. The primary objectives of the analysis are twofold; the first is to provide rigorous analyses of the characteristics of the tail-fin controlled missile including the coordinate transformation to the normal form equations and non-minimum phase behavior. The second objective is to further analyze the existing results of the linearization-oriented modeling-based AIOL, which is frequently used method to deal with the non-minimum phase behavior of the tail-fin controlled missile. The analysis starts from the missile longitudinal dynamics, Eq. (2.16), with following second-order actuator dynamics of the pitch fin deflection.

$$\ddot{\delta_p} + 2\zeta\omega_n\dot{\delta_p} + \omega_n^2\delta_p = \omega_n^2\delta_{p_c} \tag{3.1}$$

where ζ and ω_n are the damping ratio and the natural frequency of the actuator, respectively, and δ_{p_c} is the command of the pitch fin deflection. Using Eqs. (2.16) and (3.1), the missile longitudinal dynamics including the second-order actuator

dynamics can be represented as the following input-affine form.

$$\begin{aligned} \dot{x} &= f(x) + g(x)u \\ y &= h(x) \end{aligned} \tag{3.2}$$

where $x = [x_1\ x_2\ x_3\ x_4]^T = [\alpha\ q\ \delta_p\ \dot{\delta}_p]^T$, $y = a_z$, $u = \delta_{p_c}$, and

$$f(x) = \begin{bmatrix} f_1(x) \\ f_2(x) \\ f_3(x) \\ f_4(x) \end{bmatrix} = \begin{bmatrix} \frac{QS}{mV}\left(C_{Z_0}(\mathbf{M},x) + C_{Z_{\delta_p}}(\mathbf{M},x)x_3\right) + x_2 \\ \frac{QSD}{I_{yy}}\left(C_{m_0}(\mathbf{M},x) + C_{m_{\delta_p}}(\mathbf{M},x)x_3 + \frac{D}{2V}C_{m_q}(\mathbf{M},x)x_2\right) \\ x_4 \\ -\omega_n^2 x_3 - 2\zeta\omega_n x_4 \end{bmatrix}$$

$$g(x) = \begin{bmatrix} 0 \\ 0 \\ 0 \\ g_1(x) \end{bmatrix} = \begin{bmatrix} 0 \\ 0 \\ 0 \\ \omega_n^2 \end{bmatrix}, \quad h(x) = \frac{QS}{m}\left(C_{Z_0}(\mathbf{M},x) + C_{Z_{\delta_p}}(\mathbf{M},x)x_3\right)$$

with $C_{Z_0}(\mathbf{M},x) = C_{Z_\alpha}(\mathbf{M},x)x_1$ and $C_{m_0}(\mathbf{M},x) = C_{m_\alpha}(\mathbf{M},x)x_1$. Note that $C_{Z_0}(\mathbf{M},0) = C_{m_0}(\mathbf{M},0) = 0$. The analysis is performed on a following region of interest which is set to consider the normal operational range of the missile.

$$\Omega = \left\{ x \in \mathbb{R}^4 \mid |x_i| \le c_{x_i},\ i = 1, \cdots, 4 \right\} \tag{3.3}$$

where c_{x_i}, $i = 1, \cdots, 4$, is a positive constant. Within the region of interest, the following assumptions are applied.

Assumption 3.1: The total velocity is fixed.

Assumption 3.2: The center of pressure for the missile's tail-fin is located further from the missile's nose than the center of pressure for the missile body, i.e., $x_{\text{cp}} < x_{\text{cf}}$ in Fig. 2.1.

Assumption 3.3: The aerodynamic coefficients $C_{Z_{\delta_p}}(\mathbf{M}, \alpha)$ and $C_{m_{\delta_p}}(\mathbf{M}, \alpha)$ are non-zero and the partial derivative of $C_{Z_0}(\mathbf{M}, \alpha)$ with respect to the angle of attack is negative for any fixed $\mathbf{M} > 0$.

Assumption 3.4: All aerodynamic coefficients are $\mathcal{C}^k$, $k \geq 2$, functions of the angle of attack for any fixed $\mathbf{M} > 0$.

Remark 3.1: The origin of the unforced case in Eq. (3.2), i.e., $\dot{x} = f(x)$, is an equilibrium point. In addition, all aerodynamic coefficients of the missile longitudinal dynamics only depend on x_1 under **Assumption 3.1**.

3.2 Analysis Results of Missile Longitudinal Dynamics

This section includes the main analysis of the longitudinal dynamics for the characteristics of the tail-fin controlled missile and the behavior of the actual system with the AIOL-based controller. All analyses are based on the noninear control theory [30, 60].

3.2.1 Characteristics of the Tail-Fin Controlled Missile

Theorem 3.1: For the missile longitudinal dynamics with the acceleration output presented in Eq. (3.2), there exists a valid coordinate transformation to the normal form equations on Ω.

Proof of Theorem 3.1: Using Lie derivatives, the time derivative of the system output can be written as follows,

$$\dot{y} = \frac{dh}{dt} = \mathcal{L}_f h(x) + \mathcal{L}_g h(x) u \tag{3.4}$$

where $\mathcal{L}_f h(x)$ and $\mathcal{L}_g h(x)$ can be calculated based on Eq. (3.2) as

$$\begin{aligned} \mathcal{L}_f h(x) &= \frac{\partial h}{\partial x_1} f_1(x) + \frac{\partial h}{\partial x_3} f_3(x) \\ \mathcal{L}_g h(x) &= 0 \end{aligned} \tag{3.5}$$

Taking the time derivative of Eq. (3.4) yields

$$\ddot{y} = \mathcal{L}_f^2 h(x) + \mathcal{L}_g \mathcal{L}_f h(x) u \tag{3.6}$$

where $\mathcal{L}_g \mathcal{L}_f h(x)$ can be obtained as

$$\mathcal{L}_g \mathcal{L}_f h(x) = \frac{QS}{m} \omega_n^2 C_{Z_{\delta_p}}(x_1) \tag{3.7}$$

Since $\mathcal{L}_g\mathcal{L}_f h(x)$ is non-zero under **Assumption 3.3**, the relative degree of the missile longitudinal dynamics is well-defined as 2 on Ω. Now, let us consider a following nonlinear mapping.

$$\Phi(x) = \begin{bmatrix} h(x) & \mathcal{L}_f h(x) & x_1 & x_2 \end{bmatrix}^T = \begin{bmatrix} \xi_1 & \xi_2 & \eta_1 & \eta_2 \end{bmatrix}^T \tag{3.8}$$

where $\|\Phi(0)\| = 0$, and the Jacobian matrix of $\Phi(x)$ can be obtained as

$$\frac{\partial \Phi}{\partial x} = \begin{bmatrix} \frac{\partial h}{\partial x_1} & 0 & \frac{\partial h}{\partial x_3} & 0 \\ \frac{\partial \mathcal{L}_f h}{\partial x_1} & \frac{\partial \mathcal{L}_f h}{\partial x_2} & \frac{\partial \mathcal{L}_f h}{\partial x_3} & \frac{\partial \mathcal{L}_f h}{\partial x_4} \\ 1 & 0 & 0 & 0 \\ 0 & 1 & 0 & 0 \end{bmatrix} \tag{3.9}$$

Then, the determinant of Eq. (3.9) can be calculated using Eqs. (3.2) and (3.5) as

$$\mathrm{Det}\left[\frac{\partial \Phi}{\partial x}\right] = \frac{\partial h}{\partial x_3}\frac{\partial \mathcal{L}_f h}{\partial x_4} = \left(\frac{QS}{m} C_{Z_{\delta_p}}(x_1)\right)^2 \tag{3.10}$$

Note from Eq. (3.10) that the Jacobian matrix of $\Phi(x)$ is nonsingular under **Assumption 3.3**. The inverse transformation of $\Phi(x)$ is given by

$$\begin{aligned} x_1 &= \eta_1 \\ x_2 &= \eta_2 \\ x_3 &= \frac{1}{C_{Z_{\delta_p}}(\eta_1)}\left(\frac{m}{QS}\xi_1 - C_{Z_0}(\eta_1)\right) \\ x_4 &= \frac{1}{C_{Z_{\delta_p}}(\eta_1)}\left[\frac{m}{QS}\xi_2 - \left(\frac{1}{V}\xi_1 + \eta_2\right)\left\{\frac{\partial C_{Z_0}}{\partial \eta_1}\right.\right. \\ &\qquad \left.\left. + \frac{\partial C_{Z_{\delta_p}}}{\partial \eta_1}\frac{1}{C_{Z_{\delta_p}}(\eta_1)}\left(\frac{m}{QS}\xi_1 - C_{Z_0}(\eta_1)\right)\right\}\right] \end{aligned} \tag{3.11}$$

The nonlinear mapping $\Phi(x)$ can transform the missile longitudinal dynamics presented in Eq. (3.2) into the following equations in the normal form.

$$\begin{aligned}
\dot{\xi}_1 &= \xi_2 \\
\dot{\xi}_2 &= a(\xi,\eta) + b(\xi,\eta)u \\
\dot{\eta} &= q(\xi,\eta) \\
y &= \xi_1
\end{aligned} \tag{3.12}$$

where $\xi = [\xi_1\ \xi_2]^T$ is the external state vector, $\eta = [\eta_1\ \eta_2]^T$ is the internal state vector, and

$$\begin{aligned}
a(\xi,\eta) = \frac{QS}{m}\Bigg[&\Bigg\{ \left(\frac{\partial^2 C_{Z_0}}{\partial \eta_1^2} + \frac{\partial^2 C_{Z_{\delta_p}}}{\partial \eta_1^2} x_3 \right) \bar{f}_1(\xi,\eta) + \frac{QS}{mV} \left(\frac{\partial C_{Z_0}}{\partial \eta_1} + \frac{\partial C_{Z_{\delta_p}}}{\partial \eta_1} x_3 \right)^2 \\
&+ 2 \frac{\partial C_{Z_{\delta_p}}}{\partial \eta_1} \bar{f}_3(\xi,\eta) \Bigg\} \bar{f}_1(\xi,\eta) + C_{Z_{\delta_p}}(\eta_1) \bar{f}_4(\xi,\eta) \\
&+ \left(\frac{\partial C_{Z_0}}{\partial \eta_1} + \frac{\partial C_{Z_{\delta_p}}}{\partial \eta_1} x_3 \right) \left(\bar{f}_2(\xi,\eta) + \frac{QS}{mV} C_{Z_{\delta_p}}(\eta_1) \bar{f}_3(\xi,\eta) \right) \Bigg] \\
b(\xi,\eta) = &\frac{QS}{m} \omega_n^2 C_{Z_{\delta_p}}(\eta_1) \\
q(\xi,\eta) = &\begin{bmatrix} \bar{f}_1(\xi,\eta) & \bar{f}_2(\xi,\eta) \end{bmatrix}^T \\
\bar{f}_1(\xi,\eta) = &\frac{1}{V}\xi_1 + \eta_2 \\
\bar{f}_2(\xi,\eta) = &\frac{QSD}{I_{yy}} \left(C_{m_0}(\eta_1) + C_{m_{\delta_p}}(\eta_1) x_3 + \frac{D}{2V} C_{m_q}(\eta_1) \eta_2 \right) \\
\bar{f}_3(\xi,\eta) = &- \frac{1}{C_{Z_{\delta_p}}(\eta_1)} \left(\frac{\partial C_{Z_0}}{\partial \eta_1} + \frac{\partial C_{Z_{\delta_p}}}{\partial \eta_1} x_3 \right) \bar{f}_1(\xi,\eta) + \frac{m}{QSC_{Z_{\delta_p}}(\eta_1)} \xi_2 \\
\bar{f}_4(\xi,\eta) = &- \omega_n^2 x_3 - 2\zeta\omega_n \bar{f}_3(\xi,\eta)
\end{aligned}$$

Note that x_3 in Eq. (3.12) can be expressed as the function of the transformed variables ξ_1 and η_1 using Eq. (3.11), and $a(\xi,\eta)$, $b(\xi,\eta)$, and $q(\xi,\eta)$ are well-defined under **Assumptions 3.3** and **3.4**. Therefore, the nonlinear equations in the normal form presented in Eq. (3.12) are valid on Ω. □

Corollary 3.1: The missile longitudinal dynamics with the acceleration output presented in Eq. (3.2) is non-minimum phase on Ω.

Proof of Corollary 3.1: The zero dynamics of the nonlinear equations in the normal form presented in Eq. (3.12) can be obtained by substituting $\xi_1 = \xi_2 = 0$ into $q(\xi, \eta)$ as follows,

$$\begin{aligned} \dot{\eta}_1 &= \eta_2 \\ \dot{\eta}_2 &= \frac{QSD}{I_{yy}} \left(C_{m_0}(\eta_1) - \frac{C_{Z_0}(\eta_1) C_{m_{\delta_p}}(\eta_1)}{C_{Z_{\delta_p}}(\eta_1)} + \frac{D}{2V} C_{m_q}(\eta_1) \eta_2 \right) \end{aligned} \tag{3.13}$$

Now, let us find the equilibrium points of the zero dynamics on Ω. Substituting $\dot{\eta}_1 = \dot{\eta}_2 = 0$ into Eq. (3.13) yields $\eta_2 = 0$ and

$$C_{m_0}(\eta_1) - \frac{C_{Z_0}(\eta_1) C_{m_{\delta_p}}(\eta_1)}{C_{Z_{\delta_p}}(\eta_1)} = 0 \tag{3.14}$$

Note that the following relationship between the force and moment aerodynamic coefficients is considered based on the missile geometry in the longitudinal motion [38].

$$\begin{aligned} C_{m_0}(\eta_1) &= C_{Z_0}(\eta_1) \frac{x_{\text{cp}} - x_{\text{cm}}}{D} \\ C_{m_{\delta_p}}(\eta_1) &= C_{Z_{\delta_p}}(\eta_1) \frac{x_{\text{cf}} - x_{\text{cm}}}{D} \end{aligned} \tag{3.15}$$

Substituting Eq. (3.15) into Eq. (3.14) yields

$$(x_{\text{cp}} - x_{\text{cm}}) C_{Z_0}(\eta_1) C_{Z_{\delta_p}}(\eta_1) = (x_{\text{cf}} - x_{\text{cm}}) C_{Z_0}(\eta_1) C_{Z_{\delta_p}}(\eta_1) \tag{3.16}$$

Equation (3.16) implies that $x_{\text{cp}} = x_{\text{cf}}$ or $\eta_1 = 0$ under **Assumption 3.3**. Because the former contradicts **Assumption 3.2**, the origin of the zero dynamics is the only equilibrium point on Ω. To analyze the behavior of the zero dynamics near the origin, substituting Eq. (3.15) into Eq. (3.13) simplifies the

η_2-dynamics as follows,

$$\dot{\eta}_2 = \frac{QSD}{I_{yy}} \left\{ C_{Z_0}(\eta_1) \left(\frac{x_{\rm cp} - x_{\rm cf}}{D} \right) + \frac{D}{2V} C_{m_q}(\eta_1)\eta_2 \right\} \tag{3.17}$$

Using Eqs. (3.13) and (3.17), the Jacobian matrix for the zero dynamics near the origin can be obtained as

$$\left. \frac{\partial q(0,\eta)}{\partial \eta} \right|_{(\eta_1,\eta_2)=(0,0)} = \begin{bmatrix} 0 & 1 \\ \frac{QSD}{I_{yy}} \left. \frac{\partial C_{Z_0}}{\partial \eta_1} \right|_{\eta_1=0} \left(\frac{x_{\rm cp}-x_{\rm cf}}{D} \right) & \frac{QSD^2}{2I_{yy}V} C_{m_q}(0) \end{bmatrix} \tag{3.18}$$

The characteristic polynomial of the Jacobian matrix can be obtained as follows,

$$\lambda^2 - \frac{QSD^2}{2I_{yy}V} C_{m_q}(0)\lambda - \frac{QSD}{I_{yy}} \left. \frac{\partial C_{Z_0}}{\partial \eta_1} \right|_{\eta_1=0} \left(\frac{x_{\rm cp} - x_{\rm cf}}{D} \right) = 0 \tag{3.19}$$

where λ denotes the eigenvalue of the Jacobian matrix. The characteristic polynomial has positive and negative roots, respectively, because the last term on the left side of Eq. (3.19) is negative under **Assumptions 3.2** and **3.3**, which implies that the origin of the zero dynamics is an unstable saddle point. Therefore, the zero dynamics cannot have any asymptotically stable equilibrium points on Ω, and finally it can be concluded that the missile longitudinal dynamics with the acceleration output is non-minimum phase on Ω. □

Theorem 3.2: The force induced by the tail-fin deflection, i.e., $C_{Z_{\delta_p}}(x_1)x_3$ in Eq. (3.2), causes non-minimum phase behavior in the missile longitudinal dynamics on Ω.

Proof of Theorem 3.2: The longitudinal dynamics presented in Eq. (3.2) with $C_{Z_{\delta_p}}(x_1) = 0$ is defined as an approximate model. For this model, Lie

derivatives in **Theorem 3.1** are rewritten as $\mathcal{L}_{\tilde{g}}\tilde{h}(x) = \mathcal{L}_{\tilde{g}}\mathcal{L}_{\tilde{f}}\tilde{h}(x) = 0$ and

$$\begin{aligned} \mathcal{L}_{\tilde{f}}\tilde{h}(x) &= \frac{\partial \tilde{h}}{\partial x_1}\tilde{f}_1(x) \\ \mathcal{L}^2_{\tilde{f}}\tilde{h}(x) &= \frac{\partial \mathcal{L}_{\tilde{f}}\tilde{h}}{\partial x_1}\tilde{f}_1(x) + \frac{\partial \mathcal{L}_{\tilde{f}}\tilde{h}}{\partial x_2}\tilde{f}_2(x) \end{aligned} \tag{3.20}$$

where the tilde denotes a function of the approximate model. The time derivative of Eq. (3.6) for the approximate model can be obtained as follows,

$$y^{(3)} = \mathcal{L}^3_{\tilde{f}}\tilde{h}(x) + \mathcal{L}_{\tilde{g}}\mathcal{L}^2_{\tilde{f}}\tilde{h}(x)u \tag{3.21}$$

where the superscripted (k), $k \geq 3$, denotes the k-th time derivative, and the Lie derivatives can be presented as

$$\begin{aligned} \mathcal{L}^3_{\tilde{f}}\tilde{h}(x) &= \frac{\partial \mathcal{L}^2_{\tilde{f}}\tilde{h}}{\partial x_1}\tilde{f}_1(x) + \frac{\partial \mathcal{L}^2_{\tilde{f}}\tilde{h}}{\partial x_2}\tilde{f}_2(x) + \frac{\partial \mathcal{L}^2_{\tilde{f}}\tilde{h}}{\partial x_3}\tilde{f}_3(x) \\ \mathcal{L}_{\tilde{g}}\mathcal{L}^2_{\tilde{f}}\tilde{h}(x) &= 0 \end{aligned} \tag{3.22}$$

Taking the time derivative of Eq. (3.21) yields

$$y^{(4)} = \mathcal{L}^4_{\tilde{f}}\tilde{h}(x) + \mathcal{L}_{\tilde{g}}\mathcal{L}^3_{\tilde{f}}\tilde{h}(x)u \tag{3.23}$$

where $\mathcal{L}_{\tilde{g}}\mathcal{L}^3_{\tilde{f}}\tilde{h}(x)$ can be calculated as follows,

$$\mathcal{L}_{\tilde{g}}\mathcal{L}^3_{\tilde{f}}\tilde{h}(x) = \frac{\partial \mathcal{L}^3_{\tilde{f}}\tilde{h}}{\partial x_4}\tilde{g}_1(x) = \frac{(QS)^2\, D}{mI_{yy}}\frac{\partial C_{Z_0}}{\partial x_1}C_{m_{\delta_p}}(x_1)\omega_n^2 \tag{3.24}$$

Note that Eq. (3.24) is non-zero under **Assumption 3.3**, which implies that the relative degree of the approximate model is well-defined as 4 on Ω. Let us consider the following mapping for the approximate model.

$$\tilde{\Phi}(x) = \begin{bmatrix} \tilde{h}(x) & \mathcal{L}_{\tilde{f}}\tilde{h}(x) & \mathcal{L}^2_{\tilde{f}}\tilde{h}(x) & \mathcal{L}^3_{\tilde{f}}\tilde{h}(x) \end{bmatrix}^T \tag{3.25}$$

The Jacobian matrix of Eq. (3.25) can be written as

$$\frac{d\tilde{\Phi}}{dx} = \begin{bmatrix} \frac{\partial \tilde{h}}{\partial x_1} & 0 & 0 & 0 \\ \frac{\partial \mathcal{L}_{\tilde{f}}\tilde{h}}{\partial x_1} & \frac{\partial \mathcal{L}_{\tilde{f}}\tilde{h}}{\partial x_2} & 0 & 0 \\ \frac{\partial \mathcal{L}^2_{\tilde{f}}\tilde{h}}{\partial x_1} & \frac{\partial \mathcal{L}^2_{\tilde{f}}\tilde{h}}{\partial x_2} & \frac{\partial \mathcal{L}^2_{\tilde{f}}\tilde{h}}{\partial x_3} & 0 \\ \frac{\partial \mathcal{L}^3_{\tilde{f}}\tilde{h}}{\partial x_1} & \frac{\partial \mathcal{L}^3_{\tilde{f}}\tilde{h}}{\partial x_2} & \frac{\partial \mathcal{L}^3_{\tilde{f}}\tilde{h}}{\partial x_3} & \frac{\partial \mathcal{L}^3_{\tilde{f}}\tilde{h}}{\partial x_4} \end{bmatrix} \tag{3.26}$$

Using Eqs. (3.22) and (3.24), the determinant of the Jacobian matrix can be calculated as follows,

$$\begin{aligned} \mathrm{Det}\left[\frac{d\tilde{\Phi}}{dx}\right] &= \frac{\partial \tilde{h}}{\partial x_1}\frac{\partial \mathcal{L}_{\tilde{f}}\tilde{h}}{\partial x_2}\frac{\partial \mathcal{L}^2_{\tilde{f}}\tilde{h}}{\partial x_3}\frac{\partial \mathcal{L}^3_{\tilde{f}}\tilde{h}}{\partial x_4} \\ &= \left(\frac{QS}{m}\frac{\partial C_{Z_0}}{\partial x_1}\right)^4 \left(\frac{QSD}{I_{yy}} C_{m_{\delta_p}}(x_1)\right)^2 \end{aligned} \tag{3.27}$$

Note from Eq. (3.27) that the Jacobian matrix of $\tilde{\Phi}(x)$ is nonsingular under **Assumption 3.3**. Using the mapping $\tilde{\Phi}(x)$, the approximate model is transformed into the following equations in the normal form on Ω.

$$\begin{aligned} \dot{\tilde{\xi}}_1 &= \tilde{\xi}_2 \\ \dot{\tilde{\xi}}_2 &= \tilde{\xi}_3 \\ \dot{\tilde{\xi}}_3 &= \tilde{\xi}_4 \\ \dot{\tilde{\xi}}_4 &= \mathcal{L}^4_{\tilde{f}}\tilde{h}(x) + \mathcal{L}_{\tilde{g}}\mathcal{L}^3_{\tilde{f}}\tilde{h}(x)u \\ y &= \tilde{\xi}_1 \end{aligned} \tag{3.28}$$

The nonlinear equations in the normal form for the approximate model are valid and minimum phase on Ω, because there are no (unstable) internal dynamics. It means that the force induced by the tail-fin deflection causes the non-minimum phase behavior in the missile longitudinal dynamics on Ω. □

3.2.2 System Behavior with Approximate Model-Based Controller

In this section, the following approximate model-based controller is considered, which deals with the unstable internal dynamics of the tail-fin controlled missile.

$$u^* = \frac{1}{\mathcal{L}_{\tilde{g}}\mathcal{L}_{\tilde{f}}^3\tilde{h}(x)}\left(v^* - \mathcal{L}_{\tilde{f}}^4\tilde{h}(x)\right) \tag{3.29}$$

where v^* is the control input designed for linear systems. In this study, the following linear controller is considered.

$$v^* = a_{z_c}^{(4)} - \sum_{i=1}^{4} k_i\left(\tilde{\xi}_i - a_{z_c}^{(i-1)}\right) \tag{3.30}$$

where a_{z_c} is the acceleration command, and k_i is the control gain which is set to be positive constant. The reminder of this section shows the analysis for the behavior of the actual system controlled by the approximate model-based control input.

Theorem 3.3: Considering $C_{Z_{\delta_p}}(x_1)$ to be the external input, the actual missile system with the approximate model-based controller is finite-gain $\mathcal{L}_p$ stable for each $p \in [1, \infty]$ on Ω if $C_{Z_0}(x_1)$ is $\mathcal{C}^k$, $k \geq 4$, function of x_1.

Proof of Theorem 3.3: The approximate model-based mapping $\tilde{\Phi}(x)$ transforms the actual missile system into the following nonlinear system.

$$\begin{aligned}
\dot{\tilde{\xi}}_1 &= \mathcal{L}_f\tilde{h}(x) + \mathcal{L}_g\tilde{h}(x)u \\
\dot{\tilde{\xi}}_2 &= \mathcal{L}_f\mathcal{L}_{\tilde{f}}\tilde{h}(x) + \mathcal{L}_g\mathcal{L}_{\tilde{f}}\tilde{h}(x)u \\
\dot{\tilde{\xi}}_3 &= \mathcal{L}_f\mathcal{L}_{\tilde{f}}^2\tilde{h}(x) + \mathcal{L}_g\mathcal{L}_{\tilde{f}}^2\tilde{h}(x)u \\
\dot{\tilde{\xi}}_4 &= \mathcal{L}_f\mathcal{L}_{\tilde{f}}^3\tilde{h}(x) + \mathcal{L}_g\mathcal{L}_{\tilde{f}}^3\tilde{h}(x)u
\end{aligned} \tag{3.31}$$

Considering $\tilde{g}(x)$ is equal to $g(x)$, $\mathcal{L}_g\tilde{h}(x)$, $\mathcal{L}_g\mathcal{L}_{\tilde{f}}\tilde{h}(x)$, and $\mathcal{L}_g\mathcal{L}_{\tilde{f}}^2\tilde{h}(x)$ are zero, and $\mathcal{L}_f\tilde{h}(x)$, $\mathcal{L}_f\mathcal{L}_{\tilde{f}}\tilde{h}(x)$, $\mathcal{L}_f\mathcal{L}_{\tilde{f}}^2\tilde{h}(x)$, and $\mathcal{L}_f\mathcal{L}_{\tilde{f}}^3\tilde{h}(x)$ can be rewritten on Ω as follows,

$$\begin{aligned}
\mathcal{L}_f\tilde{h}(x) &= \mathcal{L}_{\tilde{f}}\tilde{h}(x) + \frac{QS}{mV}\frac{\partial\tilde{h}}{\partial x_1}C_{Z_{\delta_p}}(x_1)x_3 \\
\mathcal{L}_f\mathcal{L}_{\tilde{f}}\tilde{h}(x) &= \mathcal{L}_{\tilde{f}}^2\tilde{h}(x) + \frac{QS}{mV}\frac{\partial\mathcal{L}_{\tilde{f}}\tilde{h}}{\partial x_1}C_{Z_{\delta_p}}(x_1)x_3 \\
\mathcal{L}_f\mathcal{L}_{\tilde{f}}^2\tilde{h}(x) &= \mathcal{L}_{\tilde{f}}^3\tilde{h}(x) + \frac{QS}{mV}\frac{\partial\mathcal{L}_{\tilde{f}}^2\tilde{h}}{\partial x_1}C_{Z_{\delta_p}}(x_1)x_3 \\
\mathcal{L}_f\mathcal{L}_{\tilde{f}}^3\tilde{h}(x) &= \mathcal{L}_{\tilde{f}}^4\tilde{h}(x) + \frac{QS}{mV}\frac{\partial\mathcal{L}_{\tilde{f}}^3\tilde{h}}{\partial x_1}C_{Z_{\delta_p}}(x_1)x_3
\end{aligned} \tag{3.32}$$

Applying Eq. (3.32) to Eq. (3.31) yields

$$\begin{aligned}
\dot{\tilde{\xi}}_1 &= \tilde{\xi}_2 + \frac{QS}{mV}\frac{\partial\tilde{h}}{\partial x_1}C_{Z_{\delta_p}}(x_1)x_3 \\
\dot{\tilde{\xi}}_2 &= \tilde{\xi}_3 + \frac{QS}{mV}\frac{\partial\mathcal{L}_{\tilde{f}}\tilde{h}}{\partial x_1}C_{Z_{\delta_p}}(x_1)x_3 \\
\dot{\tilde{\xi}}_3 &= \tilde{\xi}_4 + \frac{QS}{mV}\frac{\partial\mathcal{L}_{\tilde{f}}^2\tilde{h}}{\partial x_1}C_{Z_{\delta_p}}(x_1)x_3 \\
\dot{\tilde{\xi}}_4 &= \mathcal{L}_{\tilde{f}}^4\tilde{h}(x) + \frac{QS}{mV}\frac{\partial\mathcal{L}_{\tilde{f}}^3\tilde{h}}{\partial x_1}C_{Z_{\delta_p}}(x_1)x_3 + \mathcal{L}_{\tilde{g}}\mathcal{L}_{\tilde{f}}^3\tilde{h}(x)u
\end{aligned} \tag{3.33}$$

Let us define the acceleration error of the actual missile system and the error vector of the approximate model as

$$\begin{aligned}
e &= a_z - a_{z_c} \\
\tilde{e} &= \begin{bmatrix} \tilde{e}_1 & \tilde{e}_2 & \tilde{e}_3 & \tilde{e}_4 \end{bmatrix}^T \\
&= \begin{bmatrix} \tilde{\xi}_1 & \tilde{\xi}_2 & \tilde{\xi}_3 & \tilde{\xi}_4 \end{bmatrix}^T - \begin{bmatrix} a_{z_c} & \dot{a}_{z_c} & \ddot{a}_{z_c} & a_{z_c}^{(3)} \end{bmatrix}^T
\end{aligned} \tag{3.34}$$

Substituting the AIOL-based controller presented in Eq. (3.29) into Eq. (3.33),

the error dynamics can be obtained as

$$\dot{\tilde{e}} = \tilde{A}\tilde{e} + \frac{QS}{mV}\psi(x)x_3 C_{Z_{\delta_p}}(x_1) = f_e(\tilde{e}, C_{Z_{\delta_p}}(x_1)) \tag{3.35}$$

where

$$\tilde{A} = \begin{bmatrix} 0 & 1 & 0 & 0 \\ 0 & 0 & 1 & 0 \\ 0 & 0 & 0 & 1 \\ -k_1 & -k_2 & -k_3 & -k_4 \end{bmatrix}, \quad \psi(x) = \begin{bmatrix} \psi_1(x) \\ \psi_2(x) \\ \psi_3(x) \\ \psi_4(x) \end{bmatrix} = \begin{bmatrix} \frac{\partial \tilde{h}}{\partial x_1} \\ \frac{\partial \mathcal{L}_{\tilde{f}}\tilde{h}}{\partial x_1} \\ \frac{\partial \mathcal{L}^2_{\tilde{f}}\tilde{h}}{\partial x_1} \\ \frac{\partial \mathcal{L}^3_{\tilde{f}}\tilde{h}}{\partial x_1} \end{bmatrix}$$

Note from Eq. (3.35) that the origin of the error dynamics of the approximate model is exponentially stable for the unforced case regarding $C_{Z_{\delta_p}}(x_1)$ as the external input, i.e., $\dot{\tilde{e}} = \tilde{A}\tilde{e}$. The components of $\psi(x)$ can be calculated using Eqs. (3.20) and (3.22) as follows,

$$\begin{aligned}
\frac{\partial \tilde{h}}{\partial x_1} &= \frac{QS}{m}\frac{\partial C_{Z_0}}{\partial x_1} \\
\frac{\partial \mathcal{L}_{\tilde{f}}\tilde{h}}{\partial x_1} &= \frac{QS}{m}\left\{\frac{\partial^2 C_{Z_0}}{\partial x_1^2}\tilde{f}_1(x) + \frac{QS}{mV}\left(\frac{\partial C_{Z_0}}{\partial x_1}\right)^2\right\} \\
\frac{\partial \mathcal{L}^2_{\tilde{f}}\tilde{h}}{\partial x_1} &= \frac{QS}{m}\left\{\frac{\partial^2 C_{Z_0}}{\partial x_1^2}\tilde{f}_2(x) + \frac{\partial C_{Z_0}}{\partial x_1}\left(\frac{1}{V}\frac{\partial \mathcal{L}_{\tilde{f}}\tilde{h}}{\partial x_1} + \frac{\partial \tilde{f}_2}{\partial x_1}\right)\right\} + \frac{\partial^2 \mathcal{L}_{\tilde{f}}\tilde{h}}{\partial x_1^2}\tilde{f}_1(x) \\
\frac{\partial \mathcal{L}^3_{\tilde{f}}\tilde{h}}{\partial x_1} &= \frac{QS}{m}\left[\frac{\partial^3 C_{Z_0}}{\partial x_1^3}\tilde{f}_1(x)\tilde{f}_2(x) + \frac{\partial^2 C_{Z_0}}{\partial x_1^2}\left(\frac{1}{V}\frac{\partial \mathcal{L}_{\tilde{f}}\tilde{h}}{\partial x_1} + 3\frac{\partial \tilde{f}_2}{\partial x_1}\right)\tilde{f}_1(x)\right. \\
&\quad \left. + \frac{\partial C_{Z_0}}{\partial x_1}\left\{\frac{\partial \tilde{f}_2}{\partial x_1}\frac{QSD^2}{2I_{yy}V}C_{m_q}(x_1) + \left(\frac{2}{V}\frac{\partial^2 \mathcal{L}_{\tilde{f}}\tilde{h}}{\partial x_1^2} + \frac{\partial^2 \tilde{f}_2}{\partial x_1^2}\right)\tilde{f}_1(x)\right\}\right] \\
&\quad + \frac{\partial \tilde{f}_2}{\partial x_1}\frac{\partial \mathcal{L}_{\tilde{f}}\tilde{h}}{\partial x_1} + \frac{QS}{mV}\frac{\partial C_{Z_0}}{\partial x_1}\frac{\partial \mathcal{L}^2_{\tilde{f}}\tilde{h}}{\partial x_1} + \frac{\partial^3 \mathcal{L}_{\tilde{f}}\tilde{h}}{\partial x_1^3}\tilde{f}_1(x)^2 + \frac{\partial^2 \mathcal{L}^2_{\tilde{f}}\tilde{h}}{\partial x_1 \partial x_2}\tilde{f}_2(x) \\
&\quad + \frac{(QS)^2 D}{mI_{yy}}\left(\frac{\partial^2 C_{Z_0}}{\partial x_1^2}C_{m_{\delta_p}}(x_1) + \frac{\partial C_{Z_0}}{\partial x_1}\frac{\partial C_{m_{\delta_p}}}{\partial x_1}\right)\tilde{f}_3(x)
\end{aligned} \tag{3.36}$$

where

$$\frac{\partial \tilde{f}_2}{\partial x_1} = \frac{QSD}{I_{yy}}\left(\frac{\partial C_{m_0}}{\partial x_1} + \frac{\partial C_{m_{\delta_p}}}{\partial x_1}x_3 + \frac{D}{2V}\frac{\partial C_{m_q}}{\partial x_1}x_2\right)$$

$$\frac{\partial^2 \tilde{f}_2}{\partial x_1^2} = \frac{QSD}{I_{yy}}\left(\frac{\partial^2 C_{m_0}}{\partial x_1^2} + \frac{\partial^2 C_{m_{\delta_p}}}{\partial x_1^2}x_3 + \frac{D}{2V}\frac{\partial^2 C_{m_q}}{\partial x_1^2}x_2\right)$$

$$\frac{\partial^2 \mathcal{L}_{\tilde{f}}\tilde{h}}{\partial x_1^2} = \frac{QS}{m}\left(\frac{\partial^3 C_{Z_0}}{\partial x_1^3}\tilde{f}_1(x) + 3\frac{QS}{mV}\frac{\partial C_{Z_0}}{\partial x_1}\frac{\partial^2 C_{Z_0}}{\partial x_1^2}\right)$$

$$\frac{\partial^2 \mathcal{L}_{\tilde{f}}^2\tilde{h}}{\partial x_1 \partial x_2} = \frac{(QS)^2}{mV}\left\{\frac{D^2}{2I_{yy}}\left(\frac{\partial^2 C_{Z_0}}{\partial x_1^2}C_{m_q}(x_1) + \frac{\partial C_{Z_0}}{\partial x_1}\frac{\partial C_{m_q}}{\partial x_1}\right) + \frac{1}{m}\frac{\partial C_{Z_0}}{\partial x_1}\frac{\partial^2 C_{Z_0}}{\partial x_1^2}\right\} + \frac{QS}{m}\frac{\partial^3 C_{Z_0}}{\partial x_1^3}\tilde{f}_1(x) + \frac{\partial^2 \mathcal{L}_{\tilde{f}}\tilde{h}}{\partial x_1^2}$$

$$\frac{\partial^3 \mathcal{L}_{\tilde{f}}\tilde{h}}{\partial x_1^3} = \frac{QS}{m}\left[\frac{\partial^4 C_{Z_0}}{\partial x_1^4}\tilde{f}_1(x) + \frac{QS}{mV}\left\{3\left(\frac{\partial^2 C_{Z_0}}{\partial x_1^2}\right)^2 + 4\frac{\partial C_{Z_0}}{\partial x_1}\frac{\partial^3 C_{Z_0}}{\partial x_1^3}\right\}\right]$$

Note that $\psi(x)$ is well-defined and bounded on Ω if $C_{Z_0}(x_1)$ is $\mathcal{C}^k$, $k \geq 4$, function of x_1, because $\tilde{f}_1(x)$, $\tilde{f}_2(x)$, and $\tilde{f}_3(x)$ are bounded on Ω. Consequently, the following inequality can be obtained based on the bounded property of $\psi(x)$.

$$\begin{aligned}\|f_e(\tilde{e}, C_{Z_{\delta_p}}(x_1)) - f_e(\tilde{e}, 0)\| &= \frac{QS}{mV}\|\psi(x)x_3 C_{Z_{\delta_p}}(x_1)\| \\ &\leq \frac{QS}{mV}c_\psi c_{x_3}|C_{Z_{\delta_p}}(x_1)| \end{aligned} \tag{3.37}$$

where c_ψ is a positive constant. The origin of the error dynamics of the approximate model for unforced case is exponentially stable, and therefore there exists a $\mathcal{C}^1$ function $\tilde{V}(\tilde{e})$ that satisfies the following inequalities based on the converse Lyapunov theorem [60].

$$\begin{aligned} c_1\|\tilde{e}\|^2 \leq \tilde{V}(\tilde{e}) &\leq c_2\|\tilde{e}\|^2 \\ \frac{\partial \tilde{V}}{\partial \tilde{e}}f_e(\tilde{e}, 0) &\leq -c_3\|\tilde{e}\|^2 \\ \left\|\frac{\partial \tilde{V}}{\partial \tilde{e}}\right\| &\leq c_4\|\tilde{e}\| \end{aligned} \tag{3.38}$$

where c_i for $i = 1, \cdots, 4$ are positive constants. Applying Eq. (3.38) to the time derivative of $\tilde{V}(\tilde{e})$, the following relation can be obtained.

$$\begin{aligned}\frac{d\tilde{V}}{dt} &= \frac{\partial \tilde{V}}{\partial \tilde{e}} f_e(\tilde{e}, 0) + \frac{\partial \tilde{V}}{\partial \tilde{e}} \left(f_e(\tilde{e}, C_{Z_{\delta_p}}(x_1)) - f_e(\tilde{e}, 0) \right) \\ &\leq -c_3 \|\tilde{e}\|^2 + c_4 \frac{QS}{mV} c_\psi c_{x_3} \|\tilde{e}\| |C_{Z_{\delta_p}}(x_1)| \\ &\leq -\frac{c_3}{c_2} \tilde{V}(\tilde{e}) + c_4 \frac{QS}{mV} c_\psi c_{x_3} \sqrt{\frac{\tilde{V}(\tilde{e})}{c_1}} |C_{Z_{\delta_p}}(x_1)| \end{aligned} \tag{3.39}$$

Defining $\tilde{W}(t)$ as $\sqrt{\tilde{V}(\tilde{e}(t))}$, the upper Dini derivative of $\tilde{W}(t)$ satisfies the following inequality for all $V(\tilde{e}) \geq 0$ based on Eq. (3.39).

$$D^+ \tilde{W}(t) \leq -\frac{c_3}{2c_2} \tilde{W}(t) + \frac{c_4}{2\sqrt{c_1}} \frac{QS}{mV} c_\psi c_{x_3} |C_{Z_{\delta_p}}(x_1)| \tag{3.40}$$

where D^+ denotes the upper Dini derivative. As a result, the following inequality can be obtained by the comparison lemma.

$$\tilde{W}(t) \leq e^{-\frac{c_3}{2c_2} t} \tilde{W}(0) + \frac{c_4}{2\sqrt{c_1}} \frac{QS}{mV} c_\psi c_{x_3} \int_0^t e^{-\frac{c_3}{2c_2}(t-\tau)} |C_{Z_{\delta_p}}(x_1(\tau))| d\tau \tag{3.41}$$

Considering Eq. (3.41) and $\sqrt{c_1}\|\tilde{e}(t)\| \leq \tilde{W}(t) \leq \sqrt{c_2}\|\tilde{e}(t)\|$ given in Eq. (3.38), the error vector of the approximate model satisfies the following equation.

$$\begin{aligned}\|\tilde{e}(t)\| \leq & \sqrt{\frac{c_2}{c_1}} e^{-\frac{c_3}{2c_2} t} \|\tilde{e}(0)\| \\ & + \frac{c_4}{2c_1} \frac{QS}{mV} c_\psi c_{x_3} \int_0^t e^{-\frac{c_3}{2c_2}(t-\tau)} |C_{Z_{\delta_p}}(x_1(\tau))| d\tau \end{aligned} \tag{3.42}$$

The magnitude of actual acceleration error satisfies the following inequality.

$$\begin{aligned}|e| &= \left| \tilde{h}(x) + \frac{QS}{m} x_3 C_{Z_{\delta_p}}(x_1) - a_{z_c} \right| \\ &= \left| \tilde{e}_1 + \frac{QS}{m} x_3 C_{Z_{\delta_p}}(x_1) \right| \\ &\leq \|\tilde{e}\| + \frac{QS}{m} c_{x_3} |C_{Z_{\delta_p}}(x_1)| \end{aligned} \tag{3.43}$$

Substituting Eq. (3.42) into Eq. (3.43) yields

$$|e(t)| \leq \sqrt{\frac{c_2}{c_1}} e^{-\frac{c_3}{2c_2}t} \|\tilde{e}(0)\| + \frac{QS}{m} c_{x_3} |C_{Z_{\delta_p}}(x_1(t))| + \frac{c_4}{2c_1} \frac{QS}{mV} c_\psi c_{x_3} \int_0^t e^{-\frac{c_3}{2c_2}(t-\tau)} |C_{Z_{\delta_p}}(x_1(\tau))| d\tau \tag{3.44}$$

The p-norm of truncation of the first term on the right side in Eq. (3.44) satisfies the following inequality.

$$\left\| \left[\sqrt{\frac{c_2}{c_1}} e^{-\frac{c_3}{2c_2}t} \|\tilde{e}(0)\| \right]_\tau \right\|_{\mathcal{L}_p} \leq \bar{\rho} \sqrt{\frac{c_2}{c_1}} \|\tilde{e}(0)\| \tag{3.45}$$

where the subsrcipt τ denotes the truncation of the function, and

$$\bar{\rho} = \begin{cases} 1 & \text{if } p = \infty \\ \left(\frac{2c_2}{c_3 p}\right)^p & \text{if } p \in [1, \infty) \end{cases}$$

Likewise, the p-norms of truncation of other terms on the right side in Eq. (3.44) satisfy the following equations.

$$\begin{aligned} &\left\| \left[\frac{QS}{m} c_{x_3} |C_{Z_{\delta_p}}(x_1)| \right]_\tau \right\|_{\mathcal{L}_p} \leq \frac{QS}{m} c_{x_3} \left\| \left[C_{Z_{\delta_p}}(x_1) \right]_\tau \right\|_{\mathcal{L}_p} \\ &\left\| \left[\frac{c_4}{2c_1} \frac{QS}{mV} c_\psi c_{x_3} \int_0^t e^{-\frac{c_3}{2c_2}(t-\tau)} |C_{Z_{\delta_p}}(x_1(\tau))| d\tau \right]_\tau \right\|_{\mathcal{L}_p} \\ &\qquad \leq \frac{c_2 c_4}{c_1 c_3} \frac{QS}{mV} c_\psi c_{x_3} \left\| \left[C_{Z_{\delta_p}}(x_1) \right]_\tau \right\|_{\mathcal{L}_p} \end{aligned} \tag{3.46}$$

Based on Eqs. (3.45), (3.46), and the triangle inequality, the p-norm of truncation of the acceleration error satisfies the following inequality.

$$\|[e]_\tau\|_{\mathcal{L}_p} \leq \frac{QS}{m} c_{x_3} \left(1 + \frac{c_2 c_4 c_\psi}{c_1 c_3 V} \right) \left\| \left[C_{Z_{\delta_p}}(x_1) \right]_\tau \right\|_{\mathcal{L}_p} + \sqrt{\frac{c_2}{c_1}} \bar{\rho} \|\tilde{e}(0)\| \tag{3.47}$$

Equation (3.47) implies that the actual system controlled by the AIOL-based control input is finite-gain $\mathcal{L}_p$ stable on Ω for each $p \in [1, \infty]$ and $C_{Z_{\delta_p}}(x_1)$ included in the extended $\mathcal{L}_p$ space considering $C_{Z_{\delta_p}}(x_1)$ to be the external input. □

Corollary 3.2: The approximate model-based controller presented in Eq. (3.29) perfectly regulates the output of the actual missile system for a sufficiently small $C_{Z_{\delta_p}}(x_1)$.

Proof of Corollary 3.2: For the zero acceleration command, Eq. (3.35) can be rewritten as

$$\dot{\tilde{\xi}} = \tilde{A}\tilde{\xi} + \frac{QS}{mV}\psi(x)x_3 C_{Z_{\delta_p}}(x_1) \tag{3.48}$$

where $\tilde{\xi} = [\tilde{\xi}_1 \ \tilde{\xi}_2 \ \tilde{\xi}_3 \ \tilde{\xi}_4]^T$. Based on Eqs. (3.20), (3.22), (3.25), and (3.26), it can be seen that $\|\tilde{\Phi}(x)\| = 0$ if and only if $\|x\| = 0$ under **Assumption 3.3**. Consequently, since the mapping $\tilde{\Phi}(x)$ is bounded on Ω, there exists a positive constant c_x satisfying the following inequality except for $\|x\| = 0$.

$$\frac{1}{c_x} \leq \frac{\|\tilde{\Phi}(x)\|}{\|x\|} = \frac{\|\tilde{\xi}\|}{\|x\|} \tag{3.49}$$

Using Eq. (3.49) and the bounded properties of $\psi(x)$ and $C_{Z_{\delta_p}}(x_1)$ on Ω, the following can be obtained.

$$\left\| \frac{QS}{mV}\psi(x)x_3 C_{Z_{\delta_p}}(x_1) \right\| \leq \frac{QS}{mV} c_\psi c_{\delta_p} \|x\| \leq \frac{QS}{mV} c_\psi c_{\delta_p} c_x \|\tilde{\xi}\| \tag{3.50}$$

where c_{δ_p} is a positive constant such that $|C_{Z_{\delta_p}}(x_1)| \leq c_{\delta_p}$. Equation (3.48) with $C_{Z_{\delta_p}} = 0$ still holds the inequailities presented in Eq. (3.38) based on the converse Lyapunov theorem. Therefore, the time derivative of $\tilde{V}(\tilde{\xi})$ satisfies the following inequality considering Eqs. (3.38) and (3.50).

$$\begin{aligned} \frac{d\tilde{V}}{dt} &\leq -c_3\|\tilde{\xi}\|^2 + \left\| \frac{\partial \tilde{V}}{\partial \tilde{\xi}} \right\| \left\| \frac{QS}{mV}\psi(x)x_3 C_{Z_{\delta_p}}(x_1) \right\| \\ &\leq -\left(c_3 - c_4 \frac{QS}{mV} c_\psi c_{\delta_p} c_x \right) \|\tilde{\xi}\|^2 \end{aligned} \tag{3.51}$$

Equation (3.51) implies that the origin of Eq. (3.48) is asymptotically stable if the following condition holds.

$$c_3 - c_4 \frac{QS}{mV} c_\psi c_{\delta_p} c_x > 0 \tag{3.52}$$

The magnitude of the acceleration error also satisfies the following inequality.

$$|a_z| = \left| \tilde{\xi}_1 + \frac{QS}{m} C_{Z_{\delta_p}}(x_1) x_3 \right| \leq |\tilde{\xi}_1| + \frac{QS}{m} c_{\delta_p} \|x\| \leq \left(1 + \frac{QS}{m} c_{\delta_p} c_x \right) \|\tilde{\xi}\| \tag{3.53}$$

Note from Eq. (3.53) that the actual acceleration converges to zero as $t \to \infty$ for the small $C_{Z_{\delta_p}}(x_1)$ satisfying the condition presented in Eq. (3.52). □

Remark 3.2: If the approximate model-based controller is designed neglecting the actuator dynamics based on the singular perturbation theory, **Theorem 3.3** and **Corollary 3.2** hold true without the condition that $C_{Z_0}(x_1)$ is $\mathcal{C}^k$, $k \geq 4$, function of x_1. The reason is that all functions required for the proofs associated with the missile system neglecting the actuator dynamics are well-defined and bounded under **Assumption 3.4**.

3.3 Numerical Example

In this section, numerical example is presented to illustrate the analysis for the missile longitudinal dynamics using the hypothetical aerodynamic data and physical parameters of the missile. The physical parameters are summarized in Table. 3.1. The following aerodynamic models at a specified altitude of $6,096$ m and Mach number of 2 are used [45].

$$\begin{aligned} C_Z(\alpha) &= C_{Z_0}(\alpha) + C_{Z_{\delta_p}}\delta_p = a_n\alpha^3 + b_n\alpha + c_n\delta_p \\ C_m(\alpha) &= C_{m_0}(\alpha) + C_{m_{\delta_p}}\delta_p + \frac{D}{2V}C_{m_q}q = a_m\alpha^3 + b_m\alpha + c_m\delta_p + d_mq \end{aligned} \tag{3.54}$$

where the numerical values of the aerodynamic coefficients are summarized in Table 3.2. Note that **Assumptions 3.3** and **3.4** are satisfied for the considered hypothetical aerodynamic models. The constants for the region of interest presented in Eq. (3.3) are set as

$$c_{x_1} = \frac{\pi}{6} \text{ rad}, \quad c_{x_2} = 2\pi \text{ rad/s}, \quad c_{x_3} = \frac{\pi}{6} \text{ rad}, \quad c_{x_4} = 6\pi \text{ rad/s} \tag{3.55}$$

Numerical simulation is performed for the missile longtudinal dynamics controlled by the approximate model-based controller presented in Eq. (3.29) with following control gains.

$$k_1 = 2.5 \times 10^6, \quad k_2 = 2.4 \times 10^5, \quad k_3 = 1.5 \times 10^4, \quad k_4 = 100 \tag{3.56}$$

To demonstrate the effects of $C_{Z_{\delta_p}}(x_1)$ on the actual missile system, $C_{Z_{\delta_p}}(x_1)$ is replaced with $\epsilon C_{Z_{\delta_p}}(x_1)$, for $\epsilon = 0, 1, 2, 3$, in the simulation. Note that the case of $\epsilon = 0$ shows the behavior of the approximate model controlled by the approximate model-based controller. The parameters of the actuator dynamics are set as $\omega_n = 15$ Hz and $\zeta = 0.8$, and all the initial conditions are set to zero.

Table 3.1 Physical parameters of the missile

Symbol	Name	Value
m	Mass	204.023 kg
I_{yy}	Moment of Inertia	247.429 kg $\cdot$ m^2
S	Reference Area	0.041 m^2
D	Reference Length	0.229 m
$\bar{a}$	Speed of Sound	316.032 m/s
ρ	Density of Air	0.653 kg/m^2

Table 3.2 Numerical values of aerodynamic coefficients

Normal Force	Pitch Moment
$a_n = -39.571$	$a_m = -81.189$
$b_n = -12.956$	$b_m = -4.871$
$c_n = -1.948$	$c_m = -11.803$
	$d_m = -1.719$

Figures 3.1 and 3.2 show the simulation results, where the dash line represents the acceleration command signal, the solid line without marker represents the responses for the case of $\epsilon = 0$, and the solid lines with the triangle, square, and circle markers represent the responses for the cases of $\epsilon = 1, 2, 3$, respectively. Figure 3.1 shows the time responses of the acceleration output for the cases of $\epsilon = 0, 1, 2, 3$. For the desired non-zero acceleration command, the larger tracking errors and effects of the undershoot are shown for the larger ϵ values. Furthermore, all responses have zero steady-state errors for the desired zero command. These results are consistent with the analyses of **Theorem 3.3** and **Corollary 3.2**. For the case of $\epsilon = 0$, no undershoot phenomenon appears, which implies that the force induced by the fin deflection, non-zero ϵ case, causes the non-minimum phase behavior shown in **Theorem 3.2**. Figure 3.2 shows the time responses of the state variables including the angle of attack, pitch rate, pitch fin delflection, and its time derivative for the cases of $\epsilon = 0, 1, 2, 3$. These results show that all responses for each ϵ of state variables are nearly identical and within the region of interest, which is set as in Eq. (3.55).

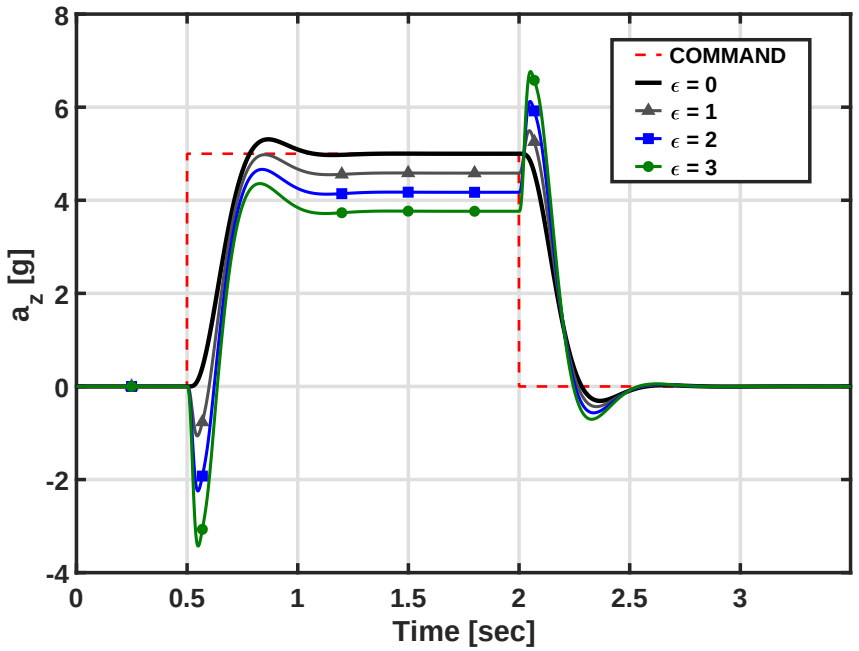

Figure 3.1 Time responses of the pitch acceleration for $\epsilon = 0, 1, 2, 3$

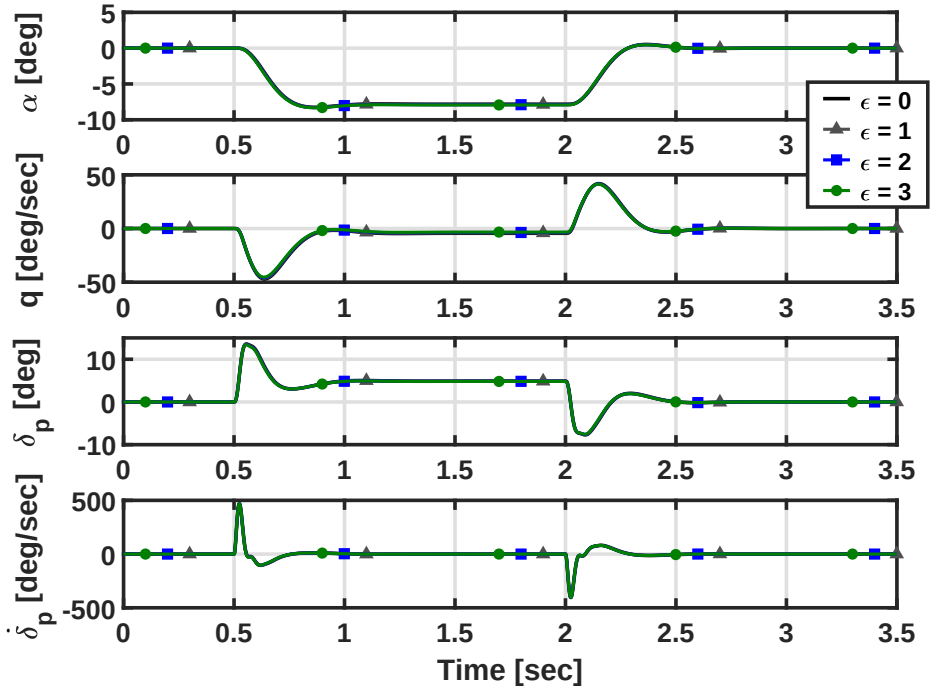

Figure 3.2 Time responses of the state variables for $\epsilon = 0, 1, 2, 3$

Chapter 4

Analysis of State-Dependent Riccati Equation Method for Missile Longitudinal Autopilot

4.1 Problem Statement

In this chapter, the analysis of the SDRE method is performed for the missile longitudinal autopilot. First, the analytic solution of the state-dependent ARE is obtained. Note that the state-dependent ARE is usually solved at each step using the numerical algorithm due to the difficulty of obtaining the analytic solution. The properties of the analytic solution including the nonsingularity and symmetry of matrices are also shown. Second, the missile acceleration autopilot for the longitudinal dynamics is designed based on the SDRE method. The analytic representation of the closed-loop system is obtained using the analytic solution of the state-dependent ARE. Finally, the stability of the missile longitudinal closed-loop system controlled by the SDRE method is analyzed based on the Lyapunov stability theorem using the analytic solution of the SDRE method.

4.2 Analytic Solution of State-Dependent Riccati Equation

This section presents the analytic solution of the following two-dimensional state-dependent ARE.

$$F(x)^T X(x) + X(x)F(x) - X(x)G(x)X(x) + H(x) = 0 \tag{4.1}$$

where $F(x)$, $G(x)$, $H(x)$, and $X(x) \in \mathbb{R}^{2\times 2}$ are the state-dependent matrices. Note that the state-dependent matrices $G(x)$ and $H(x)$ match the matrices $B(x)R(x)^{-1}B(x)^T$ and $Q(x)$ in Eq. (2.22), respectively. To obtain the positive definite stabilizing solution $X(x)$, it is assumed that **Conditions 2.1-2.3** are satisfied for the state-dependent matrices in Eq. (4.1). The components of the state-dependent matrices $F(x)$, $G(x)$, and $H(x)$ are defined as

$$F(x) = \begin{bmatrix} f_1 & f_2 \\ f_3 & f_4 \end{bmatrix}, \quad G(x) = \begin{bmatrix} g_1 & g_2 \\ g_2 & g_3 \end{bmatrix}, \quad H(x) = \begin{bmatrix} h_1 & h_2 \\ h_2 & h_3 \end{bmatrix} \tag{4.2}$$

where the dependence of x is omitted for notational convenience.

Remark 4.1: Equation (4.2) shows that there is no restriction on the components of the state-dependent matrices included in Eq. (4.1) except for **Conditions 2.1-2.3**, which are necessary for the existence of the positive definite stabilizing solution. In contrast, the existing works which obtain the analytic solution of the SDRE method impose restrictions on the components of the state-dependent matrices. For example, f_1, f_3, g_1, and g_2 are zero in Ref. [11], and f_1, g_1, and g_3 are zero in Ref. [12] under **Conditions 2.1-2.3**.

4.2.1 Process of Obtaining Analytic Solution

This section presents the process of obtaining the analytic solution of the state-dependent ARE using the matrix sign function with the following lemma [61].

Lemma 4.1: The solution of the ARE can be obtained as $X = W_{22}W_{12}^{-1}$, where W_{12}, $W_{22} \in \mathbb{R}^{2\times 2}$ are block matrices of the following matrix.

$$W = \frac{1}{2}\left\{\text{sign}[\bar{M}] - I_4\right\} = \begin{bmatrix} W_{11} & W_{12} \\ W_{21} & W_{22} \end{bmatrix} \tag{4.3}$$

where sign$[\cdot]$ denotes a matrix sign function, $\bar{M}$ is the Hamiltonian matrix that corresponds to the ARE, and I_4 is a 4×4 identity matrix.

The proof of **Lemma 4.1** can be found in Ref. [61]. Note that **Lemma 4.1** is generally used to solve the ARE numerically. However, in this study, **Lemma 4.1** is used to obtain the analytic solution of the state-dependent ARE by representing the matrix sign function of the Hamiltonian matrix. Assuming that $\text{Re}[\lambda[\bar{M}]] \neq 0$, the following definition of the matrix sign function via the principal matrix square root is used [62].

$$\text{sign}(\bar{M}) = \bar{M}^{-1}\left(\sqrt{\bar{M}^2}\right) \tag{4.4}$$

where $\lambda[\cdot]$ denotes the eigenvalue of matrix, and Re$[\cdot]$ denotes the real part. The principal square root of $\bar{M}^2$, which is denoted as $\sqrt{\bar{M}^2}$, is defined as [63]

$$\left(\sqrt{\bar{M}^2}\right)^2 = \bar{M}^2 \quad \text{and} \quad \text{Re}\left[\lambda_k\left(\sqrt{\bar{M}^2}\right)\right] > 0 \quad \text{for all } k \tag{4.5}$$

For the state-dependent ARE presented in Eq. (4.1), the state-dependent Hamiltonian matrix is constructed as follows,

$$\bar{M}(x) = \begin{bmatrix} F(x) & -G(x) \\ -H(x) & -F(x)^T \end{bmatrix} \tag{4.6}$$

Considering the property of the Hamiltonian matrix, if λ is the eigenvalue of $\bar{M}(x)$, then $-\lambda$, $\bar{\lambda}$, and $-\bar{\lambda}$ are also eigenvalues of $\bar{M}(x)$. Therefore, the eigenvalues of $\bar{M}(x)$ can be expressed for the real eigenvalue case (Case 1) and for the complex eigenvalue case (Case 2) as follows [64],

$$\lambda\left[\bar{M}(x)\right] = \begin{cases} a, -a,\ b, -b & \text{(Case 1)} \\ a+bi, -a+bi,\ a-bi, -a-bi & \text{(Case 2)} \end{cases} \tag{4.7}$$

where $a, b \in \mathbb{R}^+$. Because the Hamiltonian matrix has no eigenvalue on the imaginary axis under **Condition 2.3**, a and b are non-zero. The square of $\bar{M}(x)$ can be written as

$$\bar{M}(x)^2 = \begin{bmatrix} p_1 & q_1 & 0 & r_1 \\ q_2 & p_2 & -r_1 & 0 \\ 0 & -r_2 & p_1 & q_2 \\ r_2 & 0 & q_1 & p_2 \end{bmatrix} \tag{4.8}$$

where

$$\begin{aligned} p_1 &= f_1^2 + f_2 f_3 + g_1 h_1 + g_2 h_2, & p_2 &= f_4^2 + f_2 f_3 + g_2 h_2 + g_3 h_3 \\ q_1 &= f_1 f_2 + f_2 f_4 + g_1 h_2 + g_2 h_3, & q_2 &= f_1 f_3 + f_3 f_4 + g_2 h_1 + g_3 h_2 \\ r_1 &= f_3 g_1 + f_4 g_2 - f_1 g_2 - f_2 g_3, & r_2 &= f_2 h_1 + f_4 h_2 - f_1 h_2 - f_3 h_3 \end{aligned}$$

The characteristic polynomial of $\bar{M}(x)$ can be obtained as follows,

$$\lambda[\bar{M}(x)]^4 - (p_1 + p_2)\lambda[\bar{M}(x)]^2 + \Delta_{\bar{M}} = 0 \tag{4.9}$$

where $\Delta_{\bar{M}}$ is the determinant of $\bar{M}(x)$. Note that the characteristic polynomial of a real Hamiltonian matrix is even [64], which is consistent with Eq. (4.9). The determinant of $\bar{M}(x)$ can be written using Eq. (4.8) as

$$\Delta_{\bar{M}} = p_1 p_2 - q_1 q_2 - r_1 r_2 \tag{4.10}$$

Since the determinant of matrix is equal to the product of its eigenvalues, the determinant of $\bar{M}(x)$ can be rewritten for each case as

$$\Delta_{\bar{M}} = \begin{cases} a^2 b^2 & \text{(Case 1)} \\ \left(a^2 + b^2\right)^2 & \text{(Case 2)} \end{cases} \tag{4.11}$$

Note from Eq. (4.11) that $\Delta_{\bar{M}}$ is positive for any a, $b \in \mathbb{R}^+$. Consequently, the following inverse matrix of $\bar{M}(x)$ is non-singular.

$$\bar{M}(x)^{-1} = \frac{1}{\Delta_{\bar{M}}} \begin{bmatrix} m_1 & m_3 & m_5 & m_7 \\ m_4 & m_2 & m_7 & m_6 \\ m_8 & m_{10} & -m_1 & -m_4 \\ m_{10} & m_9 & -m_3 & -m_2 \end{bmatrix} \tag{4.12}$$

where

$$\begin{aligned}
m_1 &= f_1 f_4^2 + f_1 g_3 h_3 + f_4 g_2 h_2 - f_2 f_3 f_4 - f_2 g_3 h_2 - f_3 g_2 h_3 \\
m_2 &= f_1^2 f_4 + f_1 g_2 h_2 + f_4 g_1 h_1 - f_1 f_2 f_3 - f_2 g_2 h_1 - f_3 g_1 h_2 \\
m_3 &= f_2^2 f_3 + f_2 g_2 h_2 + f_3 g_1 h_3 - f_1 f_2 f_4 - f_1 g_2 h_3 - f_4 g_1 h_2 \\
m_4 &= f_2 f_3^2 + f_2 g_3 h_1 + f_3 g_2 h_2 - f_1 f_3 f_4 - f_1 g_3 h_2 - f_4 g_2 h_1 \\
m_5 &= g_2^2 h_3 + 2 f_2 f_4 g_2 - f_2^2 g_3 - f_4^2 g_1 - g_1 g_3 h_3 \\
m_6 &= g_2^2 h_1 + 2 f_1 f_3 g_2 - f_1^2 g_3 - f_3^2 g_1 - g_1 g_3 h_1 \\
m_7 &= f_1 f_2 g_3 + f_3 f_4 g_1 + g_1 g_3 h_2 - f_1 f_4 g_2 - f_2 f_3 g_2 - g_2^2 h_2 \\
m_8 &= g_3 h_2^2 + 2 f_3 f_4 h_2 - f_3^2 h_3 - f_4^2 h_1 - g_3 h_1 h_3 \\
m_9 &= g_1 h_2^2 + 2 f_1 f_2 h_2 - f_1^2 h_3 - f_2^2 h_1 - g_1 h_1 h_3 \\
m_{10} &= f_1 f_3 h_3 + f_2 f_4 h_1 + g_2 h_1 h_3 - f_1 f_4 h_2 - f_2 f_3 h_2 - g_2 h_2^2
\end{aligned}$$

Lemma 4.2: The principal square root of $\bar{M}(x)^2$ can be obtained as follows,

$$\sqrt{\bar{M}(x)^2} = \frac{1}{\sqrt{d}}\left(\bar{M}(x)^2 + \sqrt{\Delta_{\bar{M}}} I_4\right)$$
$$= \frac{1}{\sqrt{d}} \begin{bmatrix} p_1 + \sqrt{\Delta_{\bar{M}}} & q_1 & 0 & r_1 \\ q_2 & p_2 + \sqrt{\Delta_{\bar{M}}} & -r_1 & 0 \\ 0 & -r_2 & p_1 + \sqrt{\Delta_{\bar{M}}} & q_2 \\ r_2 & 0 & q_1 & p_2 + \sqrt{\Delta_{\bar{M}}} \end{bmatrix} \tag{4.13}$$

where $d = p_1 + p_2 + 2\sqrt{\Delta_{\bar{M}}}$.

Proof of Lemma 4.2: Using the property of the matrix trace, the following relation can be obtained.

$$p_1 + p_2 = \frac{1}{2}\mathrm{tr}\left[\bar{M}(x)^2\right] \tag{4.14}$$

where tr[·] denotes the matrix trace. Based on Eq. (4.14), d in Eq. (4.13) can be rewritten as

$$d = \frac{1}{2}\mathrm{tr}\left[\bar{M}(x)^2\right] + 2\sqrt{\Delta_{\bar{M}}} \tag{4.15}$$

The trace of $\bar{M}(x)^2$ can be expressed using the eigenvalue of the Hamiltonian matrix for each case as

$$\mathrm{tr}\left[\bar{M}(x)^2\right] = \sum_{i=1}^{4}\left(\lambda_i\left[\bar{M}(x)\right]\right)^2 = \begin{cases} 2(a^2+b^2) & \text{(Case 1)} \\ 4(a^2-b^2) & \text{(Case 2)} \end{cases} \tag{4.16}$$

Substituting Eqs. (4.11) and (4.16) into Eq. (4.15) yields

$$d = \begin{cases} a^2 + b^2 + 2|ab| & \text{(Case 1)} \\ 4a^2 & \text{(Case 2)} \end{cases} \tag{4.17}$$

Equation (4.17) shows that d is positive for any a, $b \in \mathbb{R}^+$. Applying the Cayley-Hamilton theorem to Eq. (4.9), the following matrix equation can be obtained.

$$\bar{M}(x)^4 - (p_1 + p_2)\bar{M}(x)^2 + \Delta_{\bar{M}} I_4 = 0 \tag{4.18}$$

Substituting Eq. (4.18) into the square of Eq. (4.13) yields

$$\begin{aligned}\left(\sqrt{\bar{M}(x)^2}\right)^2 &= \frac{1}{d}\left(\bar{M}(x)^2 + \sqrt{\Delta_{\bar{M}}} I_4\right)^2 \\ &= \frac{1}{d}\left(\bar{M}(x)^4 + 2\sqrt{\Delta_{\bar{M}}}\bar{M}(x)^2 + \Delta_{\bar{M}} I_4\right) \\ &= \frac{1}{d}\left\{(p_1 + p_2)\bar{M}(x)^2 + 2\sqrt{\Delta_{\bar{M}}}\bar{M}(x)^2\right\} = \bar{M}(x)^2\end{aligned} \tag{4.19}$$

Equation (4.19) shows that the square of Eq. (4.13) is equal to $\bar{M}(x)^2$, which is consistent with the definition of the principal square root of matrix in Eq. (4.5). The eigenvalues of Eq. (4.13) with even algebraic multiplicity can be expressed as follows,

$$\lambda\left[\sqrt{\bar{M}(x)^2}\right] = \frac{1}{2\sqrt{d}}\left(d \pm \sqrt{(p_1 + p_2)^2 - 4\Delta_{\bar{M}}}\right) \tag{4.20}$$

Substituting Eqs. (4.11), (4.16), and (4.17) into Eq. (4.20), we have

$$\lambda\left[\sqrt{\bar{M}(x)^2}\right] = \begin{cases} \frac{1}{2\sqrt{d}}\left(a^2 + b^2 + 2|ab| \pm |a^2 - b^2|\right) & \text{(Case 1)} \\ \frac{2}{\sqrt{d}}\left(a^2 \pm |ab| i\right) & \text{(Case 2)} \end{cases} \tag{4.21}$$

From Eq. (4.21), the real part of the eigenvalues of $\sqrt{\bar{M}(x)^2}$ can be obtained as follows,

$$\mathrm{Re}\left[\lambda\left[\sqrt{\bar{M}(x)^2}\right]\right] = \begin{cases} \frac{a^2+|ab|}{\sqrt{d}} \text{ or } \frac{b^2+|ab|}{\sqrt{d}} & \text{(Case 1)} \\ \frac{2}{\sqrt{d}} a^2 & \text{(Case 2)} \end{cases} \tag{4.22}$$

Equation (4.22) implies that all the real parts of the eigenvalues of $\sqrt{\bar{M}(x)^2}$ are positive for any a, $b \in \mathbb{R}^+$. Therefore, based on Eq. (4.5), it can be concluded that Eq. (4.13) is the principal square root of $\bar{M}(x)^2$. □

Using Eqs. (4.12), (4.13), and the relation $\bar{M}(x)^{-1}\bar{M}(x)^2 = \bar{M}(x)$, $W_{12}(x)$ and $W_{22}(x)$ in Eq. (4.3) can be obtained as follows,

$$\begin{aligned} W_{12}(x) &= \frac{1}{2\sqrt{d\Delta_{\bar{M}}}} \begin{bmatrix} w_1 & w_2 \\ w_2 & w_3 \end{bmatrix} \\ W_{22}(x) &= -\frac{1}{2\sqrt{d\Delta_{\bar{M}}}} \begin{bmatrix} w_4 & w_5 \\ w_6 & w_7 \end{bmatrix} \end{aligned} \tag{4.23}$$

where

$$\begin{aligned} &w_1 = m_5 - g_1\sqrt{\Delta_{\bar{M}}}, \quad w_2 = m_7 - g_2\sqrt{\Delta_{\bar{M}}}, \quad w_3 = m_6 - g_3\sqrt{\Delta_{\bar{M}}} \\ &w_4 = m_1 + \left(f_1 + \sqrt{d}\right)\sqrt{\Delta_{\bar{M}}}, \quad w_5 = m_4 + f_3\sqrt{\Delta_{\bar{M}}} \\ &w_6 = m_3 + f_2\sqrt{\Delta_{\bar{M}}}, \quad w_7 = m_2 + \left(f_4 + \sqrt{d}\right)\sqrt{\Delta_{\bar{M}}} \end{aligned}$$

From Eq. (4.23), the inverse matrix of $W_{12}(x)$ can be expressed as follows,

$$W_{12}(x)^{-1} = \frac{1}{2\Delta_W\sqrt{d\Delta_{\bar{M}}}} \begin{bmatrix} w_3 & -w_2 \\ -w_2 & w_1 \end{bmatrix} \tag{4.24}$$

where Δ_W is the determinant of $W_{12}(x)$. Using Eqs. (4.23) and (4.24), the analytic solution of the state-dependent ARE in Eq. (4.1) can be obtained based on **Lemma 4.1** as follows,

$$X(x) = \frac{1}{4d\Delta_{\bar{M}}\Delta_W} \begin{bmatrix} \hat{x}_1 & \hat{x}_2 \\ \hat{x}_2' & \hat{x}_3 \end{bmatrix} = \begin{bmatrix} x_{1,1} & x_{1,2} \\ x_{2,1} & x_{2,2} \end{bmatrix} \tag{4.25}$$

where

$$\begin{aligned} &\hat{x}_1 = w_2w_5 - w_3w_4, \quad \hat{x}_2 = w_2w_4 - w_1w_5 \\ &\hat{x}_2' = w_2w_7 - w_3w_6, \quad \hat{x}_3 = w_2w_6 - w_1w_7 \end{aligned}$$

4.2.2 Properties of Analytic Solution

Lemma 4.3: $W_{12}(x)$ in Eq. (4.23) is a non-singular matrix.

Proof of Lemma 4.3: For the non-singular matrix $G(x)$ in Eq. (4.1), it was proven that $W_{12}(x)$ is non-singular [65]. Now, let us investigate the case that $G(x)$ is the singular matrix. If $G(x)$ is singular, i.e., $g_1 g_3 - g_2^2 = 0$, the determinant of W_{12} can be rewritten as

$$\Delta_W = \frac{1}{4d\sqrt{\Delta_{\bar{M}}}}(f_3 g_1 + f_4 g_2 - f_1 g_2 - f_2 g_3)^2 \tag{4.26}$$

The state-dependent controllability matrix of the pair $(F(x), G(x))$ can be constructed as follows,

$$C_{F,G}(x) = \begin{bmatrix} g_1 & g_2 & f_1 g_1 + f_2 g_2 & f_1 g_2 + f_2 g_3 \\ g_2 & g_3 & f_3 g_1 + f_4 g_2 & f_3 g_2 + f_4 g_3 \end{bmatrix} = \begin{bmatrix} C_{O_1}(x) \\ C_{O_2}(x) \end{bmatrix} \tag{4.27}$$

Let us assume that the determinant of $W_{12}(x)$ is zero. Then, the following equality is satisfied based on Eq. (4.26).

$$f_3 g_1 + f_4 g_2 = f_1 g_2 + f_2 g_3 \tag{4.28}$$

Noth that, if g_2 is non-zero, g_1 and g_3 are also non-zero because $g_1 g_3 - g_2^2 = 0$, and $g_2 C_{O_1}(x) = g_1 C_{O_2}(x)$ based on Eqs. (4.27) and (4.28). Otherwise, if g_2 is zero, $g_1 g_3$ should be zero, and the state-dependent controllability matrix in Eq. (4.27) should have at least one row of all zeros. Therefore, if the determinant of $W_{12}(x)$ is zero, the controllability matrix cannot be a full-rank matrix, which implies that the pair $(F(x), G(x))$ is point-wise uncontrollable. This assumption contradicts **Condition 2.3**, and therefore the determinant of $W_{12}(x)$ cannot be zero, i.e., $W_{12}(x)$ is a non-singular matrix. □

Lemma 4.4: The analytic solution $X(x)$ in Eq. (4.25) is a symmetric matrix.

Proof of Lemma 4.4: Based on Eq. (4.23), $\hat{x}_2 - \hat{x}_2'$ can be expressed as

$$\begin{aligned} \hat{x}_2 - \hat{x}_2' &= w_2 w_4 + w_3 w_6 - w_1 w_5 - w_2 w_7 \\ &= r_1 \Delta_{\bar{M}} + u_1 \sqrt{\Delta_{\bar{M}}} + u_2 \end{aligned} \tag{4.29}$$

where

$$\begin{aligned} u_1 &= -g_2(m_1 - m_2) - g_3 m_3 + g_1 m_4 - f_3 m_5 + f_2 m_6 + (f_1 - f_4) m_7 \\ u_2 &= m_1 m_7 + m_3 m_6 - m_2 m_7 - m_4 m_5 \end{aligned}$$

Using the relation that $\bar{M}(x)^{-1}\bar{M}(x) = I_4$, the following relations can be obtained.

$$\begin{aligned} g_2 m_1 + g_3 m_3 + f_3 m_5 + f_4 m_7 = 0 \\ g_2 m_2 + g_1 m_4 + f_2 m_6 + f_1 m_7 = 0 \end{aligned} \tag{4.30}$$

Applying Eq. (4.30) to Eq. (4.29) yields that u_1 is zero, and the following relation can be obtained based on $\left(\bar{M}(x)^{-1}\right)^2 = \left(\bar{M}(x)^2\right)^{-1}$.

$$\begin{aligned} u_2 &= m_1 m_7 + m_3 m_6 - m_2 m_7 - m_4 m_5 \\ &= -p_1 p_2 r_1 + q_1 q_2 r_1 + r_1^2 r_2 \end{aligned} \tag{4.31}$$

Equation (4.31) can be rewritten as $u_2 = -r_1 \Delta_{\bar{M}}$ using Eq. (4.10). Finally, based on Eq. (4.29) and $u_1 = 0$, it can be concluded that $\hat{x}_2 - \hat{x}_2' = 0$, i.e., $X(x)$ is a symmetric matrix. □

4.3 Stability Analysis of Missile Longitudinal Closed-Loop System

In this section, stability analysis is performed for the missile longitudinal closed-loop system controlled by the SDRE method using the analytic solution of the state-dependent ARE, which is obtained in the previous section.

4.3.1 Design of Missile Longitudinal Autopilot Using State-Dependent Riccati Equation Method

The autopilot is designed based on the missile longitudinal dynamics in Eq. (2.16). Assuming the fast and stable actuator of the missile, the actuator dynamics is neglected based on the singular perturbation theory. Now, the missile longitudinal dynamics in Eq. (2.16) can be rewritten as follows,

$$\begin{aligned} \dot{x}_l &= f_l(x_l) + g_l(x_l)u_l \\ z_l &= h_l(x_l) \end{aligned} \tag{4.32}$$

where $x_l = [\alpha \ q]^T$, $u_l = \delta_p$, $z_l = a_z$, and

$$f_l(x_l) = \begin{bmatrix} \frac{QS}{mV} C_{Z_\alpha}(\mathbf{M}, x_l)\alpha + q \\ \frac{QSD}{I_{yy}} \left(C_{m_\alpha}(\mathbf{M}, x_l)\alpha + \frac{D}{2V} C_{m_q}(\mathbf{M}, x_l) q \right) \end{bmatrix}$$

$$g_l(x_l) = \begin{bmatrix} \frac{QS}{mV} C_{Z_{\delta_p}}(\mathbf{M}, x_l) \\ \frac{QSD}{I_{yy}} C_{m_{\delta_p}}(\mathbf{M}, x_l) \end{bmatrix}$$

$$h_l(x_l) = \frac{QS}{m} \left(C_{Z_\alpha}(\mathbf{M}, x_l)\alpha + C_{Z_{\delta_p}}(\mathbf{M}, x_l)\delta_p \right)$$

The region of interest of x_l is defined as $\Omega_l = \{(\alpha, q) |\ \alpha \in \Omega_\alpha \text{ and } q \in \mathbb{R}\}$, where Ω_α is the normal operational range of the angle of attack, and the following assumptions are considered.

Assumption 4.1: The total velocity is fixed.

Assumption 4.2: The aerodynamic force and moment coefficients $C_{Z_\alpha}(\mathbf{M}, x_l)$, $C_{Z_{\delta_p}}(\mathbf{M}, x_l)$, $C_{m_\alpha}(\mathbf{M}, x_l)$, $C_{m_{\delta_p}}(\mathbf{M}, x_l)$, and $C_{m_q}(\mathbf{M}, x_l)$ are negative on Ω_l for any fixed $\mathbf{M} > 0$.

Note from **Assumption 4.1** that the aerodynamic force and moment coefficients only depend on the angle of attack. Also, under **Assumption 4.2**, $f_l(0) = 0$ and $g_l(x_l) \neq 0$ on Ω_l. Therefore, Eq. (4.32) can be transformed into the following pseudo-linear system using the SDC transformation.

$$\begin{aligned} \dot{x}_l &= A(x_l)x_l + B(x_l)x_l \\ z_l &= H(x_l)x_l + L(x_l)u_l \end{aligned} \tag{4.33}$$

where

$$\begin{aligned} A(x_l) &= \begin{bmatrix} \frac{QS}{mV}C_{Z_\alpha}(x_l) & 1 \\ \frac{QSD}{I_{yy}}C_{m_\alpha}(x_l) & \frac{QSD^2}{2I_{yy}V}C_{m_q}(x_l) \end{bmatrix} = \begin{bmatrix} a_1 & 1 \\ a_2 & a_3 \end{bmatrix} \\ B(x_l) &= \begin{bmatrix} \frac{QS}{mV}C_{Z_{\delta_p}}(x_l) \\ \frac{QSD}{I_{yy}}C_{m_{\delta_p}}(x_l) \end{bmatrix} = \begin{bmatrix} b_1 \\ b_2 \end{bmatrix} \\ E(x_l) &= \begin{bmatrix} a_1 V & 0 \end{bmatrix}, \quad L(x_l) = b_1 V \end{aligned}$$

Under **Assumption 4.2**, a_1, a_2, a_3, b_1, and b_2 are negative on Ω_l. To design the SDRE-based control input, the following quadratic cost function is considered.

$$J = \frac{1}{2}\int_0^\infty \left(z_l^2 q_w + u_l^2 r_w\right) dt \tag{4.34}$$

where q_w and r_w are weighting parameters which are set to be positive constant. Substituting Eq. (4.33) into Eq. (4.34) yields

$$J = \frac{1}{2}\int_0^\infty \left(x_l^T Q(x_l)x_l + u_l^T R(x_l)u_l + 2x_l^T N(x_l)u_l\right) dt \tag{4.35}$$

where

$$Q(x_l) = q_w E(x_l)^T E(x_l), \quad R(x_l) = r_w + q_w L(x_l)^2, \quad N(x_l) = q_w L(x_l) E(x_l)^T$$

The following state-dependent ARE is constructed based on the quadratic cost function in Eq. (4.35).

$$\begin{aligned} &A(x_l)^T X(x_l) + X(x_l) A(x_l) + Q(x_l) \\ &- \left(X(x_l) B(x_l) + N(x_l)\right) R(x_l)^{-1} \left(B(x_l)^T X(x_l) + N(x_l)^T\right) = 0 \end{aligned} \tag{4.36}$$

Using the solution of the state-dependent ARE $X(x_l)$, the full-state feedback control input based on the SDRE method can be obtained as follows,

$$u_l = -R(x_l)^{-1} \left(B(x_l)^T X(x_l) + N(x)^T\right) x_l = -K(x_l) x_l \tag{4.37}$$

The state-dependent ARE in Eq. (4.36) can be modified as follows,

$$\begin{aligned} &\hat{A}(x_l)^T X(x_l) + X(x_l) \hat{A}(x_l) \\ &- X(x_l) B(x_l) R(x_l)^{-1} B(x_l)^T X(x_l) + \hat{Q}(x_l) = 0 \end{aligned} \tag{4.38}$$

where

$$\hat{A}(x_l) = A(x_l) - B(x_l) R(x_l)^{-1} N(x_l)^T = \begin{bmatrix} \hat{a}_1 & 1 \\ \hat{a}_2 & a_3 \end{bmatrix}$$

$$\hat{Q}(x_l) = Q(x_l) - N(x_l) R(x_l)^{-1} N(x_l)^T = \begin{bmatrix} \hat{q} & 0 \\ 0 & 0 \end{bmatrix}$$

and

$$\hat{a}_1 = \frac{r_w}{r_w + b_1^2 V^2 q_w} a_1, \quad \hat{a}_2 = a_2 - \frac{b_1 b_2 V^2 q_w}{r_w + b_1^2 V^2 q_w} a_1, \quad \hat{q} = \frac{V^2 q_w r_w}{r_w + b_1^2 V^2 q_w} a_1^2$$

Note that $\hat{a}_1$ and $\hat{q}$ are negative and positive, respectively, because a_1 is negative on Ω_l. The state-dependent ARE presented in Eq. (4.38) has the same form of Eq. (4.1) with the following relations.

$$\begin{aligned} F(x_l) &= \hat{A}(x_l) \\ G(x_l) &= B(x_l)R(x_l)^{-1}B(x_l)^T \\ H(x_l) &= \hat{Q}(x_l) \end{aligned} \tag{4.39}$$

The analytic solution of the state-dependent ARE obtained in the privious section can be applied to the state-dependent ARE for the missile longitudinal autopilot based on the matrix relations presented in Eq. (4.39). The components of $B(x_l)R(x_l)^{-1}B(x_l)^T$ can be represented as

$$B(x_l)R(x_l)^{-1}B(x_l)^T = \begin{bmatrix} \hat{r}_1 & \sqrt{\hat{r}_1\hat{r}_2} \\ \sqrt{\hat{r}_1\hat{r}_2} & \hat{r}_2 \end{bmatrix} \tag{4.40}$$

where

$$\hat{r}_1 = \frac{b_1^2}{r_w + b_1^2 V^2 q_w}, \quad \hat{r}_2 = \frac{b_2^2}{r_w + b_1^2 V^2 q_w}$$

From Eq. (4.40), it is clear that $\hat{r}_1$ and $\hat{r}_2$ are positive on Ω_l.

4.3.2 Stability Analysis Using Analytic Solution

To analyze the stability of the closed-loop system controlled by the SDRE method, the following two assumptions are considered based on the properties of the tail-fin controlled missile.

Assumption 4.3: The term $4a_1b_1 + b_2$ is negative on Ω_l.

Assumption 4.4: The term $(a_3b_1 + b_2)a_1 - 2a_2b_1$ is positive on Ω_l.

Remark 4.2: Assumption 4.3 is valid for most tail-fin controlled missiles, because b_2 usually dominates $4a_1b_1$. That is because QSD/I_{yy} is generally much greater than $QS/(mV)$ in normal operational range of the missile. Moreover, $C_{m_{\delta_p}}(x_l)$ is greater than $C_{Z_{\delta_p}}(x_l)$ considering Eq. (3.15). Therefore, the magnitude of b_2 is usually much greater than those of a_1 and b_1 considering Eq. (4.33). Similarly, **Assumption 4.4** is reasonable for most tail-fin controlled missiles. Using Eq. (4.33), the term $(a_3b_1 + b_2)a_1 - 2a_2b_1$ in **Assumption 4.4** can be rewritten as follows,

$$\begin{aligned}&(a_3b_1 + b_2)a_1 - 2a_2b_1\\ =&\frac{Q^2S^2D}{mVI_{yy}}C_{Z_\alpha}(x_l)C_{Z_{\delta_p}}(x_l)\left\{\frac{(x_{\rm cf} - x_{\rm cp}) - (x_{\rm cp} - x_{\rm cm})}{D} + \frac{QS}{mV}\hat{C}_{m_q}(x_l)\right\}\end{aligned} \quad (4.41)$$

where $\hat{C}_{m_q}(x_l) = (D/2V)C_{m_q}(x_l)$. Note that $x_{\rm cf} - x_{\rm cp}$ represents the distance from the aerodynamic center of the tail-fin to the center of pressure for the missile's body, and $x_{\rm cp} - x_{\rm cm}$ represents the distance from the center of pressure to the center of mass. Considering the normal operational range of the tail-fin controlled missile, the magnitude of the former is generally much greater than that of the latter. Also, because $QS/(mV)$ usually has a small value, it is valid to assume that $(a_3b_1 + b_2)a_1 - 2a_2b_1$ is positive on Ω_l.

Before analyzing the stability of the closed-loop system, **Conditions 2.1-2.3** should be examined for the designed longitudinal autopilot for the existence of the positive definite stabilizing solution of the state-dependent ARE. First of all, it is obvious that **Conditions 2.1** and **2.2** are satisfied on Ω_l considering Eqs. (4.33) and (4.35). For **Condition 2.3**, the point-wise controllability can be examined using the pair $(\hat{A}(x_l), B(x_l))$, which has the following controllability

matrix.

$$C_{\hat{A},B}(x_l) = \begin{bmatrix} b_1 & \hat{a}_1 b_1 + b_2 \\ b_2 & \hat{a}_2 b_1 + a_3 b_2 \end{bmatrix} \tag{4.42}$$

The determinant of $C_{\hat{A},B}(x_l)$ can be expressed as

$$\mathrm{Det}[C_{\hat{A},B}(x_l)] = \hat{a}_2 b_1^2 + a_3 b_1 b_2 - b_2(\hat{a}_1 b_1 + b_2) \tag{4.43}$$

From Eq. (4.38), the following relation can be obtained.

$$\begin{aligned} \hat{a}_1 b_2 - \hat{a}_2 b_1 &= \frac{r_w}{r_w + b_1^2 V^2 q_w} a_1 b_2 - \left(a_2 - \frac{b_1 b_2 V^2 q_w}{r_w + b_1^2 V^2 q_w} a_1 \right) b_1 \\ &= \frac{1}{r_w + b_1^2 V^2 q_w} (a_1 b_2 r_w + a_1 b_1^2 b_2 V^2 q_w) - a_2 b_1 \\ &= a_1 b_2 - a_2 b_1 \end{aligned} \tag{4.44}$$

Using Eq. (4.44), the determinant of $C_{\hat{A},B}(x_l)$ can be rewritten as

$$\mathrm{Det}[C_{\hat{A},B}(x_l)] = a_2 b_1^2 + a_3 b_1 b_2 - b_2(a_1 b_1 + b_2) \tag{4.45}$$

Under **Assumption 4.3**, $a_1 b_1 + b_2$ is negative on Ω_l. Therefore, the determinant of $C_{\hat{A},B}(x_l)$ is negative, because a_2, a_3, b_1, and b_2 are all negative on Ω_l, which implies that the pair $(\hat{A}(x_l), B(x_l))$ is point-wise controllable on Ω_l under **Assumption 4.3**. Similarly, the observability matrix of the pair $(\hat{A}(x_l), \hat{Q}(x_l))$ can be obtained as follows,

$$O_{\hat{A},\hat{Q}}(x_l) = \hat{q} \begin{bmatrix} 1 & 0 & \hat{a}_1 & 0 \\ 0 & 0 & 1 & 0 \end{bmatrix}^T \tag{4.46}$$

Because $\hat{q}$ is positive, the observability matrix has rank 2, and it implies that the pair $(\hat{A}(x_l), \hat{Q}(x_l))$ is point-wise observable on Ω_l. Therefore, **Condition 2.3** is satisfied on Ω_l under **Assumption 4.3**.

The stability analysis starts from representing the closed-loop system controlled by the designed autopilot using the analytic solution of the state-dependent ARE as follows,

$$\begin{aligned}
\dot{x}_l &= A(x_l)x_l - B(x_l)K(x_l)x_l \\
&= A(x_l)x_l - B(x_l)R(x_l)^{-1}(B(x_l)^T X(x_l) + N(x_l)^T)x_l \\
&= (\hat{A}(x_l) - B(x_l)R(x_l)^{-1}B(x_l)^T X(x_l))x_l \\
&= A_c(x_l)x_l
\end{aligned} \tag{4.47}$$

where $A_c(x_l)$ can be expressed as

$$\begin{aligned}
A_c(x_l) &= \begin{bmatrix} \hat{a}_1 - \frac{\hat{r}_1\hat{x}_1 + \sqrt{\hat{r}_1\hat{r}_2}\hat{x}_2}{4d\Delta_{\bar{M}}\Delta_W} & 1 - \frac{\hat{r}_1\hat{x}_2 + \sqrt{\hat{r}_1\hat{r}_2}\hat{x}_3}{4d\Delta_{\bar{M}}\Delta_W} \\ \hat{a}_2 - \frac{\sqrt{\hat{r}_1\hat{r}_2}\hat{x}_1 + \hat{r}_2\hat{x}_2}{4d\Delta_{\bar{M}}\Delta_W} & a_3 - \frac{\sqrt{\hat{r}_1\hat{r}_2}\hat{x}_2 + \hat{r}_2\hat{x}_3}{4d\Delta_{\bar{M}}\Delta_W} \end{bmatrix} \\
&= \begin{bmatrix} a_{c,1} & a_{c,2} \\ a_{c,3} & a_{c,4} \end{bmatrix}
\end{aligned} \tag{4.48}$$

Using Eqs. (4.12), (4.23), (4.25), and (4.38), $a_{c,1}$ can be derived as follows,

$$a_{c,1} = \frac{1}{\mathrm{Det}[C_{\hat{A},B}(x_l)]} \left\{ \left(a_3 b_1 - b_2 + b_1\sqrt{d} \right) t_1 + b_1 b_2 \sqrt{\Delta_{\bar{M}}} \right\} \tag{4.49}$$

where $t_1 = a_1 b_2 - a_2 b_1$. Using the relationship between the force and moment aerodynamic coefficients, which are presented in Eq. (3.15), and Eq. (4.33), t_1 can be rewritten as

$$\begin{aligned}
t_1 &= \frac{Q^2 S^2 D}{m V I_{yy}} \left(C_{Z_\alpha}(x_l) C_{m_{\delta_p}}(x_l) - C_{Z_{\delta_p}}(x_l) C_{m_\alpha}(x_l) \right) \\
&= \frac{Q^2 S^2 D}{m V I_{yy}} \left(\frac{x_{\mathrm{cf}} - x_{\mathrm{cp}}}{D} \right) C_{Z_\alpha}(x_l) C_{Z_{\delta_p}}(x_l)
\end{aligned} \tag{4.50}$$

Note from Eq. (4.50) that t_1 is positive on Ω_l considering the tail-fin controlled missile geometry as shown in Fig. 2.1. Similarly, the other components of $A_c(x_l)$

can be derived as follows,

$$
\begin{aligned}
a_{c,2} &= -\frac{1}{\mathrm{Det}[C_{\hat{A},B}(x_l)]}\left\{(a_3b_1-b_2)(a_3b_1-b_2+b_1\sqrt{d})+b_1^2\sqrt{\Delta_{\bar{M}}}\right\} \\
a_{c,3} &= \frac{1}{\mathrm{Det}[C_{\hat{A},B}(x_l)]}\left\{(t_1+b_2\sqrt{d})t_1+b_2^2\sqrt{\Delta_{\bar{M}}}\right\} \\
a_{c,4} &= -\frac{1}{\mathrm{Det}[C_{\hat{A},B}(x_l)]}\left\{(a_3b_1-b_2)(t_1+b_2\sqrt{d})+b_1b_2\sqrt{\Delta_{\bar{M}}}\right\}
\end{aligned}
\tag{4.51}
$$

Substituting Eq. (4.8) into Eq. (4.10), and substituting Eqs. (4.38) and (4.40) into the resulting equation, $\Delta_{\bar{M}}$ can be rewritten as

$$
\Delta_{\bar{M}} = a_2^2 + \frac{a_1b_2V^2(a_1b_2-2a_2b_1)\bar{w}+a_1a_3(a_1a_3-2a_2)}{b_1^2V^2\bar{w}+1} \tag{4.52}
$$

where $\bar{w} = q_w/r_w$. Then, the partial derivative of $\Delta_{\bar{M}}$ with respect to $\bar{w}$ can be obtained as follows,

$$
\frac{\partial\Delta_{\bar{M}}}{\partial\bar{w}} = \frac{(b_2-a_3b_1)\{(a_3b_1+b_2)a_1-2a_2b_1\}V^2a_1}{(b_1^2V^2\bar{w}+1)^2} \tag{4.53}
$$

Under **Assumption 4.4**, the partial derivative of $\Delta_{\bar{M}}$ is positive on Ω_l, and $\Delta_{\bar{M}}$ satisfies the following relations for any fixed $\alpha \in \Omega_\alpha$.

$$
\begin{aligned}
\inf_{\bar{w}\in\mathbb{R}^+}[\Delta_{\bar{M}}] &= \lim_{\bar{w}\to 0^+}[\Delta_{\bar{M}}] = (a_2-a_1a_3)^2 \\
\sup_{\bar{w}\in\mathbb{R}^+}[\Delta_{\bar{M}}] &= \lim_{\bar{w}\to\infty}[\Delta_{\bar{M}}] = \left(\frac{t_1}{b_1}\right)^2
\end{aligned}
\tag{4.54}
$$

Using Eqs. (4.8), (4.38), and (4.40), p_1+p_2 can be expressed as

$$
p_1+p_2 = 2a_2+a_3^2-\frac{2a_1b_1b_2V^2\bar{w}-a_1^2}{b_1^2V^2\bar{w}+1} \tag{4.55}
$$

The partial derivative of p_1+p_2 with respect to $\bar{w}$ can be obtained as follows,

$$
\frac{\partial(p_1+p_2)}{\partial\bar{w}} = -\frac{a_1b_1V^2(a_1b_1+2b_2)}{(b_1^2V^2\bar{w}+1)^2} \tag{4.56}
$$

Note that the partial derivative of $p_1 + p_2$ is positive on Ω_l, because $a_1 b_1 + 2b_2$ is negative under **Assumption 4.3**. Considering the relation that $d = p_1 + p_2 + 2\sqrt{\Delta_{\bar{M}}}$, the partial derivative of d with respect to $\bar{w}$ is also positive on Ω_l. Therefore, the following relations of d can be obtained for any fixed $\alpha \in \Omega_\alpha$.

$$\begin{aligned} \inf_{\bar{w}\in\mathbb{R}^+}[d] &= \lim_{\bar{w}\to 0^+}[d] = a_1^2 + 2a_2 + a_3^2 + 2|a_2 - a_1 a_3| = (a_1 + a_3)^2 \\ \sup_{\bar{w}\in\mathbb{R}^+}[d] &= \lim_{\bar{w}\to \infty}[d] = -2\left(\frac{b_2}{b_1}\right) a_1 + 2a_2 + a_3^2 + 2\left|\frac{t_1}{b_1}\right| = a_3^2 - \frac{4t_1}{b_1} \end{aligned} \tag{4.57}$$

Lemma 4.5: Under **Assumptions 4.1-4.4**, $a_{c,1}$ and $a_{c,2}$ are negative and positive, respectively, on Ω_l.

Proof of Lemma 4.5: Using Eq. (4.57), the following relation of the term $a_3 b_1 - b_2 + b_1\sqrt{d}$ can be obtained for any fixed $\alpha \in \Omega_\alpha$.

$$\begin{aligned} a_3 b_1 - b_2 + b_1\sqrt{d} &> a_3 b_1 - b_2 + b_1 \sup_{\bar{w}\in\mathbb{R}^+}\left[\sqrt{d}\right] \\ &= a_3 b_1 - b_2 + b_1\sqrt{a_3^2 - \frac{4t_1}{b_1}} \\ &= a_3 b_1 - b_2 - \sqrt{(a_3 b_1)^2 - 4b_1 t_1} \end{aligned} \tag{4.58}$$

Defining $c_5 = a_3 b_1 - b_2$ and $c_6 = \sqrt{(a_3 b_1)^2 - 4b_1 t_1}$, their squares satisfy the following relation.

$$\begin{aligned} c_5^2 - c_6^2 &= (a_3 b_1 - b_2^2) - \{(a_3 b_1)^2 - 4b_1 t_1\} \\ &= b_2^2 - 2a_3 b_1 b_2 + 4b_1(a_1 b_2 - a_2 b_1) \\ &= b_2(4a_1 b_1 + b_2) - 2a_3 b_1 b_2 - 4a_2 b_1^2 \end{aligned} \tag{4.59}$$

Under **Assumption 4.3**, Eq. (4.59) is positive on Ω_l. Therefore, because c_5 and c_6 are positive, c_5 is greater than c_6, which implies that the right side of

Eq. (4.58) is positive on Ω_l. From this result, it can be noticed that the term $a_3b_1 - b_2 + b_1\sqrt{d}$ is positive, and therefore $a_{c,1}$ and $a_{c,2}$ are negative and positive, respectively, on Ω_l considering Eqs. (4.49) and (4.51). □

Lemma 4.6: Under **Assumptions 4.1-4.4**, $a_{c,4}$ is negative on Ω_l.

Proof of Lemma 4.6: Using Eq. (4.51), the partial derivative of $a_{c,4}$ with respect to $\bar{w}$ can be obtained as follows,

$$\frac{\partial a_{c,4}}{\partial \bar{w}} = -\frac{b_2}{2\mathrm{Det}[C_{\hat{A},B}(x_l)]}\left\{(a_3b_1 - b_2)\frac{1}{\sqrt{d}}\frac{\partial d}{\partial \bar{w}} + b_1\frac{1}{\sqrt{\Delta_{\bar{M}}}}\frac{\partial \Delta_{\bar{M}}}{\partial \bar{w}}\right\} \tag{4.60}$$

Using Eqs. (4.53) and (4.56), Eq. (4.60) can be rewritten as

$$\frac{\partial a_{c,4}}{\partial \bar{w}} = \frac{a_1b_2c_7(a_3b_1 - b_2)V^2}{2\mathrm{Det}[C_{\hat{A},B}(x_l)]\sqrt{d\Delta_{\bar{M}}}(b_1^2V^2\bar{w} + 1)^2} \tag{4.61}$$

where

$$c_7 = b_1(a_1b_1 + 2b_2)\sqrt{\Delta_{\bar{M}}} + \{(a_3b_1 + b_2)a_1 - 2a_2b_1\}(a_3b_1 - b_2 + b_1\sqrt{d})$$

Because $a_3b_1 - b_2 + b_1\sqrt{d}$ is positive, which is proved in **Lemma 4.5**, c_7 is positive on Ω_l under **Assumption 4.3** and **4.4**, which implies that the partial derivative of $a_{c,4}$ with respect to $\bar{w}$ is negative on Ω_l. Therefore, the following relation of $a_{c,4}$ can be obtained for any fixed $\alpha \in \Omega_\alpha$.

$$\begin{aligned}\sup_{\bar{w}\in\mathbb{R}^+}[a_{c,4}] &= \lim_{\bar{w}\to 0}[a_{c,4}] \\ &= \lim_{\bar{w}\to 0}\left[-\frac{1}{\mathrm{Det}[C_{\hat{A},B}(x_l)]}\left\{(a_3b_1 - b_2)(t_1 + b_2\sqrt{d}) + b_1b_2\sqrt{\Delta_{\bar{M}}}\right\}\right]\end{aligned} \tag{4.62}$$

Substituting Eqs. (4.54) and (4.57) into Eq. (4.62) yields

$$\begin{aligned}\sup_{\bar{w}\in\mathbb{R}^+}[a_{c,4}] &= -\frac{1}{\mathrm{Det}[C_{\hat{A},B}(x_l)]}\{(a_3b_1 - b_2)(t_1 - b_2(a_1 + a_3)) - b_1b_2(a_2 - a_1a_3)\} \\ &= -\frac{1}{\mathrm{Det}[C_{\hat{A},B}(x_l)]}\{a_3b_2(a_1b_1 + b_2) - a_3b_1(a_2b_1 + a_3b_2)\}\end{aligned} \tag{4.63}$$

From Eq. (4.63), the supremum of $a_{c,4}$ with respect to $\bar{w}$ is negative on Ω_l under **Assumption 4.3**, and therefore it can be concluded that $a_{c,4}$ is negative on Ω_l under **Assumption 4.1-4.4**. □

Theorem 4.1: Under **Assumptions 4.1-4.4**, the closed-loop system represented by Eq. (4.47) is asymptotically stable on Ω_l, if there exists a constant κ satisfying the following inequality.

$$\sup_{\alpha\in\Omega_\alpha}\left[\left(\frac{\Delta_{\bar{M}}^{\frac{1}{4}}-\sqrt{a_{c,1}a_{c,4}}}{a_{c,2}}\right)^2\right]<\kappa<\inf_{\alpha\in\Omega_\alpha}\left[\left(\frac{\Delta_{\bar{M}}^{\frac{1}{4}}+\sqrt{a_{c,1}a_{c,4}}}{a_{c,2}}\right)^2\right] \tag{4.64}$$

Proof of Theorem 4.1: To analyze the stability of the closed-loop system controlled by the designed autopilot, let us consider a following Lyapunov candidate function.

$$V_L=\frac{1}{2}\left(\kappa\alpha^2+q^2\right) \tag{4.65}$$

Note that V_L is positive except for $\alpha=q=0$. Considering Eqs. (4.47) and (4.48), the time derivative of V_L can be obtained as follows,

$$\begin{aligned}\dot{V}_L&=\kappa\alpha\dot{\alpha}+q\dot{q}=\kappa a_{c,1}\alpha^2+(\kappa a_{c,2}+a_{c,3})\alpha q+a_{c,4}q^2\\&=\begin{bmatrix}\alpha & q\end{bmatrix}\begin{bmatrix}\kappa a_{c,1} & \frac{\kappa a_{c,2}+a_{c,3}}{2}\\ \frac{\kappa a_{c,2}+a_{c,3}}{2} & a_{c,4}\end{bmatrix}\begin{bmatrix}\alpha\\ q\end{bmatrix}=x_l^TA_\kappa(x_l)x_l\end{aligned} \tag{4.66}$$

The matrix $A_\kappa(x_l)$ is symmetric, and its characteristic polynomial can be obtained as follows,

$$\begin{aligned}&\lambda[A_\kappa(x_l)]^2-(\kappa a_{c,1}+a_{c,4})\lambda[A_\kappa(x_l)]+\kappa a_{c,1}a_{c,4}-\frac{1}{4}(\kappa a_{c,2}+a_{c,3})^2\\&=\lambda[A_\kappa(x_l)]^2-u_3\lambda[A_\kappa(x_l)]+\frac{1}{4}u_4=0\end{aligned} \tag{4.67}$$

where

$$u_3 = \kappa a_{c,1} + a_{c,4}, \quad u_4 = -a_{c,2}^2\kappa^2 + 2(2a_{c,1}a_{c,4} - a_{c,2}a_{c,3})\kappa - a_{c,3}^2$$

Note that u_3 is negative, because $a_{c,1}$ and $a_{c,4}$ are negative on Ω_l as proven in **Lemma 4.5** and **4.6**, respectively. Therefore, if u_4 is positive, $A_\kappa(x_l)$ is negative definite on Ω_l. Using Eqs. (4.49) and (4.51), the following relation can be obtained.

$$a_{c,1}a_{c,4} - a_{c,2}a_{c,3} = \sqrt{\Delta_{\bar{M}}} \tag{4.68}$$

Using Eq. (4.68), u_4 can be rewritten as follows,

$$u_4 = -a_{c,2}^2 \left(\kappa - \kappa_{\min}\right)\left(\kappa - \kappa_{\max}\right) \tag{4.69}$$

where

$$\kappa_{\min} = \left(\frac{\Delta_{\bar{M}}^{\frac{1}{4}} - \sqrt{a_{c,1}a_{c,4}}}{a_{c,2}}\right)^2, \quad \kappa_{\max} = \left(\frac{\Delta_{\bar{M}}^{\frac{1}{4}} + \sqrt{a_{c,1}a_{c,4}}}{a_{c,2}}\right)^2$$

Here, $\kappa_{\max}$ is greater than $\kappa_{\min}$, because $\Delta_{\bar{M}}^{\frac{1}{4}}$ and $\sqrt{a_{c,1}a_{c,4}}$ are positive on Ω_l. If $\kappa = (\kappa_{\min} + \kappa_{\max})/2$, u_4 is positive which can be written as follows,

$$u_4 = \frac{4a_{c,1}a_{c,4}\sqrt{\Delta_{\bar{M}}}}{a_{c,2}^2} > 0 \quad \text{at} \quad \kappa = \frac{\kappa_{\min} + \kappa_{\max}}{2} \tag{4.70}$$

Considering Eqs. (4.69) and (4.70), the relation between u_4 and κ for any fixed $\alpha \in \Omega_\alpha$ can be plotted as shown in Fig. 4.1. If the constant κ is chosen as a value between $\kappa_{\min}$ and $\kappa_{\max}$ for all $\alpha \in \Omega_\alpha$, then u_4 is positive on Ω_l. Therefore, the following condition for the constant κ can be obtained.

$$\sup_{\alpha\in\Omega_\alpha}\left[\kappa_{\min}\right] < \kappa < \inf_{\alpha\in\Omega_\alpha}\left[\kappa_{\max}\right] \tag{4.71}$$

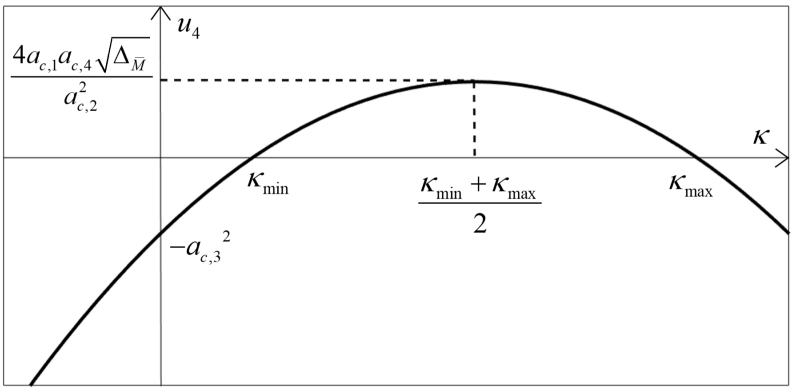

Figure 4.1 The relation between u_4 and κ for any fixed $\alpha \in \Omega_\alpha$

Now, $A_\kappa(x_l)$ is negative definite for the constant κ satisfying Eq. (4.71), and therefore the state vector x_l of the closed-loop system converges to the origin on Ω_l under **Assumptions 4.1-4.4**. □

Remark 4.3: Theorem 4.1 guarantees that the region of attraction contains the operational range of the missile for the closed-loop system controlled by the designed autopilot. In other words, if the constant κ satisfying Eq. (4.71) exists for the defined operational range and weighting parameters, then the states converge to the origin in finite-time and are maintained thereafter for any initial points on the defined operational range. This conclusion provides a solid theoretical basis for the SDRE method to be used in real practices with the guaranteed stable region. The characteristic provided by **Theorem 4.1** is significant in that it outweighs the existing studies which are limited only to the local version of stability properties.

4.4 Numerical Example

This section provides a numerical example of the analytical results which are shown in this chapter. The hypothetical aerodynamic data and physical parameters of the tail-fin controlled missile in Sec. 3.3 are used in this section. The operational range of angle of attack is set as

$$\Omega_\alpha = \{\alpha \in \mathbb{R} | -\pi/6 < \alpha < \pi/6\} \tag{4.72}$$

The coefficients in Eq. (4.33) are obtained from Eq. (3.54) as follows,

$$\begin{aligned} &C_{Z_\alpha}(x_l) = -39.571\alpha^2 - 12.956, \quad C_{m_\alpha}(x_l) = -81.189\alpha^2 - 4.871 \\ &C_{Z_{\delta_p}} = -1.948, \quad C_{m_{\delta_p}} = -11.803, \quad \hat{C}_{m_q} = -1.719 \end{aligned} \tag{4.73}$$

Note that all coefficients in Eq. (4.73) are negative for $\alpha \in \Omega_\alpha$. Using the missile data, a_1, a_2, a_3, b_1, and b_2 can be calculated as

$$\begin{aligned} &a_1 = 0.042C_{Z_\alpha}(x_l), \quad a_2 = 4.950C_{m_\alpha}(x_l), \quad a_3 = 4.950\hat{C}_{m_q} \\ &b_1 = 0.042C_{Z_{\delta_p}}, \quad b_2 = 4.950C_{m_{\delta_p}} \end{aligned} \tag{4.74}$$

Using Eqs. (4.73) and (4.74), the value of $4a_1b_1 + b_2$ in **Assumption 4.3** is expressed as

$$4a_1b_1 + b_2 = 0.544\alpha^2 - 58.247 \tag{4.75}$$

Because Eq. (4.75) is negative for $\alpha \in \Omega_\alpha$, **Assumption 4.3** is satisfied for the numerical values of the considered missile model. Similarly, $(a_3b_1+b_2)a_1-2a_2b_1$ in **Assumption 4.4** can be expressed as

$$(a_3b_1 + b_2)a_1 - 2a_2b_1 = 30.183\alpha^2 + 27.468 \tag{4.76}$$

Note that Eq. (4.76) is positive for $\alpha \in \Omega_\alpha$. Therefore, **Assumption 4.4** is also satisfied for the numerical values of the considered missile model.

To examine the effects of aerodynamic uncertainty on the analytical results, the uncertainties of $C_{m_\alpha}(x_l)$ and $C_{m_{\delta_p}}$ are considered as follows,

$$\begin{aligned} C_{m_\alpha}(x_l) &= \bar{C}_{m_\alpha} + \Delta C_{m_\alpha} \\ C_{m_{\delta_p}} &= \bar{C}_{m_{\delta_p}} + \Delta C_{m_{\delta_p}} \end{aligned} \tag{4.77}$$

where $\bar{C}_{m_\alpha}$ and $\bar{C}_{m_{\delta_p}}$ represent nominal values of the coefficients, and the uncertainties ΔC_{m_α} and $\Delta C_{m_{\delta_p}}$ are modeled as values proportional to the nominal values, i.e., $\Delta C_{m_\alpha} = \gamma_1 \bar{C}_{m_\alpha}$ and $\Delta C_{m_{\delta_p}} = \gamma_2 \bar{C}_{m_{\delta_p}}$ with $\gamma_1, \gamma_2 \in \mathbb{R}$. Considering the relation between the force and moment aerodynamic coefficients, the force coefficients including the uncertainties can be expressed as follows,

$$\begin{aligned} C_{Z_\alpha}(x_l) &= \bar{C}_{Z_\alpha} + \gamma_1 \bar{C}_{Z_\alpha} \\ C_{Z_{\delta_p}} &= \bar{C}_{Z_{\delta_p}} + \gamma_2 \bar{C}_{Z_{\delta_p}} \end{aligned} \tag{4.78}$$

where $\bar{C}_{Z_\alpha}$ and $\bar{C}_{Z_{\delta_p}}$ represent nominal values of the coefficients. For **Assumption 4.3**, $4a_1b_1 + b_2$ including the uncertainties can be obtained as follows,

$$4a_1b_1 + b_2 = 0.544(1 + \gamma_1 + \gamma_2 + \gamma_1\gamma_2)\alpha^2 + (1 + \gamma_2)(0.178\gamma_1 - 58.247) \tag{4.79}$$

Figure 4.2 shows the supremum value of Eq. (4.79) with respect to $\alpha \in \Omega_\alpha$ for γ_1, $\gamma_2 \in [-1.5, 1.5]$, where γ_2 has the most influence on the supremum value compared with γ_1. Note that the range of γ_2 guaranteeing the negative value for the supremum of Eq. (4.79) can be computed as $|\gamma_2| < 1$ for $\gamma_1 \in [-1.5, 1.5]$. Therefore, **Assumption 4.3** holds for the uncertainties of the aerodynamic coefficients less than 100% of the nominal value. To examine the robustness of **Assumption 4.4**, $(a_3b_1 + b_2)a_1 - 2a_2b_1$ is expressed including the uncertainties as

$$(a_3b_1 + b_2)a_1 - 2a_2b_1 = (\gamma_1 + 1)(\gamma_2 + 1)(30.183\alpha^2 + 27.468) \tag{4.80}$$

where $30.183\alpha^2+27.468$ is positive for $\alpha \in \Omega_\alpha$. Figure 4.3 shows the sign of $(\gamma_1+1)(\gamma_2+1)$ for γ_1, $\gamma_2 \in [-1.5, 1.5]$, where blue and red areas represent positive and negative signs, respectively. In Fig. 4.3, the positive sign of $(\gamma_1+1)(\gamma_2+1)$ holds if both γ_1 and γ_2 are greater than -1, which implies that **Assumption 4.4** also holds if both uncertainties of the aerodynamic coefficients are less than 100% of the nominal values.

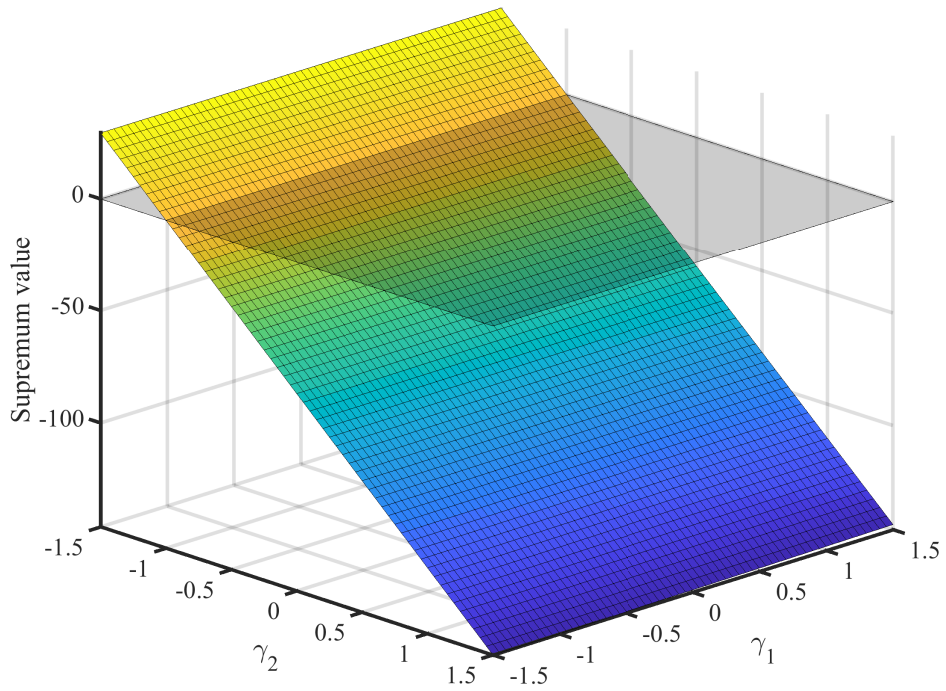

Figure 4.2 Supremum value of $4a_1b_1 + b_2$ with respect to $\alpha \in \Omega_\alpha$ for γ_1, $\gamma_2 \in [-1.5, 1.5]$

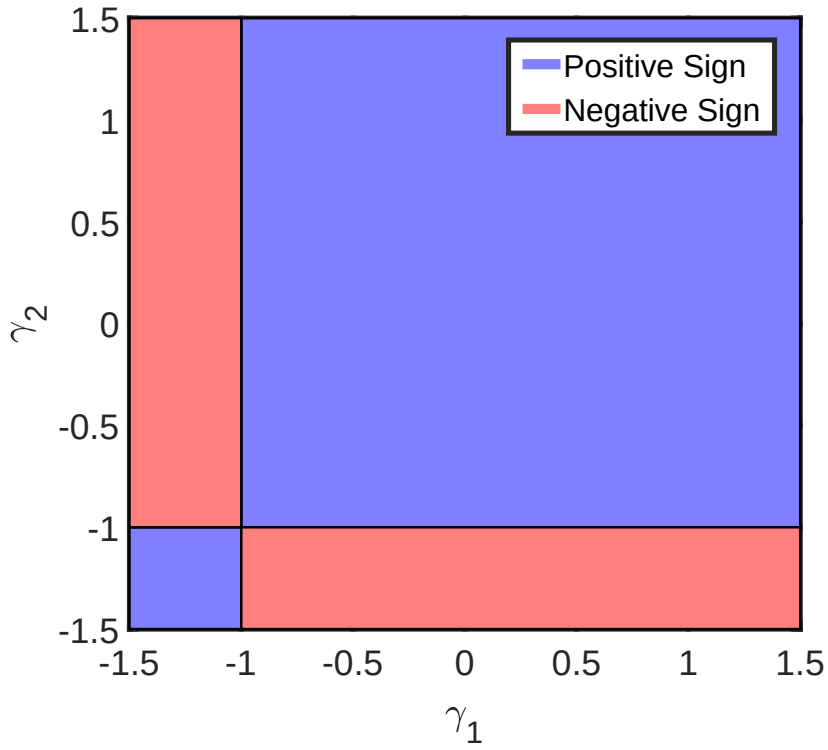

Figure 4.3 Sign of $(\gamma_1 + 1)(\gamma_2 + 1)$ for γ_1, $\gamma_2 \in [-1.5, 1.5]$

Numerical simulation is performed for the missile model to demonstrate the performance of the designed autopilot and to verify the analytical results. The weighting parameters q_w and r_w are set to be 1 and 20,000, respectively. Now, the following values of $\kappa_{\min}$ and $\kappa_{\max}$ at $\bar{w} = 5 \times 10^{-5}$ can be calculated.

$$\begin{aligned} \sup_{\alpha \in \Omega_\alpha} [\kappa_{\min}] &= \sup_{\alpha \in \Omega_\alpha} \left[\left(\frac{\Delta_{\bar{M}}^{\frac{1}{4}} - \sqrt{a_{c,1} a_{c,4}}}{a_{c,2}} \right)^2 \right] = 127.767 \\ \inf_{\alpha \in \Omega_\alpha} [\kappa_{\max}] &= \inf_{\alpha \in \Omega_\alpha} \left[\left(\frac{\Delta_{\bar{M}}^{\frac{1}{4}} + \sqrt{a_{c,1} a_{c,4}}}{a_{c,2}} \right)^2 \right] = 227.279 \end{aligned} \tag{4.81}$$

Since the supremum of $\kappa_{\min}$ with respect to $\alpha \in \Omega_\alpha$ is smaller than the infimum of $\kappa_{\max}$ with respect to $\alpha \in \Omega_\alpha$, the closed-loop system controlled by the designed autopilot for the considered missile model is asymptotically stable on Ω_l based on **Theorem 4.1**.

Figures 4.4-4.6 show the simulation results. Figure 4.4 shows the time responses of the Z-axis acceleration and the pitch fin deflection, where the solid line represents the responses of the designed autopilot and the dotted line represents the signal of the acceleration command. Figure 4.5 shows the time responses of the states, i.e., the angle of attack and pitch rate. As shown in the simulation results, the designed autopilot has satisfactory tracking performance within the defined operational range of the missile. Furthermore, to verify the correctness of the analytic solution of the SDRE method, which is obtained in Sec. 4.2, the solution of the state-dependent ARE is computed in two ways: i) the analytic way presented in Eq. (4.25), and ii) the online computation using the numerical algorithm [66]. Figure 4.6 shows the time response of the differences of the solution components calculated by the analytic and numerical ways, where $e_{i,j}$ represents the difference of the components $x_{i,j}$ computed in

two ways. As shown in Fig. 4.6, the magnitude of $e_{i,j}$ is smaller than 1×10^{-10} for all i and j. Therefore, the time response of the analytic solution is same as the solution obtained by the online computation, which verifies that the analytic solution obtained in Sec. 4.2 is correct.

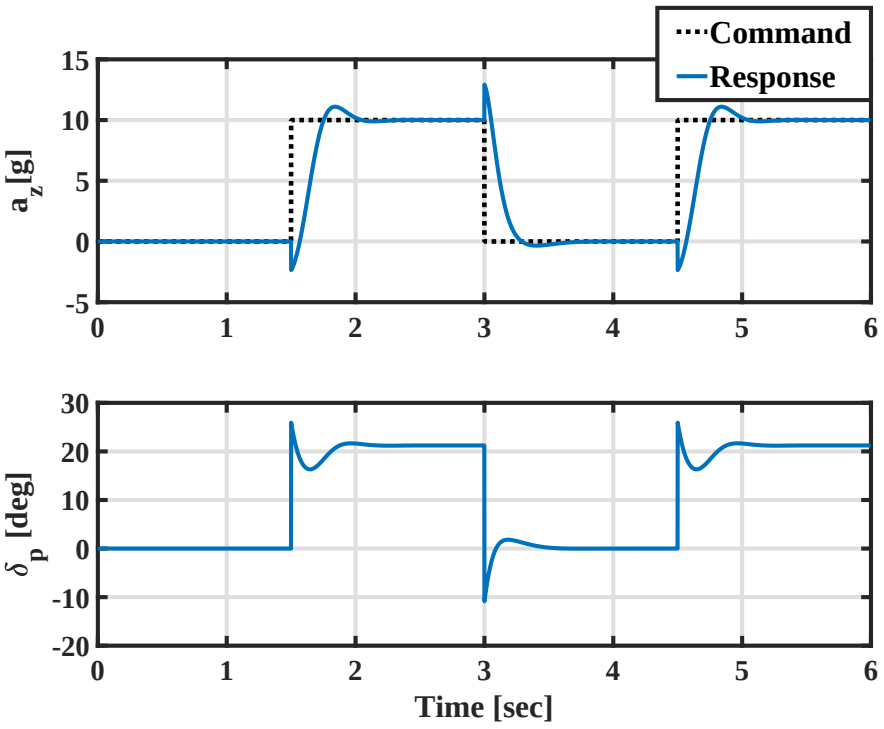

Figure 4.4 Time responses of Z-axis acceleration and pitch fin deflection

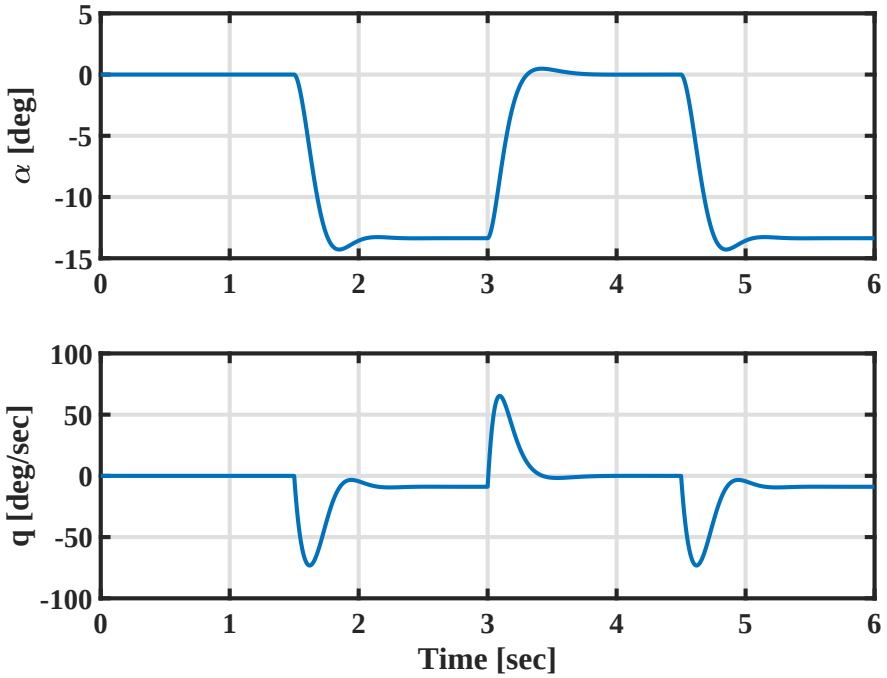

Figure 4.5 Time responses of the state variables

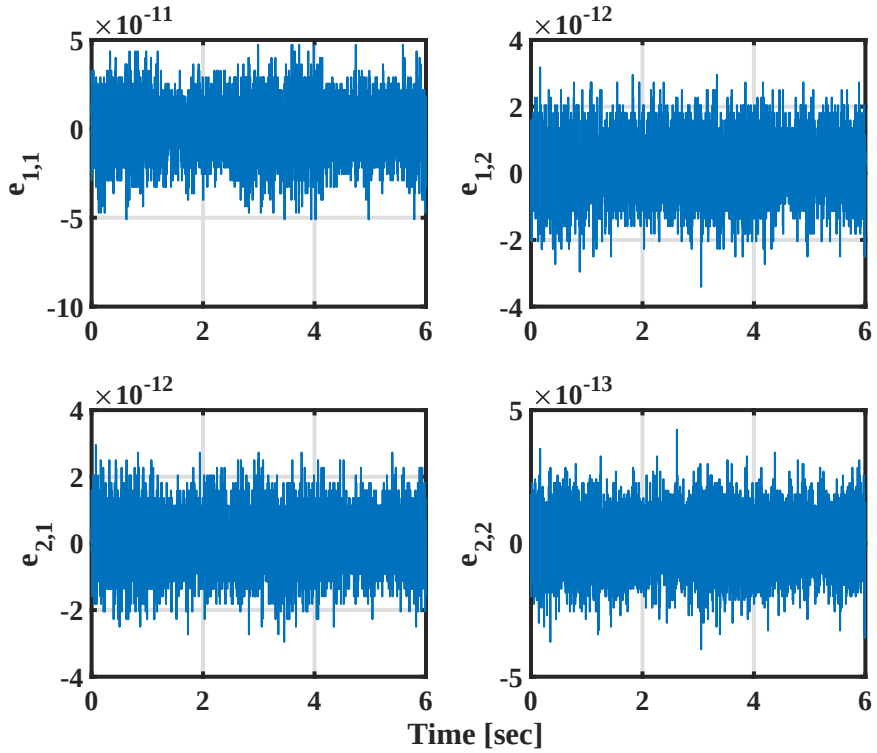

Figure 4.6 Time responses of the differences between the solution components

Chapter 5

Three-Axes and Full-Order Missile Autopilots

5.1 Problem Statement

In this chapter, the three-axes missile autopilot is designed using the longitudinal autopilot proposed in Chap. 4. Because of the axial symmetry of the skid-to-turn maneuver missile considered in this study, the pitch and yaw planes of the missile can be handled separately if the roll motion is stabilized. Accordingly, the autopilot design based on the longitudinal dynamics of the missile is applied to both pitch and yaw planes of the missile, while a proportional-derivative (PD) controller stabilizes the roll motion. Note that the sideslip angle and yaw rate are specified as the state variables in yaw plane instead of the angle of attack and pitch rate. Furthermore, a design procedure of the SDRE-based missile autopilot is provided based on the full-order missile model for comparison. In the numerical simulation, the control performance of the three-axes missile autopilot is compared with that of the full-order missile model-based autopilot.

5.2 Three-Axes and Full-Order Autopilot Design

5.2.1 Three-Axes Autopilot Design

To apply the autopilot design proposed in Chap. 4 to the six-degrees-of-freedom model of the tail-fin controlled missile, this section designs the three-axes autopilot. In this study, the skid-to-turn maneuver missile is considered which has the axial symmetric around X-axis of the missile body. Therefore, if the fast roll stabilization is assumed, the pitch and yaw planes of the missile can be controlled separately. Using this property, the proposed autopilot designed on the longitudinal motion of the missile is applied to both pitch and yaw planes, and the roll motion is stabilized using the PD controller.

Figure 5.1 shows the block diagram of the three-axes acceleration autopilot proposed in the study, where $\delta_{r,c}$, $\delta_{p,c}$, and $\delta_{y,c}$ are the commands of the roll, pitch, and yaw fin deflections, respectively. As shown in this figure, the SDRE-based pitch and yaw controllers designed in Chap. 4 generate the commands of the pitch and yaw fin deflections, respectively, while the PD controller generates the command of the roll fin deflection for stabilizing the roll motion of the missile, which is designed as follows,

$$u_\phi = -K_p\phi - K_d\dot{\phi} \tag{5.1}$$

where ϕ is the roll angle of the missile, u_ϕ is the PD control input, and K_p and K_d are the proportional and derivative control gains of the PD controller, respectively. Similar to the pitch controller designed in Chap. 4, the SDRE-based yaw controller is designed except for specifying the sideslip angle and yaw rate as the state variables instead of the angle of attack and pitch rate, where the lateral equations of motions are used as described in Eq. (2.18).

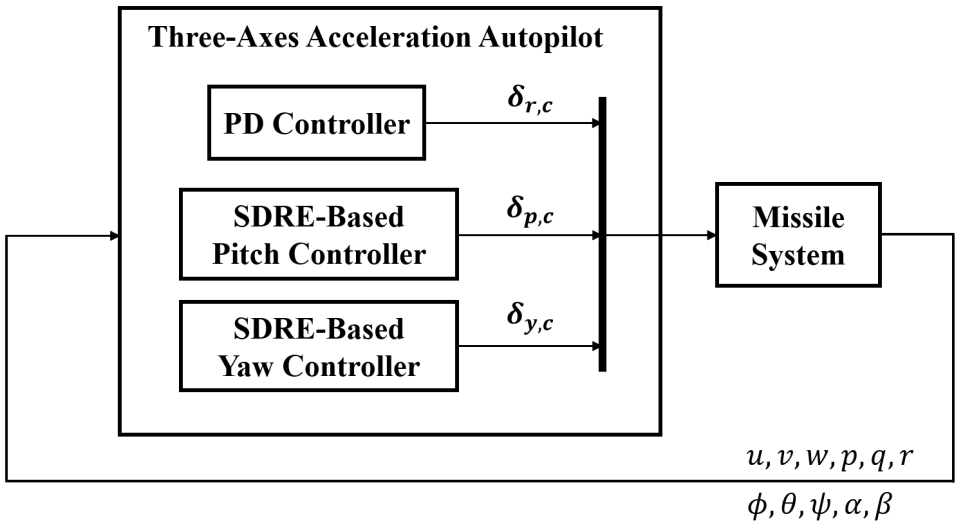

Figure 5.1 Block diagram of three-axes acceleration autopilot

5.2.2 Full-Order Autopilot Design

In this subsection, the SDRE-based acceleration autopilot based on the full-order missile model is designed for comparison with the designed acceleration autopilot based on the reduced-order missile model. Figure 5.2 shows the block diagram of the full-order missile model-based acceleration autopilot, where p_c, q_c, and r_c are the commands of the angular rates. As shown in Fig. 5.2, the full-order autopilot has a two-loop structure consisting of the inner- and outer-loops. The outer-loop controller generates the command inputs of the angular rates and sends them to the inner-loop controller. Then, the inner-loop controller generates the commands of the fin deflections corresponding to the commands of the angular rates. The two-loop design enables the tail-fin controlled missile to be controlled more efficiently by separating relatively fast and slow variables. Furthermore, it provides more design flexibility and computational efficiency by handling small SDC matrices in the SDRE method. First of all, applying small-perturbation theory and first-order Taylor expansion to the aerodynamic

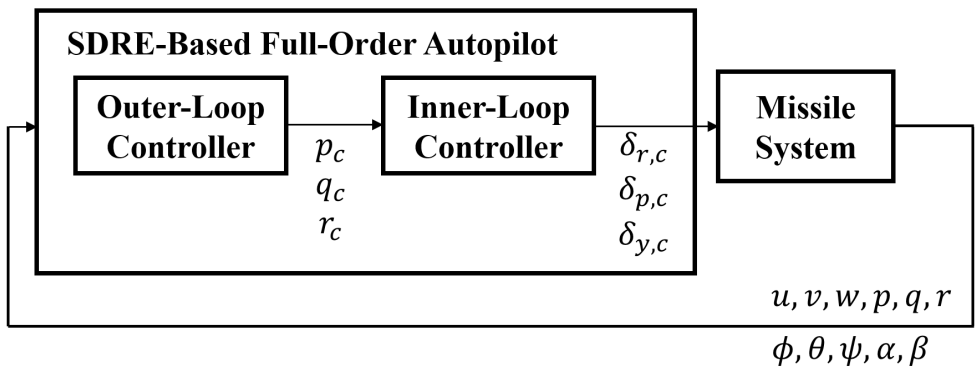

Figure 5.2 Block diagram of full-order acceleration autopilot

coefficients presented in Eqs. (2.5) and (2.7), the following types of aerodynamic coefficients are used in designing the full-order acceleration autopilot.

$$\begin{aligned}
\hat{C}_Y &= C_{Y_0} + C_{Y_{\mathbf{M}}}\mathbf{M} + C_{Y_\alpha}\alpha + C_{Y_\beta}\beta + C_{Y_{\delta_r}}\delta_r + C_{Y_{\delta_p}}\delta_p + C_{Y_{\delta_y}}\delta_y \\
\hat{C}_Z &= C_{Z_0} + C_{Z_{\mathbf{M}}}\mathbf{M} + C_{Z_\alpha}\alpha + C_{Z_\beta}\beta + C_{Z_{\delta_r}}\delta_r + C_{Z_{\delta_p}}\delta_p + C_{Z_{\delta_y}}\delta_y \\
\hat{C}_l &= C_{l_0} + C_{l_\alpha}\alpha + C_{l_\beta}\beta + C_{l_{\delta_r}}\delta_r + C_{l_{\delta_p}}\delta_p + C_{l_{\delta_y}}\delta_y \\
\hat{C}_m &= C_{m_0} + C_{m_\alpha}\alpha + C_{m_\beta}\beta + C_{m_{\delta_r}}\delta_r + C_{m_{\delta_p}}\delta_p + C_{m_{\delta_y}}\delta_y \\
\hat{C}_n &= C_{n_0} + C_{n_\alpha}\alpha + C_{n_\beta}\beta + C_{n_{\delta_r}}\delta_r + C_{n_{\delta_p}}\delta_p + C_{n_{\delta_y}}\delta_y
\end{aligned} \tag{5.2}$$

Substituting Eq. (5.2) into Eq. (2.9), the rotational equations of the missile can be obtained as follows,

$$\begin{aligned}
\dot{p} &= \frac{QSD}{I_{xx}}\left(C_{l_0} + C_{l_\alpha}\alpha + C_{l_\beta}\beta + C_{l_{\delta_r}}\delta_r + C_{l_{\delta_p}}\delta_p + C_{l_{\delta_y}}\delta_y + \frac{D}{2V}C_{l_p}p\right) \\
&= L_{bias} + L_p p + L_{\delta_r}\delta_r + L_{\delta_p}\delta_p + L_{\delta_y}\delta_y \\
\dot{q} &= \frac{I_{zz} - I_{xx}}{I_{yy}}pr + \frac{QSD}{I_{yy}}\Bigg(C_{m_0} + C_{m_\alpha}\alpha + C_{m_\beta}\beta \\
&\qquad + C_{m_{\delta_r}}\delta_r + C_{m_{\delta_p}}\delta_p + C_{m_{\delta_y}}\delta_y + \frac{D}{2V}C_{m_q}q\Bigg) \\
&= M_{bias} + M_q q + M_{pr}pr + M_{\delta_r}\delta_r + M_{\delta_p}\delta_p + M_{\delta_y}\delta_y \\
\dot{r} &= \frac{I_{xx} - I_{yy}}{I_{zz}}pq + \frac{QSD}{I_{zz}}\Bigg(C_{n_0} + C_{n_\alpha}\alpha + C_{n_\beta}\beta \\
&\qquad + C_{n_{\delta_r}}\delta_r + C_{n_{\delta_p}}\delta_p + C_{n_{\delta_y}}\delta_y + \frac{D}{2V}C_{n_r}r\Bigg) \\
&= N_{bias} + N_r r + N_{pq}pq + N_{\delta_r}\delta_r + N_{\delta_p}\delta_p + N_{\delta_y}\delta_y
\end{aligned} \tag{5.3}$$

where L_{bias}, M_{bias}, and N_{bias} are the terms that do not depend on the angular rates and the fin deflections, and $L_{(\cdot)}$, $M_{(\cdot)}$, and $N_{(\cdot)}$ are dimensional coefficients with respect to $(\cdot)$. Also, the following kinematic equation of the roll angle is

used.

$$\dot{\phi} = p + q\sin\phi\tan\theta + r\cos\phi\tan\theta \tag{5.4}$$

where θ is the pitch angle of the missile. To derive the dynamics of Y- and Z-axes acceleration, differentiating $\hat{C}_Y$ and $\hat{C}_Z$ in Eqs. (5.2) with respect to time and substituting the resulting equation and Eqs. (2.12) and (2.13) into the time derivative of the Y- and Z-axes acceleration yield

$$\begin{aligned}
\dot{a}_y &= \frac{2QS}{Vm}(a_x\cos\alpha\cos\beta + a_y\sin\beta + a_z\sin\alpha\cos\beta)\hat{C}_Y \\
&\quad + \frac{QS}{m}\Bigg[\frac{1}{a_s}(a_x\cos\alpha\cos\beta + a_y\sin\beta + a_z\sin\alpha\cos\beta)C_{Y_{\mathbf{M}}} \\
&\qquad + \{q - (p\cos\alpha + r\sin\alpha)\tan\beta + \frac{1}{V\cos\beta}(a_z\cos\alpha - a_x\sin\alpha)\}C_{Y_\alpha} \\
&\qquad + \{p\sin\alpha - r\cos\alpha - \frac{1}{V}(a_x\cos\alpha\sin\beta - a_y\cos\beta + a_z\sin\alpha\sin\beta)\}C_{Y_\beta} \\
&\quad + C_{Y_{\delta_r}}\dot{\delta}_r + C_{Y_{\delta_p}}\dot{\delta}_p + C_{Y_{\delta_y}}\dot{\delta}_y\Bigg] \\
&= Y_{bias} + Y_{a_z}a_z + Y_{a_y}a_y + Y_p p + Y_q q + Y_r r \\
\dot{a}_z &= \frac{2QS}{Vm}(a_x\cos\alpha\cos\beta + a_y\sin\beta + a_z\sin\alpha\cos\beta)\hat{C}_Z \\
&\quad + \frac{QS}{m}\Bigg[\frac{1}{a_s}(a_x\cos\alpha\cos\beta + a_y\sin\beta + a_z\sin\alpha\cos\beta)C_{Z_{\mathbf{M}}} \\
&\qquad + \{q - (p\cos\alpha + r\sin\alpha)\tan\beta + \frac{1}{V\cos\beta}(a_z\cos\alpha - a_x\sin\alpha)\}C_{Z_\alpha} \\
&\qquad + \{p\sin\alpha - r\cos\alpha - \frac{1}{V}(a_x\cos\alpha\sin\beta - a_y\cos\beta + a_z\sin\alpha\sin\beta)\}C_{Z_\beta} \\
&\quad + C_{Z_{\delta_r}}\dot{\delta}_r + C_{Z_{\delta_p}}\dot{\delta}_p + C_{Z_{\delta_y}}\dot{\delta}_y\Bigg] \\
&= Z_{bias} + Z_{a_z}a_z + Z_{a_y}a_y + Z_p p + Z_q q + Z_r r
\end{aligned} \tag{5.5}$$

where a_s is the speed of sound, Y_{bias} and Z_{bias} are the terms that do not depend on the accelerations and the angular rates, and $Y_{(\cdot)}$ and $Z_{(\cdot)}$ are dimensional coefficients with respect to $(\cdot)$.

The outer-loop controller is designed to deal with the Y- and Z-axes accelerations and roll angle of the missile. Therefore, Eqs. (5.4) and (5.5) are transformed into the following pseudo-linear system using the SDC transformation.

$$\dot{x}_O = A_O(x_O)x_O + B_O(x_O)u_O \tag{5.6}$$

where

$$x_O = [\ \phi \quad a_z \quad a_y \quad s_o\ ]^T, \quad u_O = [\ p \quad q \quad r\ ]^T$$

$$A_O(x_O) = \begin{bmatrix} 0 & 0 & 0 & 0 \\ 0 & Z_{a_z} & Z_{a_y} & Z_{bias}/s_o \\ 0 & Y_{a_z} & Y_{a_y} & Y_{bias}/s_o \\ 0 & 0 & 0 & -\lambda_o \end{bmatrix}$$

$$B_O(x_O) = \begin{bmatrix} 1 & \sin\phi\tan\theta & \cos\phi\tan\theta \\ Z_p & Z_q & Z_r \\ Y_p & Y_q & Y_r \\ 0 & 0 & 0 \end{bmatrix}$$

Note that s_o is an additional state to treat the bias terms, which is governed by the following stable dynamics.

$$\dot{s}_o = -\lambda_o s_o \tag{5.7}$$

where λ_o is a positive constant. Similarly, the inner-loop controller deals with the angular rates of the missile, and Eq. (5.3) is transformed into the following pseudo-linear system using the SDC transformation.

$$\dot{x}_I = A_I(x_I)x_I + B_I(x_I)u_I \tag{5.8}$$

where

$$x_I = [\ p \quad q \quad r \quad s_i\ ]^T, \quad u_I = [\ \delta_r \quad \delta_p \quad \delta_y\ ]^T$$

$$A_I(x_I) = \begin{bmatrix} L_p & 0 & 0 & L_{bias}/s_i \\ \sigma_{pr} M_{pr} r & M_q & (1-\sigma_{pr}) M_{pr} p & M_{bias}/s_i \\ \sigma_{pq} N_{pq} q & (1-\sigma_{pq}) N_{pq} p & N_r & N_{bias}/s_i \\ 0 & 0 & 0 & -\lambda_i \end{bmatrix}$$

$$B_I(x_I) = \begin{bmatrix} L_{\delta_r} & L_{\delta_p} & L_{\delta_y} \\ M_{\delta_r} & M_{\delta_p} & M_{\delta_y} \\ N_{\delta_r} & N_{\delta_p} & N_{\delta_y} \\ 0 & 0 & 0 \end{bmatrix}$$

Note that $\sigma_{pr} \in [0,1]$ and $\sigma_{pq} \in [0,1]$ are design parameters that provide the non-uniqueness of the SDC transformation. A variable s_i is an additional state to augment bias terms L_{bias}, M_{bias}, and N_{bias} in the SDC matrix, and its dynamics is described as

$$\dot{s_i} = -\lambda_i s_i \tag{5.9}$$

where λ_i is a positive constant. For each pseudo-linear system in Eqs. (5.6) and (5.8), the state-dependent ARE can be constructed as presented in Eq. (2.22). Then, by solving the state-dependent ARE, the following inner- and outer-loop control inputs can be generated.

$$\begin{aligned} u_I &= -R_I(x_I)^{-1} B_I(x_I)^T X_I(x_I) x_I \\ u_O &= -R_O(x_O)^{-1} B_O(x_O)^T X_O(x_O) x_O \end{aligned} \tag{5.10}$$

where $R_I(x_I)$ and $R_O(x_O)$ are the weighting matrices, and $X_I(x_I)$ and $X_O(x_O)$ are the state-dependent ARE solutions for the inner- and outer-loops, respectively.

Remark 5.1: In the full-order acceleration autopilot, each loop deals with a four-dimensional system, and accordingly the dimensions of their solutions of the state-dependent ARE are also four. Because the four-dimensional ARE cannot be solved analytically, each state-dependent ARE should be numerically solved at each step. It leads not only the high computational burden but also preventing the closed-loop system from being analytically represented. Therefore, the only local asymptotic stability of the closed-loop system can be guaranteed for a narrow unknown region of attraction around the equilibrium point based on the point-wise controllability and observability. This lack of the guaranteed stable region is considered as a major obstacle to use the SDRE method in practice, because the autopilot may fail for arbitrary initial states.

5.3 Numerical Simulation

5.3.1 Simulation Setup

To demonstrate the performance of the proposed autopilots, numerical simulations are performed for the two types of missile acceleration autopilots, which are the three-axes autopilot and full-order missile model-based autopilot. In this simulation, the gliding phase of the missile is considered, and therefore no thrust forces of the missile exist and the inertial properties including the mass and the moment of inertia are fixed. For the actuator dynamics of the missile's tail, the second-order dynamics is considered. Table 5.1 summarizes the characteristics of the missile in the numerical simulation. For the skid-to-turn maneuver missile, zero roll angle should be maintained for the entire flight time. Therefore, the roll command is set as zero during the simulation. The commands of the Y- and Z-axes accelerations are summarized in Table. 5.2 for each time interval, where a_{y_c} and a_{z_c} are the commands of the Y- and Z-axes

Table 5.1 Missile characteristics in simulation

Symbol	Name	Value
m	Mass	50.502 kg
I_{xx}	X-Axis Moment of Inertia	$0.325\ \text{kg} \cdot \text{m}^2$
I_{yy}, I_{zz}	Y- and Z-Axes Moment of Inertias	$60.102\ \text{kg} \cdot \text{m}^2$
S	Reference Area	$0.022\ \text{m}^2$
D	Reference Length	0.165 m
ω_n	Natural Frequency of Actuator	30 Hz
ζ	Damping Ratio of Actuator	0.8

Table 5.2 Acceleration commands in simulation

Time Interval [sec]	[0, 0.5)	[0.5, 1.5)	[1.5, 2.5)	[2.5, 3.5)	[3.5, 4]
a_{y_c} [g]	0	10	20	-10	0
a_{z_c} [g]	0	10	20	-10	0

accelerations, respectively. The initial conditions of the total velocity and other states are set to be 950 m/s and zero, respectively, and the operational ranges for the angle of attack and sideslip angle are set as $\pm\pi/6$.

Figure 5.3 shows the time response of the total velocity, where the total velocity decreases slowly from 950 m/s to about 830 m/s due to the aerodynamic effect during the simulation. Before performing numerical simulation, the supremum of $\kappa_{\min}$ and the infimum of $\kappa_{\max}$ of both pitch and yaw plane autopilots with respect to the angle of attack and sideslip angle, respectively, are shown in Fig. 5.4 for the total velocity from 800 m/s to $1,000$ m/s. In Fig. 5.4, the solid line represents the supremum of $\kappa_{\min}$ and the dash-dotted line represents the infimum of $\kappa_{\max}$. As shown in this result, the supremum of $\kappa_{\min}$ is less than 1.15, and the infimum of $\kappa_{\max}$ is much greater than the supremum of $\kappa_{\min}$ for any fixed total velocity from 800 m/s to $1,000$ m/s. It implies that the analytical results of the asymptotic stability presented in **Theorem 4.1** can be applied to both pitch and yaw plane autopilots for any fixed total velocity in the range.

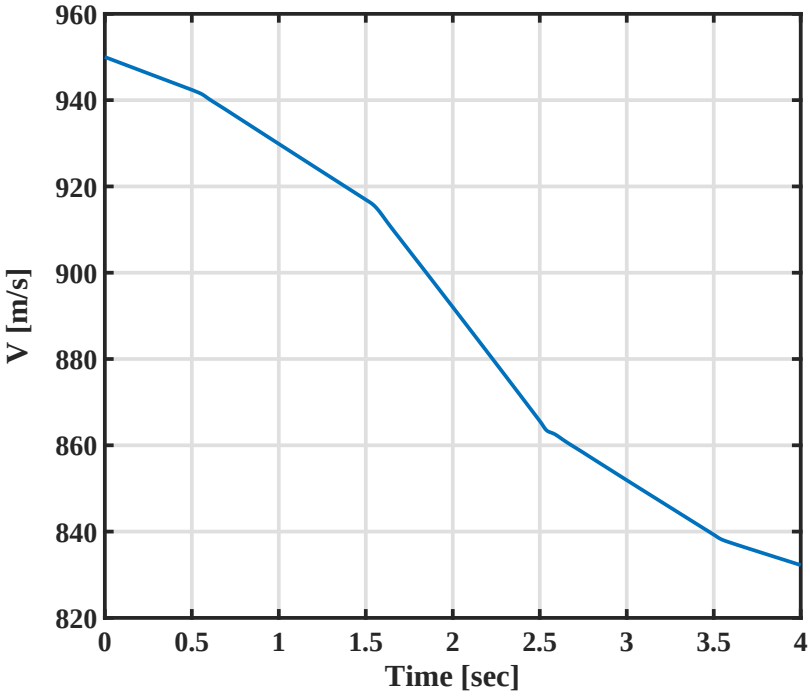

Figure 5.3 Time response of the total velocity

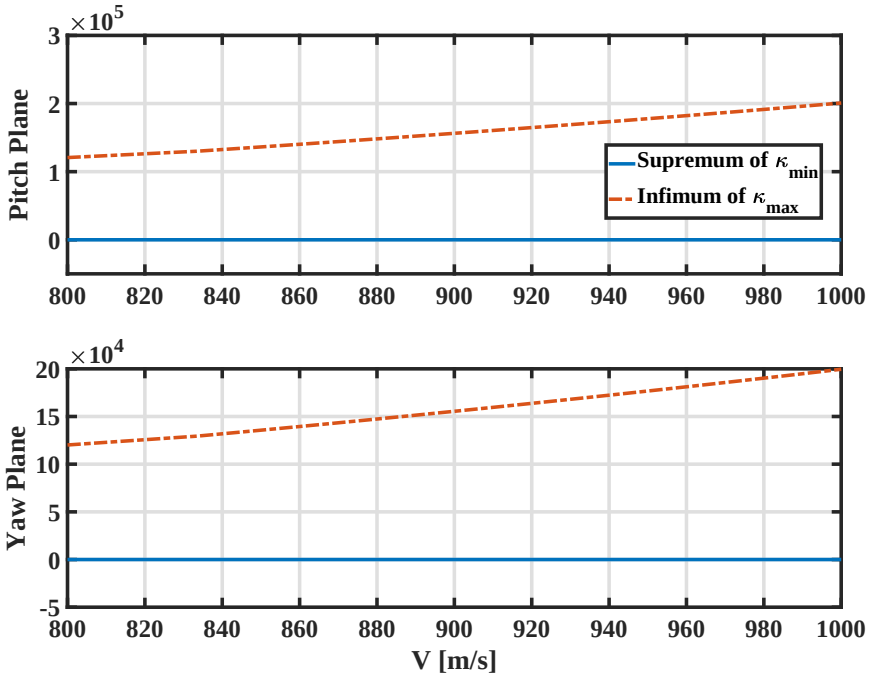

Figure 5.4 Responses of the supremum of $\kappa_{\min}$ and the infimum of $\kappa_{\max}$ versus the total velocity

5.3.2 Simulation Results

Simulation results of the three-axes and full-order autopilots are shown in Figs. 5.5-5.8, where the solid line represents the responses of the full-order autopilot, the dash-dotted line represents the responses of the three-axes autopilot, and the dashed line represents the command signal. Figure 5.5 shows the time responses of roll angle and Y- and Z-axes accelerations, and Fig. 5.6 shows the time responses of the three-channel fin deflections for the two autopilots. As shown in the results, the Y- and Z-axes accelerations of the three-axes autopilot are well regulated within ± 0.1 g. For the non-zero commands of the accelerations, the three-axes autopilot shows satisfactory tracking performance compared to the responses of the full-order autopilot, although there exist steady-state tracking errors of less than 10% due to coupling effects and aerodynamic modeling errors. The roll angle of the three-axes autopilot is regulated within ± 0.5 deg as well, while the magnitude of maximum roll error of the full-order autopilot is about 2 deg. Figure 5.7 shows the time responses of the angle of attack and sideslip angle, and Fig. 5.8 shows the time responses of roll, pitch, and yaw rates for two cases. Note that all states of both pitch and yaw planes in the three-axes autopilot are within the predefined operational ranges of the angle of attack and the sideslip angle.

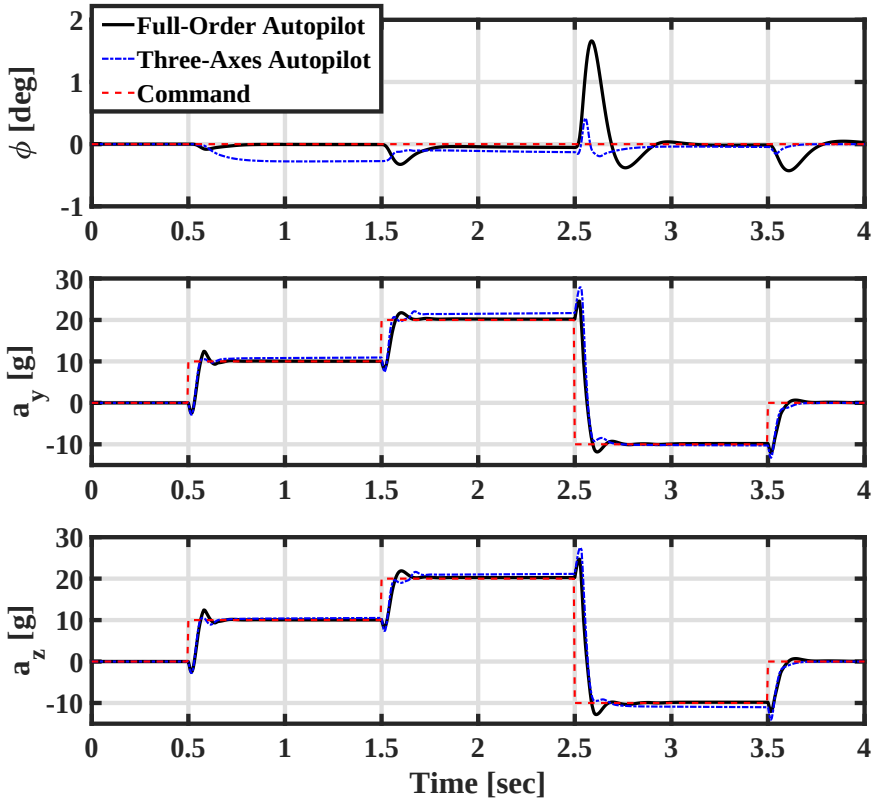

Figure 5.5 Time responses of roll angle and Y- and Z-axes accelerations

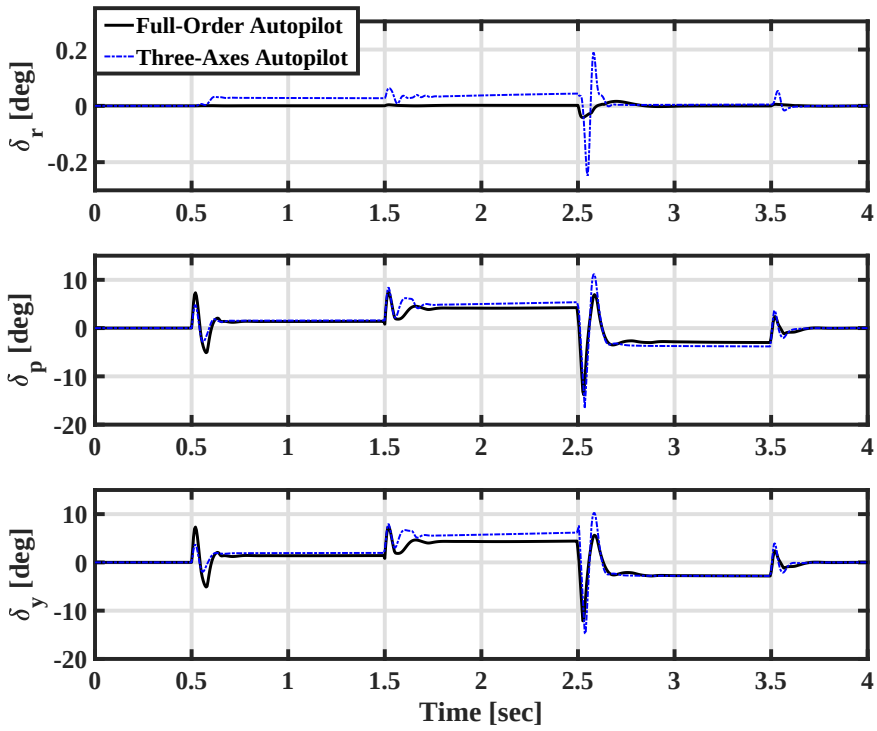

Figure 5.6 Time responses of roll, pitch, and yaw fin deflections

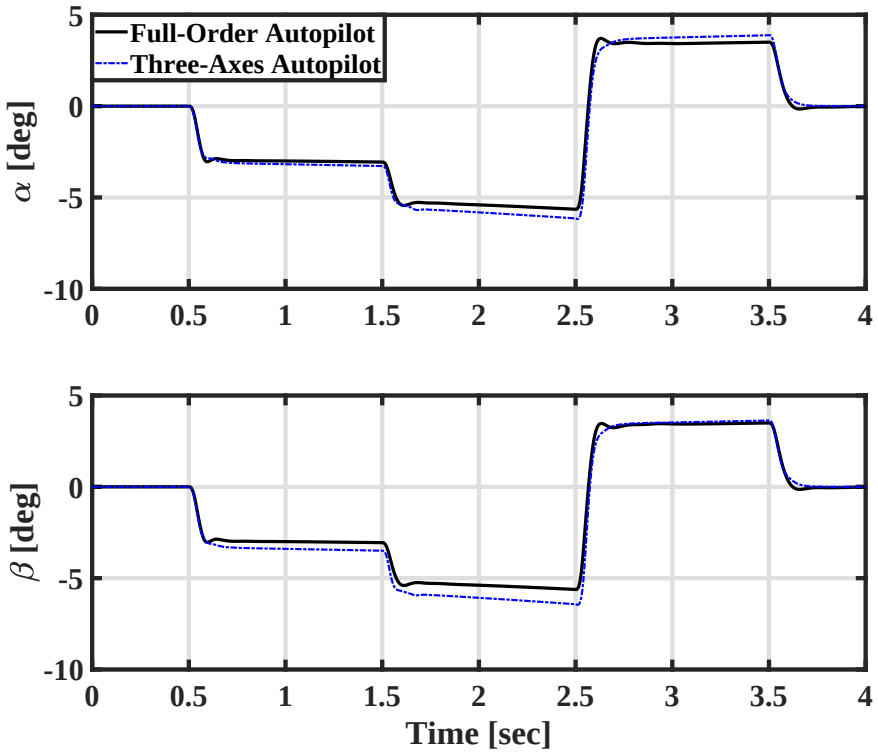

Figure 5.7 Time responses of the angle of attack and sideslip angle

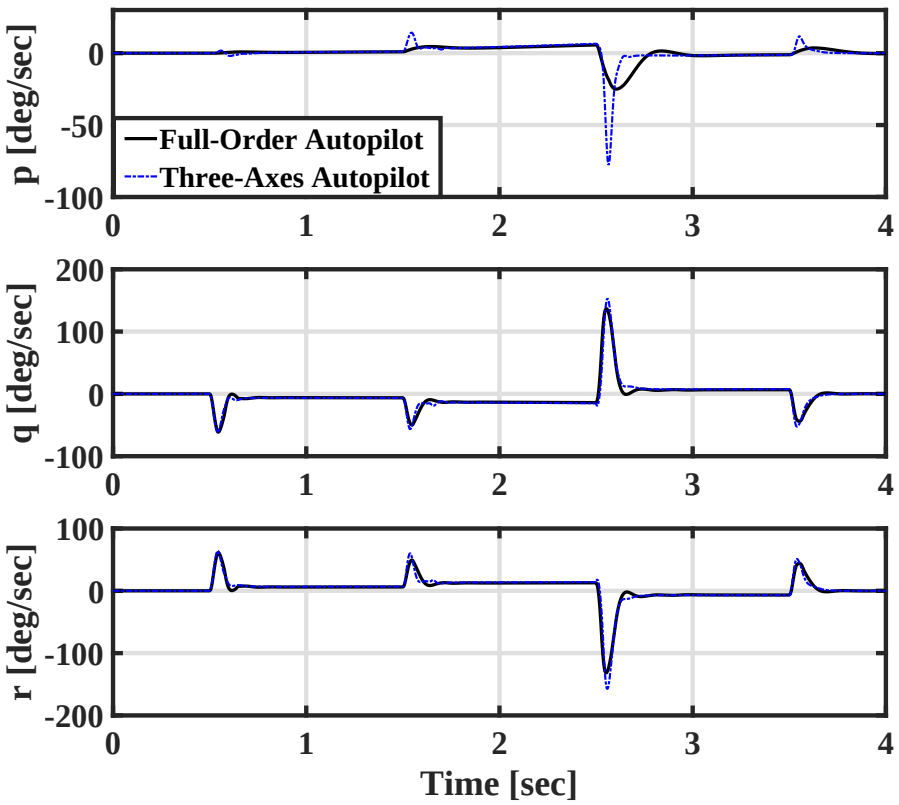

Figure 5.8 Time responses of roll, pitch, and yaw rates

Furthermore, Monte Carlo simulation is performed for the three-axes autopilot to examine the robust performance with respect to the aerodynamic uncertainties. The following force and moment aerodynamic coefficients including uncertainties are applied to the simulation.

$$\begin{aligned} C_Y &= (1+\gamma_1)\bar{C}_Y, \quad C_Z = (1+\gamma_2)\bar{C}_Z \\ C_l &= (1+\gamma_3)\bar{C}_l, \quad C_m = (1+\gamma_4)\bar{C}_m, \quad C_n = (1+\gamma_5)\bar{C}_n \end{aligned} \tag{5.11}$$

where $\bar{C}_Y$, $\bar{C}_Z$, $\bar{C}_l$, $\bar{C}_m$, and $\bar{C}_n$ denote the nominal values of the aerodynamic coefficients, and γ_i, for $i = 1, \cdots, 5$, denote the proportional value for the nominal value, which represents the aerodynamic uncertainties. To examine the robust performance of the three-axes autopilot for various uncertain environments, Monte Carlo simulation of 150 runs is performed for γ_i, for $i = 1, \cdots, 5$, where γ_i has a normal distribution with a zero mean and a standard deviation of 0.1. The acceleration commands summarized in Table 5.2 are also applied to the Monte Carlo simulation. Table 5.3 summarizes the values of the mean and standard deviation of the steady-state acceleration errors for each non-zero acceleration command interval.

Table 5.3 Steady-state errors for non-zero command intervals in Monte Carlo simulation

Time Interval [sec], Acceleration Command [g]	Magnitude of Steady-State Error [g]			
	Mean		Standard Deviation	
	a_y	a_z	a_y	a_z
[0.5, 1.5), 10	0.6012	0.9311	0.3717	0.5404
[1.5, 2.5), 20	1.3546	1.4284	0.7238	0.8691
[2.5, 3.5), -10	0.3675	0.7320	0.2252	0.2941

Figures 5.9 and 5.10 shows the results of Monte Carlo simulation of 150 runs, where the solid line represents the responses of the three-axes autopilot and the dashed line represents the command signal. Figure 5.9 shows the time responses of roll angle and Y- and Z-axes accelerations, and Fig. 5.10 shows the time responses of the three-channel fin deflections for Monte Carlo simulation. Compared to the results of the nominal simulation, the control performance degradations, especially in the transient responses, occur due to the aerodynamic uncertainties. Nevertheless, none of simulation responses of 150 runs diverge and the available levels of control performances in various uncertain environments are achieved even though certain ranges contain some steady-state errors. Additionally, all 150 responses of the roll angles are well regulated within ± 1.5 deg in various uncertain environments.

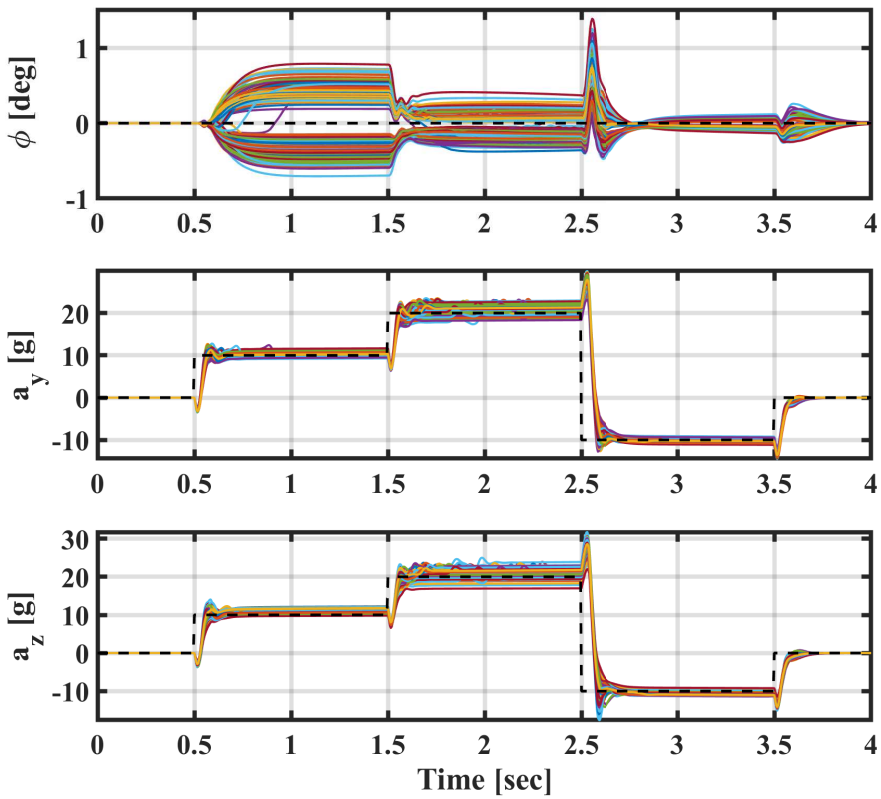

Figure 5.9 Time responses of roll angle and Y- and Z-axes accelerations in Monte Carlo simulation of 150 runs

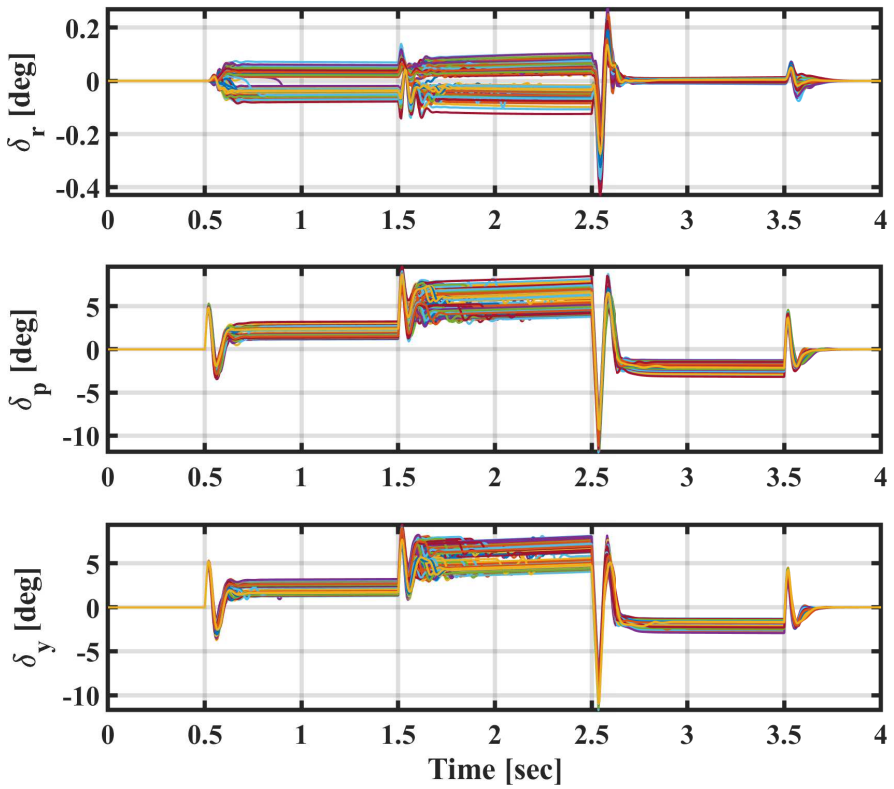

Figure 5.10 Time responses of roll, pitch, and yaw fin deflections in Monte Carlo simulation of 150 runs

Chapter 6

Conclusion

6.1 Concluding Remarks

In this study, a missile acceleration autopilot was designed based on a state-dependent Riccati equation (SDRE) method, and the asymptotic stability of its closed-loop system was analyzed, using an analytic solution of the state-dependent algebraic Riccati equation (ARE). The main results of this study are summarized as follows:

Analysis of the Tail-Fin Controlled Missile

This study provided a rigorous mathematical analysis of the tail-fin controlled missile. This has not been done in previous studies. A valid transformation to normal form equations of the missile was proposed, and the non-minimum phase behavior of the tail-fin controlled missile was analyzed, based on the normal form equations. In addition, closed-loop system behavior with an approximate model-based controller was analyzed, where input-output stability was proven, considering the term causing the non-minimum phase behavior as an external input. This is an improvement on existing work that addressed the boundedness of the tracking error for the closed-loop system.

Missile Acceleration Autopilot Using the State-Dependent Riccati Equation Method

For two-dimensional systems, an analytic solution of the state-dependent ARE was obtained, using a matrix sign function and principal square root of a Hamiltonian matrix. The acceleration autopilot for the tail-fin controlled missile was designed based on the SDRE method, and its asymptotic stability was analyzed using the analytic solution. To utilize the analytic solution for two-dimensional systems, the missile acceleration autopilot was designed based on missile longitudinal dynamics with a short-period approximation. The analytical result will provide a solid theoretical basis for the SDRE method to be practically utilized, with a clearly quantified stable region.

Six-Degrees-of-Freedom Simulation

To demonstrate the control performance of the proposed acceleration autopilot, a numerical simulation based on the six-degrees-of-freedom equations for the missile was performed. The proposed autopilot was applied to both pitch and yaw planes of the missile because of the axial symmetry of a skid-to-turn maneuver missile. For comparison, numerical simulation for a full missile model-based acceleration autopilot was also performed, and the results of two autopilots were compared. Simulation results of the proposed autopilot showed satisfactory control performance, compared with that of the full model-based autopilot.

6.2 Further Works

Generalization of Asymptotic Stability Analysis

In this study, some assumptions, based on the properties of the tail-fin controlled missile in the normal operational range, are applied for the stability analysis of the closed-loop system controlled by the SDRE method. Also, **Theorem 4.1**, which addresses the asymptotic stability of the closed-loop system, is based on the existence of a constant κ satisfying a specific inequality. Application of the analytical result may be limited because of these restrictions. Therefore, to some extent, the assumptions and conditions required to analyze the stability should be relaxed.

Analytic Solution for High-Order Nonlinear Systems

In this study, the analytic solution of the state-dependent ARE was derived for two-dimensional nonlinear systems. Accordingly, the missile acceleration autopilot was designed for the short-period approximated model, rather than the full-order missile model. To apply the analytical result proposed in this study to a wider class of systems, the analytic solution of the state-dependent ARE should be obtained for more high-order systems.

Bibliography

[1] Cimen, T., "Survey of State-Dependent Riccati Equation in Nonlinear Optimal Feedback Control Synthesis," *Journal of Guidance, Control, and Dynamics*, Vol. 35, No. 4, 2012, pp. 1025–1047.
DOI:10.2514/1.55821

[2] Mracek, C. P., and Cloutier, J. R., "Full Envelope Missile Longitudinal Autopilot Design Using the State-Dependent Riccati Equation Method," *AIAA Guidance, Navigation, and Control Conference*, New Orleans, LA, August 1997.
DOI:10.2514/6.1997-3767

[3] Vaddi, S. S., Menon, P. K., and Ohlmeyer, E. J., "Numerical State-Dependent Riccati Equation Approach for Missile Integrated Guidance Control," *Journal of Guidance, Control, and Dynamics*, Vol. 32, No. 2, 2009, pp. 699–703.
DOI:10.2514/1.34291

[4] Cimen, T., "A Generic Approach to Missile Autopilot Design Using State-Dependent Nonlinear Control," *18th IFAC World Congress*, Milano, Italy, January 2011.
DOI:10.3182/20110828-6-IT-1002.03744

[5] Lee, J., Lee, Y., Kim, Y., Moon, G., and Jun, B.-E., "Adaptive SDRE Based Boost-Phase Missile Autopilot Design Using Single and Modular Neural Networks," *IFAC Workshop on Advanced Control and Navigation for Autonomous Aerospace Vehicles*, Seville, Spain, June 2015.
DOI:10.1016/j.ifacol.2015.08.068

[6] Lee, J., Lee, Y., Kim, Y., Moon, G., and Jun, B.-E., "Design of an Adaptive Missile Autopilot Considering the Boost Phase Using the SDRE Method and Neural Networks," *Journal of the Franklin Institute*, Vol. 355, No. 18, 2018, pp. 9085–9107.
DOI:10.1016/j.jfranklin.2016.12.004

[7] Massari, M., and Zamaro, M., "Application of SDRE Technique to Orbital and Attitude Control of Spacecraft Formation Flying," *Acta Astronautica*, Vol. 94, No. 1, 2014, pp. 409–420.
DOI:10.1016/j.actaastro.2013.02.001

[8] Jagat, A., and Sinclair, A. J., "Nonlinear Control for Spacecraft Pursuit-Evasion Game Using the State-Dependent Riccati Equation Method," *IEEE Transactions on Aerospace and Electronic Systems*, Vol. 53, No. 6, 2017, pp. 3032–3042.
DOI:10.1109/TAES.2017.2725498

[9] Bogdanov, A., and Wan, E., "State-Dependent Riccati Equation Control for Small Autonomous Helicopter," *Journal of Guidance, Control, and Dynamics*, Vol. 30, No. 1, 2007, pp. 47–60.
DOI:10.2514/1.21910

[10] Langson, W., and Alleyne, A., "A Stability Result with Application to Nonlinear Regulation," *Journal of Dynamic Systems, Measurement, and Control*, Vol. 124, No. 3, 2002, pp. 452–456.
DOI:10.1115/1.1486011

[11] Erdem, E. B., and Alleyne, A. G., "Design of a Class of Nonlinear Controllers via State Dependent Riccati Equations," *IEEE Transactions on Control Systems Technology*, Vol. 12, No. 1, 2004, pp. 133–137.
DOI:10.1109/TCST.2003.819588

[12] Chen, C.-C., Liang, Y.-W., and Jhu, W.-M., "Global Stability of a System with State-Dependent Riccati Equation Controller," *Journal of Guidance, Control, and Dynamics*, Vol. 38, No. 10, 2015, pp. 2050–2054.
DOI:10.2514/1.G000989

[13] Cloutier, J. R., D'Souza, C. N., and Mracek, C. P., "Nonlinear Regulation and Nonlinear $\mathcal{H}_\infty$ Control via the State-Dependent Riccati Equation Technique: Part 1, Theory," *1st International Conference on Nonlinear Problems in Aviation and Aerospace*, Daytona Beach, FL, May 1996.

[14] Cloutier, J. R., D'Souza, C. N., and Mracek, C. P., "Nonlinear Regulation and Nonlinear $\mathcal{H}_\infty$ Control via the State-Dependent Riccati Equation Technique: Part 2, Examples," *1st International Conference on Nonlinear Problems in Aviation and Aerospace*, Daytona Beach, FL, May 1996.

[15] Potter, J. E., "Matrix Quadratic Solutions," *SIAM Journal on Applied Mathematics*, Vol. 14, No. 3, 1966, pp. 496–501.
DOI:10.1137/0114044

[16] Laub, A., "A Schur Method for Solving Algebraic Riccati Equation," *IEEE Transactions on Automatic Control*, Vol. 24, No. 6, 1979, pp. 913–921.
DOI:10.1109/CDC.1978.267893

[17] Roberts, J. D., "Linear Model Reduction and Solution of the Algebraic Riccati Equation by Use of the Sign Function," *International Journal of Control*, Vol. 32, No. 4, 1980, pp. 677–687.
DOI:10.1080/00207178008922881

[18] Incertis, F. C., "A New Formulation of the Algebraic Riccati Equation Problem," *IEEE Transactions on Automatic Control*, Vol. 26, No. 3, 1981, pp. 768–770.
DOI:10.1109/TAC.1981.1102692

[19] Incertis, F. C., "An Extension on a New Formulation of the Algebraic Riccati Equation Problem," *IEEE Transactions on Automatic Control*, Vol. 28, No. 2, 1983, pp. 235–238.
DOI:10.1109/TAC.1983.1103208

[20] Incertis, F. C., "A Skew-Symmetric Formulation of the Algebraic Riccati Equation Problem," *IEEE Transactions on Automatic Control*, Vol. 29, No. 5, 1984, pp. 467–470.
DOI:10.1109/TAC.1984.1103565

[21] Ish-Shalon, J., "On Symbolic Solution of the Matrix Algebraic and Differential Riccati Equations," *American Control Conference*, Boston, MA, June 1985.
DOI:10.23919/ACC.1985.4788881

[22] Rojas, A. J., "On the Continuous-Time Algebraic Riccati Equation and Its Closed-Form Solution," *IEEE Conference on Decision and Control*, Atlanta, GA, December 2010.
DOI:10.1109/CDC.2010.5717592

[23] Rojas, A. J., "On the Solution of a Class of Algebraic Riccati Equations with Repeated Unstable Eigenvalues," *American Control Conference*, Baltimore, MD, June-July 2010.
DOI:10.1109/ACC.2010.5530962

[24] Choi, Y., Park, J., and Lee, S., "Closed-Form Solution of Particular Case of Algebraic Riccati Equation Using Moser–Veselov Equation," *IET Control Theory & Applications*, Vol. 4, No. 5, 2010, pp. 865–870.
DOI:10.1049/iet-cta.2009.0103

[25] Shubert, H. A., "An Analytic Solution for an Algebraic Riccati Equation," *IEEE Transactions on Automatic Control*, Vol. 19, No. 3, 1974, pp. 255–256.
DOI:10.1109/TAC.1974.1100564

[26] Bierman, G. J., "Comments on "An Analytic Solution for an Algebraic Riccati Equation"," *IEEE Transactions on Automatic Control*, Vol. 20, No. 2, 1975, pp. 300–301.
DOI:10.1109/TAC.1975.1100890

[27] Ledyaev, Y., "On Analytical Solutions of Matrix Riccati Equations," *Proceedings of the Steklov Institute of Mathematics*, Vol. 273, No. 1, 2011,

pp. 214–228.
DOI:10.1134/S0081543811040109

[28] Cho, N., Lee, J., and Kim, Y., "Analytic Solution of Continuous-Time Algebraic Riccati Equation for Two-Dimensional Systems and Its Application to Wing-Rock Regulation," *AIAA Guidance, Navigation, and Control Conference*, Kissimmee, FL, January 2018.
DOI:10.2514/6.2018-0862

[29] Lee, J., Cho, N., and Kim, Y., "Analysis of Missile Longitudinal Autopilot Based on the State-Dependent Riccati Equation Method," *Journal of Guidance, Control, and Dynamics,* accepted for publication, 2019.
DOI:10.2514/1.G003679

[30] Isidori, A., *Nonlinear Control Systems,* 3rd ed., Springer-Verlag, Berlin, 1995.

[31] Devaud, E., Siguerdidjane, H., and Font, S., "Some Control Strategies for a High-Angle-of-Attack Missile Autopilot," *Control Engineering Practice*, Vol. 8, No. 8, 2000, pp. 885–892.
DOI:10.1016/S0967-0661(00)00013-7

[32] Lee, C. H., Jun, B.-E., and Lee, J. I., "Connections Between Linear and Nonlinear Missile Autopilots via Three-Loop Topology," *Journal of Guidance, Control, and Dynamics*, Vol. 39, No. 6, 2016, pp. 1424–1430.
DOI:10.2514/1.G001565

[33] Siguerdidjane, H., and Devaud, E., "Nonlinear Missile Autopilot Design Based on Angle of Attack Normal Form," *European Journal of Control*,

Vol. 6, No. 22, 2000, pp. 154–164.
DOI:10.1016/S0947-3580(00)70923-X

[34] Devaud, E., Harcaut, J. P., and Siguerdidjane, H., "Three-Axes Missile Autopilot Design: From Linear to Nonlinear Control Strategies," *Journal of Guidance, Control, and Dynamics*, Vol. 24, No. 1, 2001, pp. 64–71.
DOI:10.2514/2.4676

[35] Shtessel, Y. B., Shkolnikov, I. A., and Levant, A., "Guidance and Control of Missile Interceptor Using Second-Order Sliding Modes," *IEEE Transactions on Aerospace and Electronic Systems*, Vol. 45, No. 1, 2009, pp. 110–124.
DOI:10.1109/TAES.2009.4805267

[36] Guardabassi, G. O., and Savaresi, S. M., "Approximate Linearization via Feedback - An Overview," *Automatica*, Vol. 37, No. 1, 2001, pp. 1–15.
DOI:10.1016/S0005-1098(00)00117-5

[37] Hauser, J., Sastry, S., and Meyer, G., "Nonlinear Control Design for Slightly Non-Minimum Phase Systems: Application to V/STOL Aircraft," *Automatica*, Vol. 28, No. 4, 1992, pp. 665–679.
DOI:10.1016/0005-1098(92)90029-F

[38] Zarchan, P., *Tactical and Strategic Missile Guidance,* 5th ed., Progress in Astronautics and Aeronautics, Vol. 21, AIAA, Reston, VA, 2007.

[39] Mracek, C. P., and Ridgely, D. B., "Missile Longitudinal Autopilots: Comparison of Multiple Three Loop Topologies," *AIAA Guidance, Navigation,*

and Control Conference, San Francisco, CA, August 2005.
DOI:10.2514/6.2005-6380

[40] Mracek, C. P., and Ridgely, D. B., "Missile Longitudinal Autopilots: Connections Between Optimal Control and Classical Topologies," *AIAA Guidance, Navigation, and Control Conference*, San Francisco, CA, August 2005.
DOI:10.2514/6.2005-6381

[41] Defu, L., Junfang, F., Zaikang, Q., and Yu, M., "Analysis and Improvement of Missile Three Loop Autopilot," *Journal of Systems Engineering and Electronics*, Vol. 20, No. 4, 2009, pp. 844–851.

[42] Jackson, P., "Applying μ-Synthesis to Missile Autopilot Design," *29th IEEE Conference on Decision and Control*, Honolulu, HI, December 1990.
DOI:10.1109/CDC.1990.203333

[43] Ferreres, G., and M'Saad, M., "Parametric Robustness Evaluation of a $\mathcal{H}_\infty$ Missile Autopilot," *Journal of Guidance, Control, and Dynamics*, Vol. 19, No. 3, 1996, pp. 621–627.
DOI:10.2514/3.21666

[44] Mahmood, A., Kim, Y., and Park, J., "Robust $\mathcal{H}_\infty$ Autopilot Design for Agile Missile with Time-Varying Parameters," *IEEE Transactions on Aerospace and Electronic Systems*, Vol. 50, No. 4, 2014, pp. 3082–3089.
DOI:10.1109/TAES.2014.130750

[45] Shamma, J. S., and Cloutier, J. R., "Gain-Scheduled Missile Autopilot Design Using Linear Parameter Varying Transformations," *Journal of Guid-*

ance, Control, and Dynamics, Vol. 16, No. 2, 1993, pp. 256–263.
DOI:10.2514/3.20997

[46] Stilwell, D. J., "State-Space Interpolation for a Gain-Scheduled Autopilot," *Journal of Guidance, Control, and Dynamics*, Vol. 24, No. 3, 2001, pp. 460–465.
DOI:10.2514/2.4766

[47] Theodoulis, S., and Duc, G., "Missile Autopilot Design: Gain-Scheduling and the Gap Metric," *Journal of Guidance, Control, and Dynamics*, Vol. 32, No. 3, 2009, pp. 986–996.
DOI:10.2514/1.34756

[48] Leith, D. J., and Leithead, W. E., "Survey of Gain-Scheduling Analysis & Design," *International Journal of Control*, Vol. 73, No. 11, 2000, pp. 1001–1025.
DOI:10.1080/002071700411304

[49] Gratt, H. J., and McCowan, W. L., "Feedback Linearization Autopilot Design for the Advanced Kinetic Energy Missile Boost Phase," *Journal of Guidance, Control, and Dynamics*, Vol. 18, No. 5, 1995, pp. 945–950.
DOI:10.2514/3.21489

[50] Menon, P. K., and Yousefpor, M., "Design of Nonlinear Autopilots for High Angle of Attack Missiles," *AIAA Guidance, Navigation, and Control Conference*, San Diego, CA, July 1996.
DOI:10.2514/6.1996-3913

[51] Mattei, G., and Monaco, S., "Nonlinear Autopilot Design for an Asymmetric Missile Using Robust Backstepping Control," *Journal of Guidance, Control, and Dynamics*, Vol. 37, No. 5, 2014, pp. 1462–1476.
DOI:10.2514/1.G000434

[52] Lee, S., Kim, Y., Moon, G., and Jun, B.-E., "Missile Autopilot Design During Boost Phase Using Robust Backstepping Approch," *AIAA Guidance, Navigation, and Control Conference*, Kissimmee, FL, January 2015.
DOI:10.2514/6.2015-0860

[53] Shima, T., Idan, M., and Golan, O. M., "Sliding-Mode Control for Integrated Missile Autopilot Guidance," *Journal of Guidance, Control, and Dynamics*, Vol. 29, No. 2, 2006, pp. 250–260.
DOI:10.2514/1.14951

[54] Lee, Y., Kim, Y., Moon, G., and Jun, B.-E., "Sliding-Mode-Based Missile-Integrated Attitude Control Schemes Considering Velocity Change," *Journal of Guidance, Control, and Dynamics*, Vol. 39, No. 3, 2016, pp. 423–436.
DOI:10.2514/1.G001416

[55] Slotine, J.-J. E., and Li, W., *Applied Nonlinear Control*, Prentice Hall, Englewood Cliffs, NJ, 1991.

[56] Cloutier, J. R., and Stansbery, D. T., "The Capabilities and Art of State-Dependent Riccati Equation-Based Design," *American Control Conference*, Anchorage, AK, May 2002.
DOI:10.1109/ACC.2002.1024785

[57] Blakelock, J. H., *Automatic Control of Aircraft and Missiles*, Wiley, New York, NY, 1991.

[58] Nelson, R. C., *Flight Stability and Automatic Control,* 2nd ed., McGraw-Hill, New York, NY, 1998.

[59] Cimen, T., "Systematic and Effective Design of Nonlinear Feedback Controllers via the State-Dependent Riccati Equation (SDRE) Method," *Annual Reviews in Control*, Vol. 34, No. 1, 2010, pp. 32–51.
DOI:10.1016/j.arcontrol.2010.03.001

[60] Khalil, H. K., *Nonlinear Systems,* 3rd ed., Prentice-Hall, Upper Saddle River, NJ, 2011.

[61] Denman, E. D., "The Matrix Sign Function and Computations in Systems," *Applied Mathematics and Computation*, Vol. 2, No. 1, 1976, pp. 63–94.
DOI:10.1016/0096-3003(76)90020-5

[62] Shieh, L. S., Tsay, Y. T., and Yates, R. E., "Some Properties of Matrix Sign Functions Derived from Continued Fractions," *IEEE Proceedings of Control Theory and Application, Part D*, Vol. 131, No. 3, 1983, pp. 111–118.
DOI:10.1049/ip-d.1983.0020

[63] Higham, N. J., "Stable Iterations for the Matrix Square Root," *Numerical Algorithms*, Vol. 15, No. 2, 1997, pp. 227–242.
DOI:10.1023/A:1019150005407

[64] Meyer, K. R., and Hall, G. R., *Introduction to Hamiltonian Dynamical Systems and the N-Body Problem*, Applied Mthematical Sciences Series, Vol. 90, Springer-Verlag, New York, NY, 1992.

[65] Lu, L., and Pearce, C. E. M., "On the Matrix-Sign-Function Method for Solving Algebraic Riccati Equations," *Applied Mathematics and Computation*, Vol. 86, No. 2-3, 1997, pp. 157–170.
DOI:10.1016/S0096-3003(96)00179-8

[66] Arnold, W. F., and Laub, A. J., "Generalized Eigenproblem Algorithms and Software for Algebraic Riccati Equations," *Proceedings of the IEEE*, Vol. 72, No. 12, 1984, pp. 1746–1754.
DOI:10.1109/PROC.1984.13083

국문초록

본 논문에서는 꼬리날개를 이용한 Skid-to-turn 기동 유도탄의 가속도 자동조종장치를 SDRE(State-Dependent Riccati Equation) 기법을 이용하여 설계하고, 미리 설정된 유도탄의 운용 범위내에서 폐루프 시스템의 점근 안정성을 분석하였다. SDRE 기법 기반의 제어기를 포함한 폐루프 시스템을 해석적으로 표현하기 위해 상태변수를 포함하는 대수 리카티 방정식의 해석해를 구했으며, 이를 점근 안정성 분석에 사용하였다.

본 논문에서는 먼저 꼬리날개 제어 유도탄의 6-자유도 운동방정식을 유도하였다. 유도된 방정식을 기반으로 유도탄의 종방향 및 횡방향의 운동을 모사하는 모델을 제시하였다. 유도탄 종방향 운동방정식에 대하여 시스템 자체의 특성과 근사 모델 기반의 제어기를 포함한 폐루프 시스템의 특성을 수학적으로 분석하였다. 유도탄의 정상운용 범위내에서 유효한 정규형 방정식으로의 변환을 제시하였으며, 이를 기반으로 유도탄의 비최소 위상 특성을 분석하였다. 근사 모델 기반의 제어기를 포함한 폐루프 시스템에 대하여 비최소 위상을 유발하는 항을 외부 입력으로 고려한 입출력 안정성을 증명하였다. 그리고 수치 예시를 통해 제안한 해석 결과를 확인하였다.

한편, SDRE 기법으로 설계된 자동조종장치를 포함한 폐루프 시스템의 점근 안정성을 분석하였다. 폐루프 시스템을 해석적으로 표현하기 위해 상태변수를 포함하는 대수 리카티 방정식의 해석해를 행렬 부호 함수와 해밀토니안 행렬의 주요 제곱근을 이용하여 구하였다. SDRE 기법을 이용하여 유도탄 가속도 자동조종장치를 꼬리날개 제어 유도탄의 종방향 운동방정식을 기반으로 설계하였으며, 유도탄의 정상 운용 범위에서의 특성에 기반한 가정을 고려하여 설계한 가속도

자동조종장치를 포함한 페루프 시스템의 점근 안정성을 르야프노프 안정성 이론을 기반으로 증명하였다. 이때, 페루프 시스템의 해석적 표현을 위해 상태변수를 포함하는 대수 리카티 방정식의 해석해를 사용하였다. 수치 예시를 통해 제안한 안정성 해석 결과를 확인하였다.

본 논문에서 설계한 유도탄 가속도 자동조종장치의 제어 성능을 확인하기 위해 가속도 추종을 위한 6-자유도 수치 시뮬레이션을 수행하였다. Skid-to-turn 기동의 유도탄의 축대칭을 고려하여 유도탄 종방향 운동방정식을 기반으로 설계된 자동조종장치를 유도탄의 피치 및 요 평면에 적용한 시뮬레이션 결과를 제시하였다.

주요어: 유도탄 가속도 자동조종장치, SDRE 기법, 점근 안정성, 비선형 해석
학번: 2013-20698